MONTHLY NOTICES

OF THE

ROYAL ASTRONOMICAL SOCIETY

Volume 118 No. 5 1958

Published and Sold by the

ROYAL ASTRONOMICAL SOCIETY
BURLINGTON HOUSE
LONDON, W.1

Price £1 0s. 0d.; in U.S.A. $3

Annual Subscription for volume of six numbers: £5 5s. 0d. ; in U.S.A. $16

MONTHLY NOTICES

OF THE

ROYAL ASTRONOMICAL SOCIETY

Vol. 118 No. 5

MEETING OF 1958 MARCH 14

Dr W. H. Steavenson, President, in the Chair

The election by the Council of the following Fellows was duly confirmed :—

John Anderson, 22 Massey Park, Stormont, Belfast, N. Ireland (proposed by E. M. Lindsay);

Charles David Austin, 49 Leysdown Road, London, S.E.9 (proposed by C. W. Allen);

Frederick Henry George Best, 24 Blake Road, Croydon, Surrey (proposed by P. Moore);

Michael Gadsden, I.G.Y. Station, Invercargill, New Zealand (proposed by I. L. Thomsen);

Eugene C. Robertson, Geological Survey, Silver Spring, Maryland, U.S.A. (proposed by A. H. Cook);

Malcolm Walsh, 10 Penylan Road, Newport, Mon. (proposed by C. W. Allen); and

Jack Youdale, 21 Stanhope Road, Billingham, Co. Durham (proposed by D. Sinden).

The re-election by the Council of the following Fellow was duly confirmed:—

Victor Dumert, 88 Church Lane, London, N.2 (proposed by H. Bondi).

The election by the Council of the following Junior Members was duly confirmed :—

Robert John Dickens, Royal Greenwich Observatory, Herstmonceux Castle, Hailsham, Sussex (proposed by B. E. J. Pagel);

Roger Anthony Gordon Smith, 184 King's Hall Road, Beckenham, Kent (proposed by B. E. J. Pagel); and

Ramon David Wolstencroft, 138 Butterstile Lane, Prestwich, Lancs. (proposed by C. W. Allen).

Seventy-eight presents were announced as having been received since the last meeting, including:—

T. Maloney: *Other worlds in space* (presented by John Calder, Publishers, Ltd.).

MEETING OF 1958 APRIL 11

Dr W. H. Steavenson, President, in the Chair

The President announced that the Council had elected the following Associates of the Society :—

Francis Birch, Dunbar Laboratory, Harvard University, Cambridge 38, Mass., U.S.A.;

Boris Vassilevitch Kukarkin, Chief of the Variable Star Department of the Sternberg Astronomical Institute, Moscow, U.S.S.R.; and

Yngve Öhman, Director, Stockholms Observatorium, Saltsjöbaden, Sweden.

The election by the Council of the following Fellows was duly confirmed :—

Donald Thomas Germain-Jones, British Petroleum Company, Beaufort House, Gravel Lane, London, E.1 (proposed by L. H. Tarrant);

Alexander Leo Helm, Beech House, Holmewood, Langton Green, Tunbridge Wells, Kent (proposed by P. Moore);

Ernest George Hill, Harbour St. Bride, Durlston Road, Swanage, Dorset (proposed by H. G. Hughes);

R. Ingram-Brown, Brown, Son & Ferguson, Ltd., 52/58 Darnley Street, Pollockshields, Glasgow (proposed by C. W. T. Layton);

Roger Jackson Lee, Box 2391, Brown Station, Providence 12, Rhode Island, U.S.A. (proposed by L. M. Milne-Thomson);

Martin F. McCarthy, Specola Vaticana, Palazzo Pontificio, Castel Gandolfo, Italy (proposed by W. P. Bidelman); and

John Grahame Sutherland, 172 Overhill Road, London, S.E.22 (proposed by H. J. Lewis).

Fifty-eight presents were announced as having been received since the last meeting, including :

E. O. Tancock (ed.), *Philip's Chart of the Stars* (presented by G. Philip & Son);

F. B. Wood (ed.), *The present and the future of the telescope of moderate size* (presented by the University of Pennsylvania Press);

N. Roman (ed.), *I.A.U. Symposium No.* 5. *The large-scale structure of the galactic system* (presented by the International Astronomical Union); and

M. Migeotte, L. Neven, J. Swensson and E. Vigroux, *An atlas of nitrous oxide, methane and ozone infra-red absorption bands* (presented by the Institut d'Astrophysique de l'Université de Liège).

MEETING OF 1958 MAY 9

Dr W. H. Steavenson, President, in the Chair

The President announced the death of Knut Emil Lundmark, an Associate of the Society, and paid a tribute to his memory, the Fellows standing.

The election by the Council of the following Fellows was duly confirmed :—

Donald Murray Edwards, c/o Mapping Branch, Lands and Surveys, Perth, W. Australia (proposed by C. R. Edwards);

Hubert Basil Lewis, 8 Baker Street, Moorabbin, Australia (proposed by E. B. Walton);

Donald Malcolm, 18 Caledonia Street, Paisley, Scotland (proposed by A. E. Roy);

Seyed Mohamed Razavy, 51A Blenheim Crescent, London, W.11 (proposed by H. Wildey);

Thomas E. Sadler, Gravenhunger, Woore, Staffs. (proposed by C. D. Grimwade);

Cyril Alfred Edgar Tomes, 65 East Dulwich Road, London, S.E.22 (proposed by P. Moore);

Ernest W. Wilkes, Allendale Road, Hexham (proposed by C. Gilbert);

William Williamson, 1 Gold Street, Longton, Staffs. (proposed by C. D. Grimwade); and

Ronald William Girdler, Corpus Christi College, Cambridge (proposed by R. Stoneley).

The re-election by the Council of the following Fellow was duly confirmed :—

Herbert Gilgryst, 5 De Vere Gardens, London, W.8 (proposed by C. M. Botley).

The election by the Council of the following Junior Member was duly confirmed :—

Lionel William Moore, 190 Pickhurst Lane, Hayes, Kent (proposed by C. W. Allen).

ADDITIONAL MEETING OF 1958 JULY 11

in the Physics Lecture Theatre of the University College of North Staffordshire, Keele

Dr W. H. Steavenson, President, in the Chair

The President announced that this Additional Meeting was the ninth to take place outside the rooms of the Society in London. He expressed the thanks of the Society to Sir George Barnes, Principal of the University College of North Staffordshire, and to the College authorities, at whose invitation the Meeting was being held at Keele. The thanks of the Society were also extended to Professor H. D. Springall and Professor F. A. Vick for the use of the Departments of Chemistry and Physics respectively, to the Registrar, Mr. J. F. N. Hodgkinson, for his co-operation in making the necessary arrangements for the Society's stay, and to Dr J. N. Hodgson who, in acting as the Society's Local Secretary, had undertaken much of the detailed work involved in the local organization of the various meetings and associated activities.

One hundred and thirteen presents were announced as having been received since the last meeting, including :—

G. Alter, J. Ruprecht and V. Vanysek, *Catalogue of star clusters and associations* (presented by G. Alter);

A. Dauvillier, *Le volcanisme lunaire et terrestre* (presented by Editions Albin Michel);

G. de Vaucouleurs, *La photographie astronomique* (presented by Editions Albin Michel); and

United Nations Educational, Scientific and Cultural Organization, *The Earth as a Planet* (presented by U.N.E.S.C.O.)

Other meetings and activities in connection with the Society's visit to Keele included a colloquium on *Interplanetary Matter*, held in the morning of July 10. In the afternoon of the same day, at the kind invitation of the Director, Professor A. C. B. Lovell, and with the co-operation of his staff, there was a conducted tour of the Jodrell Bank Experimental Station. In the evening a Public Lecture entitled *Why is it dark at night* ? was delivered in the College Conference Hall by Professor H. Bondi. On July 11 a number of excursions were arranged to places of scenic and historical interest in the neighbourhood.

THE CONTRIBUTION OF THE IMPERSONAL ASTROLABE TO FUNDAMENTAL ASTRONOMY

George Darwin Lecture delivered by Professor André Danjon on 1958 *May* 9

I wish to recall that Sir George Darwin, to whom this lecture is dedicated, devoted a part of his work to rotating celestial bodies. The title of his first paper was *On the Influence of Geological Changes on the Earth's Axis of Rotation.* Since then the discovery of the movements of the poles and, later, of the variations in the length of the day have aroused a renewed interest in the problems of practical astronomy related to these phenomena. My aim in this lecture is to describe the programme of observations now being carried out at the Paris Observatory and to mention the further developments that can be anticipated in the near future.

A few years before the outbreak of the last war, I had published the description of a new type of transit instrument for the determination of right ascensions. The results obtained at Strasbourg with a prototype of small dimensions (aperture 6 cm) having been very encouraging, a new series of tests was commenced at the Paris Observatory in 1946. Meanwhile, an instrument of similar design but of 12 cm aperture was constructed. The early observations made with this larger instrument revealed unforeseen difficulties, which could have been overcome by completely redesigning the mounting. But, for the time being, the study of this instrument has been discontinued and all the facilities available in Paris Observatory, including scientific and technical staff, laboratories and workshop, etc. have been concentrated on the construction of an instrument of an entirely different type: the impersonal astrolabe, which will be the main topic of this lecture.

I had moreover another reason for giving priority to the astrolabe, of which an experimental model had already been constructed at the Observatory in 1950 and progressively improved. This reason is that, in 1952, the International Council of Scientific Unions decided to organize the International Geophysical Year and to incorporate in its programme a determination of world longitudes and latitudes. The observatories participating in the operation were recommended to observe stars selected in the Fundamental Catalogue FK3 (or in the improved catalogue FK3R). It was agreed that preference should be given to modern instruments giving simultaneously and with the highest possible accuracy the two coordinates, time and latitude. The zenith telescope, indeed, gives both coordinates but requires a special catalogue limited to zenith stars, in which therefore non-fundamental stars have to be introduced. The astrolabe is the only instrument which permits both coordinates to be determined by the observation of fundamental stars alone.

A large size astrolabe was then ordered from the Société Optique et Précision de Levallois (OPL). The design of the instrument was worked out in close co-operation with the technicians of this firm. The new instrument differs from the experimental model mainly in its dimensions, which are larger, and in the improved arrangement of the mechanical parts.

The instrument was delivered in 1956 and put into service in July of that year. Since then it has been in use without interruption. More than twelve thousand transits have been observed, which is adequate for evaluating the qualities of the instrument, if not for establishing definitive results. The observations have been carried out mainly by L. Arbey, B. Guinot and Mlle Débarbat.

Under the most favourable atmospheric conditions, the OPL astrolabe permits the transit of a star, at a well determined zenith distance, differing very slightly from thirty degrees, to be recorded with an accuracy characterized by a standard deviation of 0″·09, assuming that the errors of the catalogue have been corrected. The deviation increases with atmospheric scintillation, and its most frequent value is 0″·17. For only six per cent of the nights is it larger than 0″·26. But what is most important is that the observations have proved to be free from systematic errors, a result of outstanding importance for the use of the impersonal astrolabe as a fundamental instrument.

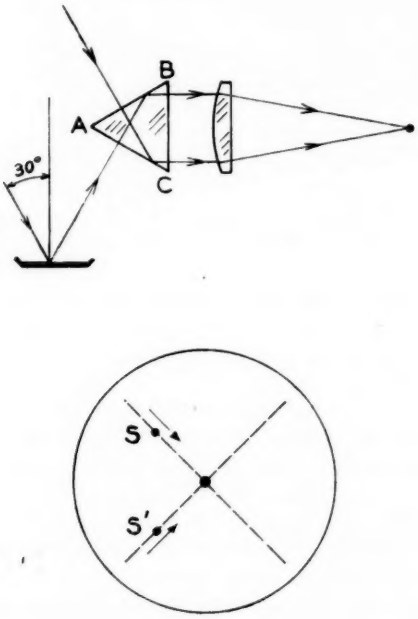

FIG. 1.

Indeed we very soon realized that this instrument was useful not only for the determination of time and latitude but that it could be used as well for the improvement of the FK3 catalogue and for the determination of the fundamental astronomical constants. The accuracy of the results is due partly to the intrinsic qualities of the instrument and partly to the application of the so-called "method of equal altitude of stars".

As for the instrument itself I wish first to recall its principle. Suppose that we fix an equilateral glass prism in front of a horizontal telescope in such a way that its edges are horizontal and one of its faces vertical (Fig. 1). A beam

of light coming from a star entering the face AB at right angles to the edge of the prism, is then reflected from AC and emerges through the lower half of BC. Another portion of the beam falls on AC after having been reflected from the surface of a bath of mercury. It is reflected by AB and emerges through the upper half of BC. Thus, looking through the telescope, two images of the star, S and S′, are seen which appear to move in opposite directions, one moving upwards and the other downwards. They appear to coincide when the star is at a zenith distance of exactly 30° and the instant of coincidence is noted. As the prism angle is not exactly of 60°, there are three unknowns in the problem, namely: the correction of the clock, the latitude, and the excess of the zenith distance over 30°. Therefore at least three stars, in different azimuths, must be observed. In fact, many more than three stars are observed, and in general each of our groups contains twenty-eight stars. The plotting of position lines, a method familiar to navigators, gives an approximate graphical solution but as our observations are very accurate a solution by least squares should be applied.

The astrolabe in its original form was designed by MM. Claude et Driencourt*. It dates back to 1900 and it was then a very simple instrument which consisted merely of a telescope, a prism, a mercury horizon and adjustment devices. The observer noted the time of coincidence of the two images of the star by the eye and ear method or by the hand tapping method. Thus, each star gave only a single determination of time, which was affected by personal equation. But it was intended to be an instrument for use in the field and not an instrument of high precision. There was indeed another source of error resulting from the images being displaced when the position of the eye-piece was changed even by a slight amount. The reason is that the images are formed by two pencils of rays the axes of which are not strictly parallel but are inclined to each other at an angle of two or three degrees. If the focusing is altered, the distance between the two pseudo-images changes, which produces the same effect as a variation in the prism angle. I will later show you that this angle has an astonishing stability, but, owing to the defective arrangement of the instrument, no full advantage of this remarkable property was taken.

Various astronomers have been successful either in correcting this optical defect or in rendering the astrolabe an impersonal instrument. The excellent results obtained by Paul Muller, the well known double star observer, with a micrometer containing a doubly refracting prism, led me to the concept of a more complete solution which I will now describe and which is the essential feature of the impersonal astrolabe†.

A doubly-refracting prism is placed at the focus of the telescope. For certain reasons, which would take too long to describe, I have selected a double Wollaston prism made of quartz. The arrangement of this prism is shown in Fig. 2. The separation angle of this prism is precisely equal to the angle between the axes a and b of the two pencils transmitted by the objective. The splitting of the pencil a gives two pencils a_1 and a_2, as is shown in the figure, while the splitting of pencil b gives pencils b_1 and b_2. It is at once seen that a_1 and b_2 are

* A. Claude and L. Driencourt, *Description et usage de l'Astrolabe à Prisme*, Paris, Gauthier-Villars, 1910.

J. Ball and Knox Shaw, *A Handbook of the Prismatic Astrolabe*, Cairo, 1919.

See also: E. Chandon and A. Gougenheim, *Les Instruments pour l'observation des Hauteurs Egales en Astronomie*, *Revue Hydrographique*, **12**, 1, 1935.

† A. Danjon, L'Astrolabe impersonnel de l'Observatoire de Paris, *Bull. Astro.*, **18**, 251, 1955.

parallel and that therefore the distance of the two corresponding images σ and σ' no longer depends on the adjustment of the eyepiece. The two other images are eliminated by suitably placed screens. Moreover, the coincidence of the two images σ and σ' can be obtained by a displacement of the quartz prism parallel to the axis of the telescope. The coincidence thus obtained can be maintained

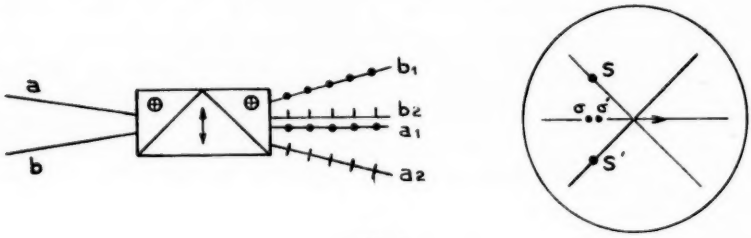

FIG. 2.

by traversing the prism at a rate proportional to the sine of the azimuth and to the cosine of the latitude. The micrometer screw which drives the prism, carries a disk with contacts connected to a chronograph. The astrolabe, already corrected for its optical defects, then becomes impersonal. The observer needs only to correct the movement produced by a motor, so as to maintain the coincidence of the two images.

In fact this coincidence is obtained not by superposing the two images, but by placing them side by side along the same horizontal line between two illuminated wires as shown in Fig. 3.

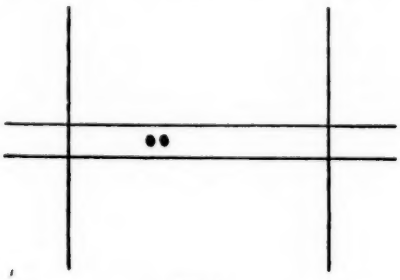

FIG. 3.

It would take too long to describe, in all details, the arrangements adopted for the component parts of the astrolabe*. Figure 4 gives a very simplified layout of the instrument. The objective of the OPL model has an aperture of ten centimetres and a focal distance of one meter. Two equal lune-shaped holes are made in a diaphragm, giving diffraction images elongated along the vertical, with axes in the ratio of three to five. The faces of the prism are rectangles of 10 cm by 8 cm. The dimensions of the micrometer screw are rather unusual: 25 mm in diameter and 5 mm in pitch. If the star is observed exactly to the East or to the West, the screw makes a complete revolution in 2·61 seconds. The speed of the motor is constant and is adjusted to suit the latitude of the station.

* A. Danjon, " L'Astrolabe impersonnel modèle OPL ", *Bull. Astro.*, to be published in 1958.

A speed reducer automatically varies the speed of rotation of the screw proportionally to the sine of the azimuth, when the astrolabe is turned around its vertical axis to observe another star. To make the instrument as compact as possible, the beam of light is broken twice by mirrors made of fused quartz and located between the objective and its focus.

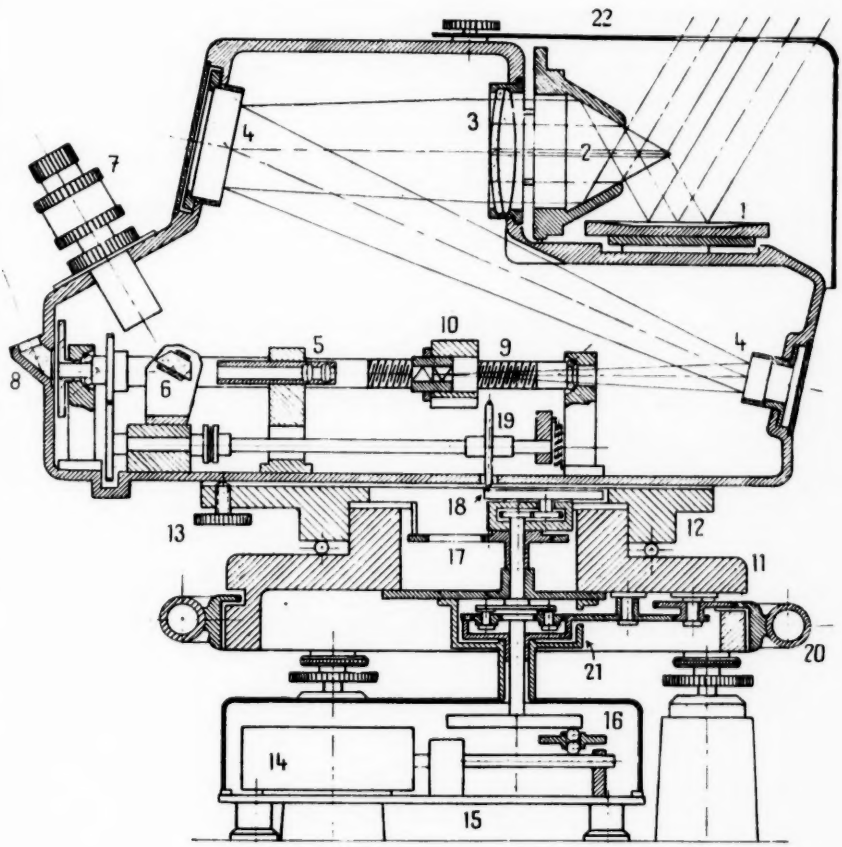

FIG. 4.

The accuracy of astrolabe observations is due to a large extent to careful manufacture by the Société OPL but equally to the working conditions and to the intrinsic properties of the equal altitude method. I shall consider these two points in turn. As the instrument rotates around a vertical axis, its flexures are not liable to vary with the azimuth. Its design provides protection against sudden changes of temperature. The results of time and latitude observations do not even depend on the absolute value of the prism angle; they could be affected only by a variation of this angle during the observation. But results obtained since July 1956 have clearly demonstrated that there is no systematic variation of this angle in the course of the night, not even in the course of a year,

and that the zenith distance remains invariable within a few hundredths of a second. Our observation programme includes twelve groups, each of twenty-eight stars chosen from the FK3 or its supplements. These groups are identified by letters a, b, . . . , k, l.

A single observer can observe, during a single night, at least two consecutive groups, often three, or even more*. The computed zenith distance, corrected for refraction, would have the same value for all these groups if the prism angle were constant and if the catalogue were not affected by any systematic error. In fact, two consecutive groups observed in the course of the same night, give different values as is shown by Fig. 5. In the course of a year, differences a–b, b–c, ... , l–a are obtained. The distribution of these differences does not reveal any systematic variation in the nature of a function of the right ascension, which indicates that the prism angle is independent of the annual variation of temperature and that errors in the catalogue are solely responsible for the differences obtained.

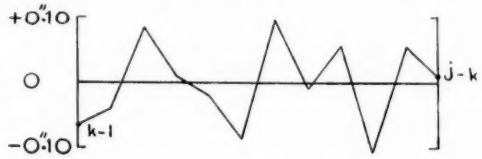

FIG. 5.

Even more, we have been able to verify that the zenith distance of transits does not vary systematically during the course of the night, although, as a general rule, the temperature of the instrument decreases from the evening to the morning. This is illustrated by the smallness of the closing error of the differences that B. Guinot has computed for a complete year. For instance, for group k this closing error was found as small as $-0''{\cdot}017 \pm 0''{\cdot}104$. At any rate it is not significant. It must be emphasized that the prism has been very carefully annealed, that its mounting does not exert any prejudicial stresses, and that these two conditions seem to be essential.

Let us now consider the method of equal altitude of stars and its advantages. Devised by Gauss about a hundred and fifty years ago for field operations, its application to problems of fundamental astronomy has so far been restricted to special cases such as, for instance, the determination of latitude by the Talcott method, which is still in use in the International Latitude Service, or the observation of transits in the prime vertical by the method of W. Struve. However, it is very valuable, in its general form, for linking together stars whose declinations differ by several tens of degrees and whose right ascensions differ by several hours.

The declinations of the stars that can be observed with the astrolabe are between $\phi - 30°$ and $\phi + 30°$, ϕ being the latitude of the station. In Paris, these two limits are theoretically $+18°50'$ and $+78°50'$, or practically $+20°$ and $+78°$. Their hour angle at the time of the transit is comprised between the limits $-H$ and $+H$, H being the solution of the equation $\sin H = \frac{1}{2} \sec \phi$. For Paris $2H = 6^h\ 36^m$ and for Herstmonceux, $6^h\ 59^m$. The observation of one group requires about one hour and a half so that it is possible to link together stars whose right ascensions differ by as much as 8 hours.

* B. Guinot, " L'Astrolabe Impersonnel. Réduction des Observations. Étude des Résultats." *Bull. Astro.*, **18**, 283, 1956.

When two transits of the same star are observed, one to the east and the the other to the west, the mean of the observed times gives its right ascension, and its declination is easily computed from the difference of the same transit times. The determination of the right ascension is not very accurate when the declination of the star is near the limits and, on the other hand, the determination of the declination is not possible when the hour angle of the transit is close to H. To fill these gaps it would be advantageous, and for more than one reason, to set up astrolabe stations in several latitudes. In Paris for instance we obtain good values of the right ascensions for declinations comprised between $+20°$ and $+78°$, and good values for the declinations in the intervals between $+20°$ and $+50°$ and between $+68°$ and $+78°$. In these intervals the application of the method of equal altitude with a high precision instrument discloses at once the indvidual errors of the catalogue, as these errors are important compared to the accuracy of the observations. I have already mentioned that the average value of the standard deviation for one transit was $0''{\cdot}17$ and that, under very favourable atmospheric conditions, this deviation is as small as $0''{\cdot}09$. As each group is observed about 20 times each year, the plotting of the position lines is correct within a few hundredths of a second. In a few years the precision of their determination will be as accurate as $0''{\cdot}01$. Individual errors being expressed by a dispersion of the position lines in the diagram, some of them intersect the circle, whose centre and radius are obtained from a least squares adjustment, and some others remain outside the circle. As for the systematic errors of the catalogue they are sometimes revealed by an asymmetry of the diagram.

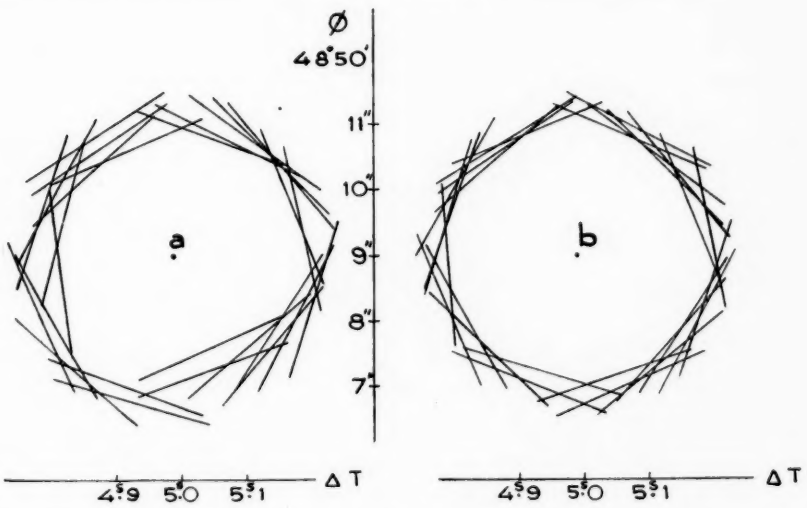

FIG. 6.

$\Delta T = 4^{s}{\cdot}987 \pm 0^{s}{\cdot}006$
$\Delta\phi = -1''{\cdot}01 \pm 0''{\cdot}06$
$R = -2''{\cdot}27 \pm 0''{\cdot}04$
$\sigma = 0''{\cdot}21$

$\Delta T = 4^{s}{\cdot}987 \pm 0^{s}{\cdot}002$
$\Delta\phi = -1''{\cdot}01 \pm 0''{\cdot}03$
$R = -2''{\cdot}27 \pm 0''{\cdot}02$
$\sigma = 0''{\cdot}09$

The diagram in Fig. 6(a) was drawn from the results obtained on 1958 January 22 on group d. The same group was observed in 1957 and the displacements to

be given to the position lines to make them tangent to the circle were already known. Fig. 6(b) shows the same diagram corrected from the observations obtained in the preceding year. Their quadratic mean error decreases from 0″·21 to 0″·09 and the asymmetry disappears. This example illustrates clearly the effectiveness of the method of equal altitudes in correcting the position of stars, but it must be remarked that this operation is merely an internal adjustment affecting each group independently and that it is by no means sufficient to correct the catalogue.

It is now essential to make a fundamental remark. Whatever be the instrument used, a single observation of a group of stars cannot disclose systematic errors of a catalogue which are equivalent to a change in the coordinate system and which do not affect the relative positions of the stars. Such are those produced by an error in the value of the precession or of the nutation. As the relative positions of the stars remain unchanged but the position of the pole and the origin of the coordinate system are erroneous, the diagram of the position lines is translated without distortion and therefore neither its symmetry nor the radius of the circle of the position lines is affected. But of course the coordinates of the centre of the circle are altered, and consequently so also are the time and the latitude. The method of equal altitude of stars, which reveals so clearly the individual errors and the localised errors affecting the various regions of the sky, cannot therefore provide any evidence of a systematic error in the reference system by a *single* observation of a given group. Errors of this sort can be found out only by a chain programme of observation, associated with group to group connections, covering at least one entire year. These errors will then appear in the group errors in the form of a variation depending on sin α.

I have said a moment ago that there was in this respect no privileged instrument. Suppose that we observe with a meridian circle the transits of a group of stars of limited range in right ascension. If the pole of the catalogue is at a distance $\Delta\nu$ from the true pole of rotation, in consequence of an error in the precession, and if α_m is the observed mean right ascension of the group, the azimuth of the meridian circle, computed from the observations, will have an error equal to $\Delta\nu \sin \alpha_m \sec \phi$, but nevertheless the representation of the observations by means of this faulty azimuth will still be excellent. Therefore no improvement of the catalogue can be expected. Here again the "chain adjustment" alone will enable the errors of the catalogue to be determined and corrected.

Theoretically the method of equal altitude of stars and the method of meridian transits are therefore equivalent in this respect. But in practice their possibilities are very different. In the first place, the stability of the astrolabe can be guaranteed with much greater certainty than that of the meridian circle. In particular, the astrolabe enables the value of the prism angle to be accurately controlled, and that is the only instrumental constant whose variation would be prejudicial to the accuracy of the observations. We now know by experience that the changes in the prism angle are negligible compared with the accidental or systematic errors of the fundamental catalogue. Moreover, the observations with the astrolabe are referred to a single terrestrial reference: the vertical. The discussion of the latitude observations have proved, as I will show you, that the daily variations of the zenithal refractions are imperceptible, at least in Paris.

The conditions are quite different in the transit instrument. The solid body which serves as the direction of reference is not now a simple glass prism but a telescope with its trunnions. The line of sight is determined by the optical centre of an objective, consisting of two lenses which cannot be linked rigidly together nor to their mounting, and by the spider's web carried by the movable frame of a micrometer. The objective and the micrometer are linked together by a metallic tube exposed to unceasingly variable conditions of temperature, as this tube radiates either from one side or the other as the star to be observed is to the north or to the south. The axis of rotation is defined by two trunnions carried by a heavy metallic part exposed to the same variations of temperature. Consequently the position of the instrument changes with respect to the vertical from one star to another, and as the flexures are not rigorously symmetrical with respect to the meridian plane, lateral deflections are unavoidable. To measure the collimation of the instrument and the inclination of its axis of rotation, the telescope is pointed towards the nadir in a direction quite different from the positions it occupies for the observation of stars. Who could say what happens to this collimation and inclination when the telescope is pointed towards a star ? To obtain an accuracy of 1/10th of a second of arc, it is necessary that the mechanical or thermal deformations of the instrument are less than 1 micron. Experience shows that they are in general much larger than this limit. More than 70 years ago, Chandler already asserted that the method of equal altitudes of stars was better suited to give accurate results than meridian astronomy*. We have reached this very conclusion by comparing the physical properties of the astrolabe and the transit instrument. But there is another reason, of a geometrical nature, which confirms this conclusion. With the method of equal altitudes, transits of stars can be observed all around a complete circle (almucantar) on the celestial sphere; and that is why the radius of the circle and its pole, which is the zenith of the station, are so well determined. Meridian observations provide different conditions, as the observations can only be made over 45° of zenith distance, that is along an arc which covers only one quarter of the circumference on the meridian; thus, the position of the pole of this arc, which defines the direction of the rotation axis of the transit instrument, is practically less accurately determined than that of the zenith of the astrolabe.

Even if it were perfect the meridian circle by itself could not conveniently provide for the " chain adjustment ", because such adjustment cannot be effected without referring, as an intermediate step, to an azimuth mark or a collimator. I know nothing more disappointing than the observation of a mark. I have often observed those of the Strasbourg Observatory which were set up very carefully by Winnecke. Even when at first sight they appeared to be stable, they suffered every now and then from sudden variations amounting frequently to one second of arc. If the mark is located not far from the instrument then its azimuth is not well defined. If it is far from the instrument its direction is

* S. C. Chandler, " The Almucantar ", *Ann. of Harvard Coll. Obs.*, **17**, 1887, 179–181.

" I think it can be successfully maintained that the almucantar system of observation constitutes a more simple and direct solution of the problem of determining the absolute time from the phenomena of diurnal motion, and consequently one more likely to be free from the systematic error, than that of the meridian transit." .... " As regards the adaptation of the instrument to purely astronomical purposes, one line of usefulness seems to be clearly marked out, in the application to the class of position measurements for which meridian instruments have heretofore been exclusively employed."

frequently deviated by lateral refractions. But in any case a terrestrial mark is far from being as reliable as the prism of the astrolabe for defining a direction of reference. Its stability cannot even be assured through the course of a night, from evening to morning, and far less during day time.

In my opinion, better results can be expected from a collimator than from a mark, because the collimator can be installed in the interior of the meridian room and can then be efficiently protected against variations of temperature, as well as its pillar and even the ground all around the pillar. That is why I have used two collimators, one to the east and the other to the west, with the transit instrument that I mentioned at the beginning of this lecture and of which I will now recall briefly the principle (Fig. 7). In front of the objective of a telescope

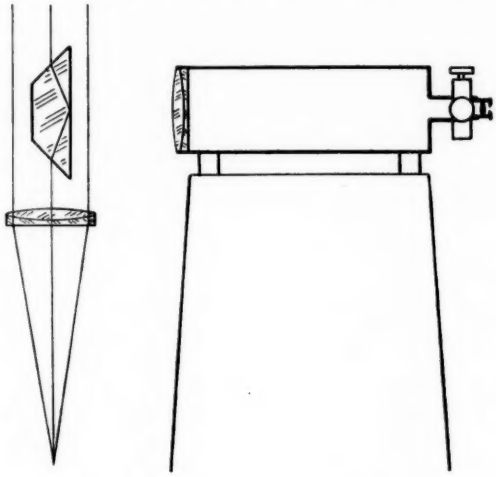

Fig. 7.

whose axis lies in the meridian plane, is mounted a reversing prism, which covers its surface with the exception of two segments which remain uncovered. In the field of the telescope two images of the star appear, which move in opposite directions. The two images coincide when the star transits the plane of the reflecting face, which differs but by a very small amount from the direction of the meridian plane. The position of the prism is then determined by auto-collimation, by means of the lateral collimator pointed towards its reflecting face. The readings made with this collimator provide the necessary correction for reducing all the transits to a same plane. The second collimator is used when the instrument is reversed. I will not mention the various operations which enable the horizontality of the collimator to be controlled by means of a mercury horizon and its azimuth to be controlled by the observation of fundamental stars. What I wish to stress is that the line of sight is much better defined by the prism than by the optical axis of the conventional meridian telescope. The major difficulties occurring in the meridian telescope are automatically eliminated, but indeed other problems arise which I am now endeavouring to overcome. If there is a noticeable difference in temperature between the interior and the exterior of the room, the reflected image of the

cross wires as seen in the collimator is unsteady. This is but a minor inconvenience which can be easily corrected. The most troublesome effect is caused by the position of the prism in front of the objective. If its temperature differs from that of the surrounding air even by a few tenths of a degree, it is enveloped by a layer of air about 1 cm thick within which there exists a marked temperature gradient. The part of the pencil of rays which crosses this layer becomes divergent if the prism is warmer than the air and convergent if it is cooler, and in both cases the image given by the free aperture is altered. If the air around the prism is stirred by means of a fan, this layer of air disappears and the image resumes its normal aspect. But if the fan is stopped, then this layer is at once formed again.

A similar effect is also produced in instruments in which metallic parts are placed across the path of the light. I have observed for instance, by a very sensitive interferometer method, that the bright extensions which surround the stellar images in a reflecting telescope are caused by the presence of the supports of the secondary mirror which, cooling off during the night by radiation, are surrounded by a layer of warmer air producing a refraction effect, and not a diffraction effect as is generally assumed. André Couder gets rid of this effect by covering the supports of the secondary mirror with sheets of polished aluminium.

The case of the reversing prism of my transit instrument cannot be treated so easily and I have had to adopt a more radical solution : the prism of the projected instrument will be placed in an atmosphere of helium, this gas having a refractivity ten times smaller than that of air and a conductivity six times higher. The idea is not a new one : Bernard Lyot had elaborated plans for a reflecting telescope of an aperture of 150 cm without a dome, to be installed at the Observatory of the Pic du Midi, the tube of which, sealed by a glass plate at its upper part, would have been filled with helium.

I have given these detailed explanations in order to recall, in a specific case, how different can be the actual properties of an instrument and its theoretical properties. When an inventor forgets this important truth, the actual use of the instrument soon reminds him of it. But let us come back to our subject and take up again the " chain adjustment ". Years will elapse before we know if this new instrument is as well adapted as the astrolabe for this particular purpose.

I will not wait any longer to answer objections raised by various authors about this chain programme, the legitimacy of which has been disputed. Their criticisms are based, in particular, on the closing errors, sometimes quite large, found for certain latitude stations equipped with zenith telescopes*. The mean value of the closing errors for the years 1956 and 1957, for the four stations of the International Latitude Service, was $-0''{\cdot}124$ between the evening group and the middle group and $-0''{\cdot}101$ between the middle group and the morning group. But the individual values show a very large scattering. The extreme annual means were $-0''{\cdot}345$ for Ukiah and $+0''{\cdot}162$ for Kitab. If these closing errors had the same value for all the stations they could be eliminated by correcting the aberration constant but they are very different from one station to the other. This dispersion can be assigned only to

* G. Cecchini, *Relazione sul attività del Servizio Internazionale delle Latitudine*, I.U.G.G. General Assembly, Toronto, 1957.

instrumental or to meteorological factors. I am myself convinced that the first occur much more frequently and are in general more harmful.

It may also occur that the local terrain or the presence of large buildings in the immediate vicinity of the instrument will give rise during the night to atmospheric turbulence which produces appreciable accidental refractions. Such cases are no doubt exceptional as the site of an observatory is as a general rule selected with full knowledge of these facts. But a fall in the temperature in the course of the night affects the level and the micrometer screw of the zenith telescope, and these effects contribute to the closing error of the chain programme.

The astrolabe does not have such disadvantages. Dr Guinot, who has determined the connections of our groups, has found for the first year of observation a very small closing error. He first smoothed the observations, as I have already stated for the group of January 22, in order to free them from individual or local errors. Then he computed the differences between consecutive groups observed *by the same observer in the course of the same night.* He started with group k and came back to the same group after a complete year. Table I gives the differences in time and latitude with the related standard deviations.

TABLE I

1956–57

Groups	Time unit : $0^{s}.001$		Latitude Unit· $0''.01$		n
j–k	+15·0	±4·1	−2·9	±3·1	5
k–l	+ 3·2	2·2	+0·5	4·0	12
l–a	− 8·0	1·7	+3·0	3·6	10
a–b	−10·0	2·5	−3·1	2·9	11
b–c	+23·0	1·7	+5·7	1·8	10
c–d	−12·1	1·7	−3·8	2·0	12
d–e	+ 3·0	1·7	+1·9	2·0	13
e–f	+ 0·5	1·1	−2·6	1·2	13
f–g	− 0·5	1·5	−7·3	1·6	14
g–h	−12·8	1·5	+7·4	2·5	13
h–i	+ 1·7	1·8	−4·9	1·4	15
i–j	− 1·6	1·5	+2·6	2·5	16
Closing error	+ 1·4	±7·1	−3·5	±8·7	

These results have been confirmed by those of the second year of observations which will end by July next.

Certain differences, mainly in right ascensions, reach surprisingly high values. In the course of the same night, groups b and c give clock-corrections differing by an amount of 23 milliseconds. But what is still more remarkable is the smallness of the closing errors *which are not significant.* We can therefore assume that the chain method of adjustment is permissible, and we can conclude that not only the astrolabe but also the atmosphere of Paris is very stable. If, contrary to my opinion, the closing errors observed elsewhere were not chiefly due to instrumental causes, we would then have to admit that, by bad fortune, these other stations had all been located in exceptionally unfavourable sites and that Paris enjoyed uniquely privileged conditions. Flattering though this last assumption may be for the pride of the French, I strongly refuse to believe in the poor quality of the other latitude stations and I persist in accusing the zenith telescopes, the control of which seems to me very difficult. By control I mean a permanent and absolute control such as that which is provided for the astrolabe,

at least twice per night, by the determination of the prism angle and not a mere testing of the instrument at long intervals.

Having conclusively established that the application of group corrections is permissible, Dr Guinot computes the corrections required to refer the determinations of time, latitude and zenith distance to a provisional system more consistent than that of the FK3.

TABLE II

	a	b	c	d	e	f	g	h	i	j	k	l
Time ($0^s.001$)	+0·1	−10·0	+12·9	+0·7	+3·6	+3·9	+3·3	−9·6	−8·0	−9·7	+5·1	+8·2
Latitude ($0''.01$)	+1·5	− 1·3	+ 4·7	+1·2	+3·6	+1·2	−5·8	+2·0	−2·1	0·0	−2·6	−1·8
Zen. Dist. ($0''.01$)	−7·3	+ 1·4	+ 2·4	+0·8	−7·4	+2·3	+1·8	+7·4	−3·2	+2·4	+2·9	−3·5

Fig. 8 represents the group corrections for time and latitude reduced to nearly the same scale, as an arc of 1 millisecond at the zenith in Paris is nearly equal to $0''.01$. It appears at first sight that the right ascensions of the FK3 are less homogeneous than the declinations. These differences may be partly

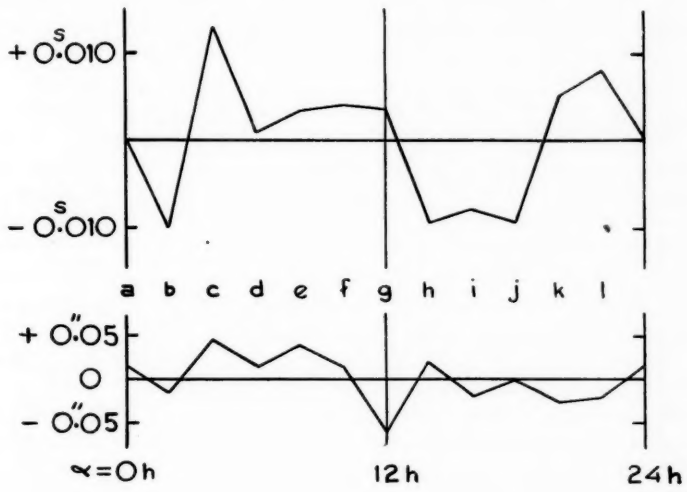

FIG. 8.

explained by the uncertainty of the proper motions, the computation of which depends to some extent upon meridian observations made before the introduction of the travelling wire micrometer. But that such deficiencies still exist in the FK3 is a proof of the inability of conventional methods to link together stars with very different right ascensions.

The analysis of group corrections discloses an irregularity of small amplitude in right ascension depending upon sin α. The corresponding error in the declinations of the form cos α is still smaller. The pole of the provisional system, which practically coincides with that of the FK3, therefore differs but little from the

true pole. But the systematic errors of the FK3 are much smaller than the local errors, which concern areas of an extent comparable to that of the constellations.

We shall know in a few years whether the corrections given in Table II are stable or whether they vary in course of time. In the latter case their variations will enable corrections to the constants both of precession and nutation to be derived. But we shall have to wait for 19 years until we can accurately sort out these two constants.

It is well known that the constant of aberration k can easily be deduced from the closing error in latitude, but the value obtained from the first year of observations, equal to 20″·48, has only a low weight. B. Guinot has shown that the time determinations could also be used for this purpose. Group d can be observed in Paris for about six months. If the conventional value of k is too small by 0″·04, as has been suggested, then the clock correction given by this group will show a sensible variation compared with the determinations made on normal groups at the same dates. It will at first decrease, by a total amount of 3 milliseconds, and will then increase by the same quantity. It seems possible to obtain evidence of this effect.

It is not surprising that the determination of the constants requires long series of observations but apart from this long-term programme the data given in Table II have immediate applications: (1) to the determination of the irregularities of Universal Time; (2) to the study of the variation of latitude; and (3) to the establishment of a catalogue of stars referred to the provisional system of the astrolabe.

The first of these applications has been studied by Dr Arbey, the two others by Dr Guinot*. My two associates have refrained from making any selection of the observational data. They have rejected no observations and have retained incomplete groups as well as those observed by personnel under training. But they have weighted the results according to their standard deviations by means of a suitably decreasing scale. They have then computed the means, including from 10 to 19 groups but more generally 13. All these means have nearly the same weight and they are shown by the points on the following figures derived from astrolabe observations grouped as just explained.

The diagram 9(a) was derived by Dr Arbey and represents the irregularities of the Universal Time TUO in Paris from 1956·5 to 1958·0.

These observations have been referred to the Uniform Time given by Dr Essen's atomic standard at the National Physical Laboratory which is at present the best tested of these standards. The time given by the crystal oscillators of Paris Observatory has been compared with Essen's standard through the intermediary of the MSF time signals. Dr and Mme Stoyko have shown that the definitive terrestrial time from 1955·5 to 1957·7 requires a correction of the form At^2 to compensate for the effect of a progressive increase in the length of the day†. The Universal Time TUO represented on Fig. 9(a) has been corrected for this term. It is then directly comparable with the curve in Fig. 9(b), which represents the difference TUO–TU2 computed by extrapolation by Dr Stoyko, in conformity with the instructions of Commission 31 of the International Astronomical Union for the rapid computation of the provisional time

* A memoir by B. Guinot is in the press, to be published in Bulletin Astronomique.

† A. et N. Stoyko, *C.R. Acad. Sci. Paris*, **246**, 235, 1958.

TU2*. Fig. 9(c) represents the difference of the ordinates of the curves 9(a) and 9(b), that is the provisional time TU2.

It is not possible at present to give an interpretation of this curve, as the final coordinates of the pole are not yet known, neither are the results obtained by other observatories which would enable the seasonal variations of the Earth's rotation to be computed. It can, however, be remarked that the rate of provisional TU2 is systematic and in particular an annual variation can be recognized. I have endeavoured to smooth out the TU2 irregularities and finally I have applied the following correction expressed in milliseconds:

$$\Delta = 6 \sin 2\pi(t+0{\cdot}15) + 2{\cdot}5 \sin 4\pi(t+0{\cdot}05) + 5(t-1957{\cdot}5)^2$$

t being the time expressed in years.

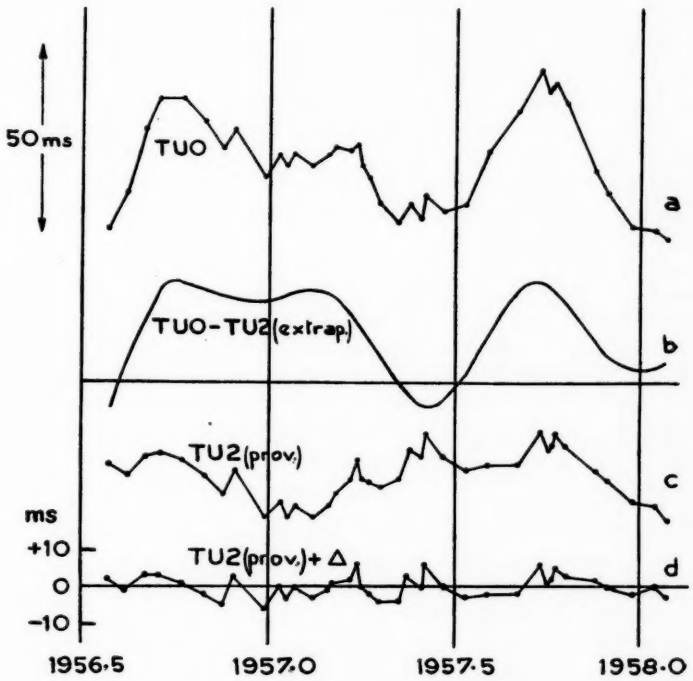

FIG. 9.

The residuals, shown on Fig. 9(d), show no systematic trend and their mean quadratic value is of 3·0 milliseconds. I wish to stress that the diagram includes 38 values for a period of 18 months, that is an average of 2 values per month.

What is the significance of the quantity Δ? The first two terms will possibly be justified when the final value of the difference TUO–TU2 is known, though it is possible that a portion of these terms should be attributed to errors in the group corrections and to the annual variation of the vertical. A slow variation would not affect in any way the closing error and therefore could not be detected.

* N. Stoyko, *Bull. Hor. du B.I.H.*, Série 4, **10**, 203, 1956.

On this particular point the question remains open. As for the third term of the expression of Δ, that is the term in t^2, it is to be added to the term identified by Dr and Mme Stoyko, the existence of which is confirmed by the present work. For the period covered by our observations, the gradual progressive rate of decrease of the terrestrial time is $0{\cdot}52\ t^2$ milliseconds, t being here expressed in months (instead of $0{\cdot}484\ t^2$).

It is not without interest to have been able to establish these empirical corrections, which make it possible to pass from the TUO time of Paris to the uniform time of the Essen's standard. When Ephemeris Time has been determined for the same period, the connection of the Essen standard to the conventional second of time will become easy. If we use the results of all the astrolabes now in operation throughout the world, including those to be delivered in the near future, it can be ascertained that this connection can be performed within 5 years with an accuracy of 10^{-9}.

But of all the problems dealt with in this lecture that of the time is indeed the most difficult. To obtain good time determination it is not enough to have available a good atomic standard and a good optical instrument. The chronograph, the time signal receivers, the propagation time of radio waves can each give rise to sources of errors or uncertainties. Great progress remains to be made in the transmission of time. In addition, with the degree of accuracy that we endeavour to obtain, the personal equations of the various observers are not negligible.

I have endeavoured to show the personal equations by plotting separately the diagram of Fig. 9(d), for the three principal observers, Dr Arbey, Dr Guinot and Mlle Débarbat. For certain periods, the same details appear on these curves as, for instance, the low values of April–May 1957, which very likely are real. But for other periods the curves do not agree so well. For instance, in January 1957, we find -7 milliseconds for the difference A–G while this difference is $+4$ milliseconds at the end of June 1957. In general, a systematic difference seems to exist between the observers, as for the whole of the observations of 1956–1957 the following values are obtained:

$$\text{A–G} = -2{\cdot}9 \text{ milliseconds}$$

$$\text{G–D} = -0{\cdot}7 \text{ milliseconds.}$$

But these figures should not be interpreted as invariable personal equations. Indeed these differences are not stable; they vary fortuitously. Nowadays the name of " noise " is given to functions characterized by such random variations. We could therefore speak of " personal noise " instead of " personal equation ".

It is very difficult to explain the persistency of such a marked difference as that of January 1957 between two well-trained observers. On one hand it is rather unlikely that the deflection of the vertical takes different values for odd and even days. On the other hand the observations are carried out in such a way that a systematic error in the appreciation of the coincidence of the two images affects only the radius of the circle defined by the position lines, but not the position of its centre. It must therefore be assumed that the observer does not time the coincidence in the same way on the east as on the west and that the error therein involved varies from week to week or from month to month. For the time being this effect remains without a satisfactory explanation. I have asked M. André Lallemand to study a photo-electric receiver designed

especially for the astrolabe in order to increase the accuracy of the observations and to obtain with confidence that of one millisecond.

The determination of the latitude offers less complexity than that of the determination of time, as it is derived straight away from the observations themselves after the group junctions are completed. Fig. 10 was derived by Dr Guinot and represents the latitude of the Paris astrolabe since the middle of the year 1956. Our groups have been selected in such a way that they will be observable without any change until the year 2000. Homogeneous data will then be available for the determination of the secular wandering of the pole which is not the case at the moment.

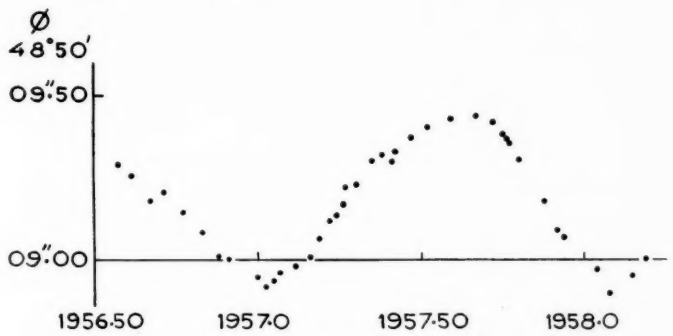

FIG. 10.

We have still to indicate what is the order of magnitude of the errors involved in both determinations. The average standard deviation of a group-observation is 4·3 milliseconds in time and of 0″·062 in latitude, including incomplete groups (the best determinations have given much smaller values, respectively 2·3 milliseconds and 0″·025). These figures refer to the consistency of the values within one group. If we compare the observations of groups between themselves by referring them to the smoothed curve, then the standard deviations take larger values, particularly for time, viz., 7·6 milliseconds and 0″·073.

I shall now present the results of B. Guinot relating to the establishment of a catalogue of fundamental stars. In 1955 he presented to the General Assembly of the International Astronomical Union a note on the error $\Delta\alpha_\delta$ of the FK3 derived from the results of the prototype astrolabe which was the only one in service at that time. Fig. 11 shows the similarity of the results obtained since then with the OPL astrolabe, although the observed stars are in general different in the two cases.

But B. Guinot has gone further. He has undertaken to determine with the astrolabe the coordinates of as many stars as possible, referred to the provisional system derived from the group corrections. He first computed the translation T which should be applied to each of the position lines to take into account:

(1) The internal smoothing of each group. It has been checked that these corrections were not affected by magnitude equations or by colour equations.

(2) The corrections of Table II.

He then derived from T the correction to the tabular coordinates of the star. If it has been observed at its two transits, east and west, and if T_E and T_W are

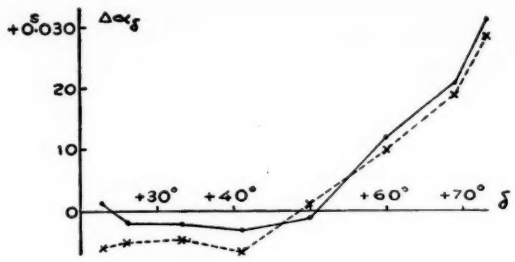

FIG. 11.—$\Delta\alpha_\delta$ (*Astrolabe—FK3*).
Continuous line: experimental astrolabe (1954).
Broken line: OPL astrolabe (1957).

the corresponding values of T, A is the azimuth of a transit reckoned from the south, positively towards the west, and η is the parallactic angle, then the corrections to apply to the coordinates of the catalogue are

$$\Delta\alpha \text{ (Astrolabe} - \text{FK3)} = \frac{T_E - T_W}{2|\sin A| \cos\phi}$$

$$\Delta\delta \text{ (Astrolabe} - \text{FK3)} = -\frac{T_E + T_W}{\cos\eta}.$$

In certain special cases, advantage can be taken of a single transit, for instance when the star is close to its maximum elongation. In that case it can be assumed that $\cos\eta = 0$ and the right ascension is then given by the following relation

$$\Delta\alpha \text{ (Astrolabe} - \text{FK3)} = -\frac{T + \Delta\delta \cos\eta}{\sin A \cos\phi}.$$

The same formula gives $\Delta\delta$ for stars close to the southern limit in declination as it then can be assumed that $\Delta\alpha \sin A = 0$.

B. Guinot compiled in that way a first catalogue of 115 stars of which 47 are known by their two coordinates, 56 by their right ascension only and 12 by their declination only. The Institut Géographique National has lent to Paris Observatory a second OPL astrolabe, and special groups of stars, different from that of the routine programme, are now being observed in order to extend this catalogue to 300 fundamental stars, that is, more than half of those of the FK3 and of its supplement contained in the Paris zone. Already, interesting remarks can be made.

As for the declination, the astrolabe catalogue and the FK3 are in good general agreement. The average of the differences is

$$\overline{\Delta\delta} \text{ (Astrolabe} - \text{FK3)} = -0''{\cdot}002$$

and is not significant. This is only a check of the adjustment. Fig. 12 shows the behaviour of $\Delta\delta_\alpha$ for stars comprised in the zone $+20°$ to $+30°$. Systematic differences are small but the statistics relate only to a limited number of stars. It is obvious that a constant error could affect the declinations of both catalogues.

In right ascension, the differences are larger and the distribution is more systematic. The chart in Fig. 13 gives a very expressive representation. Each star is there represented by a circle, whose diameter is proportional to the difference $\Delta\alpha$ (astrolabe – FK3), black when the difference is positive and open when it is negative. When the difference is smaller in absolute value than 5 milliseconds the circle is replaced by a cross. We notice at a first glance a

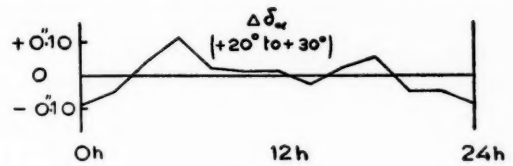

FIG. 12.

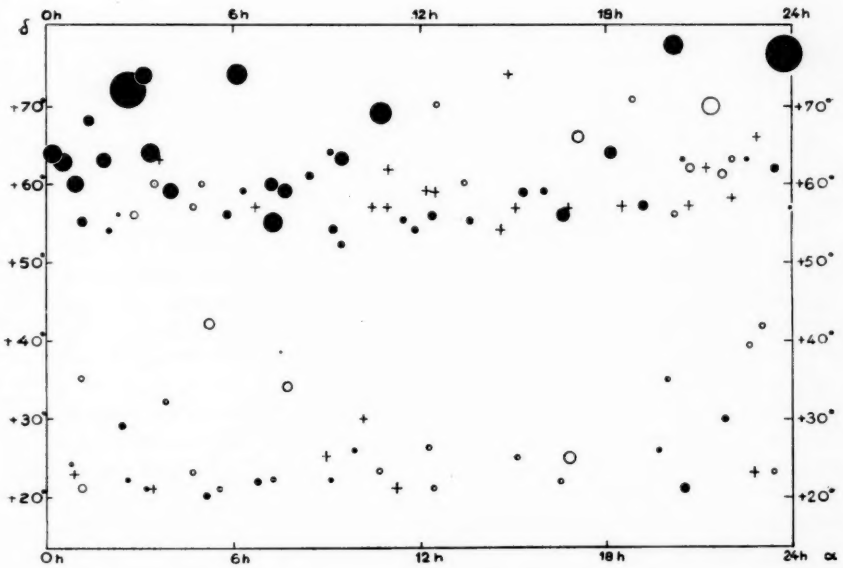

FIG. 13.

region of high declination, comprised between 23 hours and 11 hours, where the differences are very considerable and positive. It is indeed because of this anomaly that the difference $\Delta\alpha_\delta$ increases so rapidly beyond $+50°$. This illustrates the disadvantage of dividing $\Delta\alpha$ into two terms. The FK3 system is homogeneous between 11 hours and 23 hours. In this interval it would be sufficient to correct the individual positions to obtain a good catalogue with very small systematic errors for the coordinates as well as for the proper motions. On the contrary, to apply the correction $\Delta\alpha_\delta$ in this interval would be injurious. If the correction were applied it would be necessary to compensate for it by applying another correction $\Delta\alpha_\alpha$ of the opposite sign, this correction being a function both of α and of δ.

One may wonder why the astronomers have not hitherto realised the existence of these regional errors. The reason is very likely because it had become the practice to analyse the errors in an arbitrary way by means of a formula instead of considering very simply only $\Delta\alpha$ and $\Delta\delta$. In my opinion, it would be advantageous to abandon this method which can in no way be justified and which is merely confusing. For the compilation of the FK4, it would be wiser to consider rather the individual errors, the local errors, and the systematic errors, the latter mostly arising from errors in the adopted positions of the pole and of the equinox.

Fig. 14 represents the mean values of $\Delta\alpha \cos\delta$ between $+60°$ and $+75°$. There are two conspicuous discontinuities at about 11 hours and 23 hours. The representation of such residuals by trigonometrical series would of course be nonsensical. The conclusion is that the conversion of the FK3 to the FK4 cannot be derived from harmonic analysis.

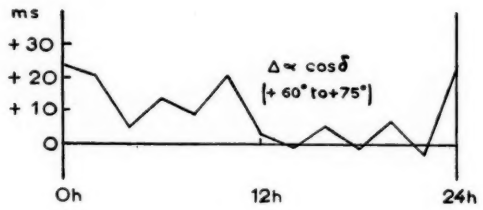

FIG. 14.

I will now make a last remark. In the case of meridian observations, the accuracy of which decreases from the equator as cos δ, the large discrepancies observed for high declinations can be allocated to random errors. But the accuracy of the measurements of right ascensions with the astrolabe depends only on sin A. It is the same at Paris for the zone from $+20°$ to $+22°$ as for the zone $+68°{\cdot}5$ to $+73°$. Hence if the $\Delta\alpha$ are much larger in the second zone than in the first, it is the catalogue that is responsible. The uncertainty of the group corrections could explain discrepancies of the order of 5 milliseconds but not of 20 milliseconds or more. The anomaly of the FK3 is found again, but to a lesser extent, in the N30 catalogue of H. R. Morgan. The discontinuities are smaller and less abrupt. However, positive corrections should still be applied to the right ascensions between 23 hours and 11 hours beyond $+50°$. But the first astrolabe catalogue has as yet too few stars to allow for further detailed discussion.

If I have taken the liberty of presenting so many provisional results, perhaps too many, it is not so much for their intrinsic value, for I do not ignore that they have to be confirmed*, as to emphasize the advantages of the method of equal altitude of stars. When this method is applied with the impersonal astrolabe, it provides for a permanent test, the zenith distance, which enables the quality of the results to be objectively evaluated. The several unknowns, namely time, latitude, corrections to the catalogue or to the fundamental constants, can be clearly separated from each other in a manner which cannot otherwise be

* All the reductions will soon be revised using the high precision ephemerides which Dr Fricke, Director of the Rechen-Institut, has kindly undertaken to compute for the stars of the Paris zone.

attained in meridian astronomy. Instead of amending the catalogue hour by hour, it enables large areas to be dealt with, which are easily linked together. The results take an expressive form and their discussion leaves hardly any obscurities. It also gives to the computer an impression of confidence which I have observed with all my associates. I am convinced that this impression is not fallacious and that favourable prospects are really opened in the difficult field of fundamental astronomy, which is by no means a dead subject.

A STUDY OF THE DETERMINATION OF SOLAR ATMOSPHERIC ABUNDANCES

D. Mugglestone

(Received 1958 May 1)

Summary

A study is made of the determination of solar atmospheric abundances from the observed intensities of faint Fraunhofer lines. The method of weighting functions, which utilizes the results of the observed limb-darkening, is considered in detail. An alternative method is proposed, the method of the Planckian gradient, which makes no recourse to limb-darkening observations and which is entirely dependent upon the physical characteristics of the solar atmospheric model considered.

Throughout the paper reference is made to the case of nitrogen (ionization potential = 14·54 volts) primarily to compare results obtained by the above two methods. Nine absorption lines are considered and the nitrogen abundance is determined from each of the nine lines. Appreciable discrepancies are found between the results obtained by the two methods. Theoretical considerations lead to the conclusion that in the case of nitrogen, and in general for all elements of high ionization potential, the method of weighting functions is quite unreliable and the Planckian gradient method should be used.

Three atmospheric models are considered, and, for nitrogen, the mean results obtained by the latter method are (on the basis $\log A_H = 12{\cdot}00$) Claas model : $\log A_N = 7{\cdot}71$, Vitense model : $\log A_N = 7{\cdot}81$, Swihart model : $\log A_N = 7{\cdot}93$ (cf. Hunaerts 9·02, Unsöld 8·61).

Introduction.—A method for the derivation of solar atmospheric abundances from observed faint Fraunhofer line intensities was proposed by Unsöld (**18**) in 1932 and later modified and improved by Minnaert (**10**). This method, that of weighting functions, has been used extensively for abundance determinations (e.g. Claas (**5**)). Here the information provided by the observed limb-darkening of the Sun is used and the method may be subject to certain limitations. It may be, for example, that the limb-darkening results, which are reliable only for the outer layers of the atmosphere, do not give adequate information concerning phenomena occurring in the deeper layers. The theoretical basis of the method of weighting functions is again considered in detail in Section 4.

An alternative method is proposed, here called the Planckian gradient method, which is determined entirely by the physical characteristics of the particular solar atmospheric model considered. This procedure makes no reference to the results of limb-darkening and is therefore free, in some degree, from the above limitations (Section 5).

The two methods are applied to the case of nitrogen, which, due to its high ionization potential, will provide appreciable absorption in the lower layers of the atmosphere, and the numerical results may then be compared. A theoretical comparison is also made in order to obtain a measure of the reliability of the two methods.

1. ***The solar atmosphere.***—The energy which is radiated from the surface of the solar atmosphere, together with its angular and spatial distribution, gives, at least in principle, complete information concerning the radiation from each elementary layer in the photosphere. Most of the radiation from the upper, cooler, layers will reach the surface of the photosphere; the radiation from the lower layers will however be modified by absorption in the intervening strata.

We consider a plane parallel atmosphere in local thermodynamic equilibrium, i.e. to each layer in the atmosphere we assign a local temperature T such that, for this temperature, Kirchoff's law is valid, i.e. $j_\nu/k_\nu = 4\pi B_\nu(T)$ at any frequency ν where k_ν and j_ν are the mass absorption and emission coefficients respectively and $B_\nu(T)$ is the Planckian function at temperature T. The emergent intensity of radiation in the continuum at an angle θ to the outward normal is given by

$$I_\nu^c(0,\theta) = \int_0^\infty B_\nu(T) e^{-\tau_\nu \sec\theta} \sec\theta \, d\tau_\nu, \tag{1.1}$$

where, in material of density ρ,

$$\tau_\nu = \int_0^x k_\nu \rho \, dx \tag{1.2}$$

expresses the transition from the linear depth x to the optical depth τ_ν in the continuum at frequency ν. Here $B_\nu(T)$ is the source function for the radiation.

In the case of the solar atmosphere the continuous absorption coefficient k_ν is almost entirely determined by the photodissociation of the negative hydrogen ion and by photo-ionization from discrete levels of the neutral hydrogen atom (bound–free transitions). In the present investigation for faint absorption lines it is assumed that the condition of local thermodynamic equilibrium is satisfied, i.e. the frequent interchange of energy between the absorption electrons and the free electrons ensures that the population of the energy states will be in accordance with Boltzmann's law, and scattering is unimportant. The formation of the Fraunhofer lines is then due to selective absorption followed by continuous absorption. If l_ν is the mass absorption coefficient for line absorption in frequency ν then the emergent intensity in the line, at an angle θ to the outward normal, is given by

$$I_\nu(0,\theta) = \int_0^\infty B_\nu(T) e^{-t_\nu \sec\theta} \sec\theta \, dt_\nu, \tag{1.3}$$

where

$$t_\nu = \int_0^x (k_\nu + l_\nu)\rho \, dx \tag{1.4}$$

is the optical depth in the line.

2. *Solar atmospheric models.*—Using equation (1.1) it is possible in principle to obtain the temperature distribution with optical depth for any wave-length from the observed limb-darkening of the Sun. Chalonge and Kourganoff (**4**) and Barbier (**2**) have made most careful studies of the limb-darkening observations and many models are based on these results.

For example, we may represent the Planckian function in the form

$$B_\nu(\tau_\nu) = a_\nu + b_\nu \tau_\nu + c_\nu \tau_\nu^2, \tag{2.1}$$

and derive the values of the constants a_ν, b_ν and c_ν in accordance with the method outlined in Section 4.1. For a given wave-length the Planckian function $B_\nu(\tau_\nu)$

is a function of T only and hence equation (2.1), a quadratic in τ_ν, gives the solution $\tau_\nu = \tau_\nu(T)$.

Since we may obtain the relationship $\tau_\nu = \tau_\nu(T)$ for any wave-length, we are able to compare the optical depths in the several wave-lengths corresponding to a single value of T, i.e. to a single layer in the atmosphere. Since $\tau_{\nu,1}/\tau_{\nu,2} = k_{\nu,1}/k_{\nu,2}$ we are also able to determine the ratio of absorption coefficients in several wave-lengths. As we are able to correlate the optical depths in the various colours we may select one wave-length as typical ($\lambda = 5000$ A) and express the temperature variation in the photosphere in terms of this optical depth τ_0 (see Section 4.2).

Since it will be of interest, in the abundance determinations which follow, to examine the sensitivity of the results to the model atmosphere chosen, three models will be used with slightly different characteristics (especially surface temperature).

(*a*) *Model adopted by Claas.*—The model adopted by Claas (**5**), which we will refer to hereafter as the "Claas model", is based on the limb-darkening calculations of Barbier (**2**). With regard to the structure of the atmosphere only two assumptions are made, i.e. the layers are in radiative and local thermodynamic equilibrium. The calculations of the gas pressure P_g and the electron pressure P_e were carried out in accordance with the method developed by Barbier (**2**) except that a fourth approximation based upon Barbier's third approximation for P_g and P_e was made.

The model is defined by Claas from the surface down to optical depth $\tau_0 = 2{\cdot}2$; this was found to be sufficient for the application of the method of the weighting function (Section 4), but quite insufficient for the method of the Planckian gradient (Section 5). Below this depth the relationship $\tau_0 = \tau_0(T)$ derived from limb-darkening observations is rather uncertain. Lyttkens (**9**) has extended the model to greater optical depth using the relationship

$$T^4 = \tfrac{3}{4} T_e^4 [\tau + q(\tau)], \tag{2.2}$$

where T_e is the effective temperature of the Sun ($T_e = 5713$ °K) and τ is the Rosseland mean optical depth. The function $q(\tau)$ varies between $1/\sqrt{3}$ at $\tau = 0{\cdot}0$ and $0{\cdot}710$ at infinitely large optical depth, for the present model the value $0{\cdot}710$ is adopted for the whole range below $\tau_0 = 2{\cdot}2$. Lyttkens further calculated the $P_g = P_g(\tau)$ relationship utilizing the tables of Strömgren (**15**). The electron pressure can now be found directly from the same tables (Table 8 in Strömgren's publication).

By conversion to the standard optical depth τ_0 in wave-length $\lambda = 5000$ A by the relationship

$$\tau_0 = \int_0^\tau \frac{k_0}{\bar{k}}\, d\tau \tag{2.3}$$

utilizing tables of $k_\nu/\bar{k} = k_\nu/\bar{k}(\theta, P_e)$ kindly supplied by Dr B. Strömgren (unpublished), and by numerical interpolation in the results of Lyttkens, the Claas model was extended in regular numerical interval in τ_0 to the depth $\tau_0 = 4{\cdot}2$.

(*b*) *Vitense model* (**20**).—The method adopted for the determination of the $\tau_0 = \tau_0(T)$ relationship is essentially the same as the method used in the foregoing model. Here however the limb-darkening results of Chalonge and Kourganoff were preferred to those of Barbier and corrections were made to conform to the more recent values of the radiation constants in the Planck function. Vitense (**20**) however took into account that the measured values of $I_\nu^c(0, \theta)$ are available

only for $0{\cdot}3 \leqslant \cos\theta \leqslant 1{\cdot}0$, and therefore the derived function $B_\nu(\tau_\nu)$ is reliable only in the corresponding region of τ_ν, i.e. approximately $\tau_\nu > 0{\cdot}2$. The temperature stratification of the uppermost layers, $0 \leqslant \tau_\nu \leqslant 0{\cdot}2$, was found from the limb-darkening variations of the residual intensities of the strong Balmer lines of hydrogen and the strong lines of iron. This resulted in a much lower value of the surface temperature, viz. $T_0 = 3800 \pm 100$ °K, compared with that used by Claas ($T_0 = 4900$ °K). Using this value of the surface temperature, the intermediate temperatures, i.e. $0 \leqslant \tau_\nu \leqslant 0{\cdot}2$, were found by interpolation.

In the model used in this investigation (Model (ii) in Vitense's publication) a slightly steeper temperature gradient, found by D. Labs, was adopted, resulting in a slightly higher surface temperature ($T_0 = 4006$ °K). It was found however that the uncertainties in the temperature and pressure in the superficial layers do not influence the distribution in the region $\tau_\nu > 0{\cdot}2$.

Again the model derived is defined only from the surface to optical depth $\tau_0 = 2{\cdot}0$. The results of Lyttkens were again used to extend the model to much lower layers, the fitting being made at $\log P_g = 5{\cdot}10$ for $\theta = 0{\cdot}706$ (a small error may have been introduced here).

(*c*) *Swihart model.*—Swihart (**16**) produced, initially, a standard model of the solar atmosphere in which the observed integrated flux of radiation is reproduced by the assumed $\tau = \tau(T)$ relationship.

The flux $\mathscr{F}$ at the surface is obtained by integrating the surface intensity over all solid angles, i.e.

$$\mathscr{F} = \int I^c(0,\theta)\cos\theta\, d\omega = 2\pi \int_0^{\pi/2} I^c(0,\theta)\cos\theta \sin\theta\, d\theta = \pi F. \tag{2.4}$$

Introducing equation (1.1) we have for the monochromatic flux

$$F_\nu = 2\int_0^\infty B_\nu(T)\, d\tau_\nu \int_0^{\pi/2} \mathrm{e}^{-\tau_\nu \sec\theta} \sin\theta\, d\theta. \tag{2.5}$$

If we now introduce the variable

$$\sec\theta = y, \qquad \text{i.e.} \quad \sin\theta\, d\theta = y^{-2}\, dy,$$

and the exponential integral function

$$E_n(x) = \int_1^\infty \frac{\mathrm{e}^{-xy}}{y^n}\, dy, \tag{2.6}$$

equation (2.5) becomes

$$F_\nu = 2\int_0^\infty B_\nu(T) E_2(\tau_\nu)\, d\tau_\nu. \tag{2.7}$$

More generally for the flux at any depth τ_ν, where there is an inward flowing contribution from the layers above τ_ν, we have

$$F_\nu(\tau_\nu) = 2\int_{\tau_\nu}^\infty B_\nu(T) E_2(t_\nu - \tau_\nu)\, dt_\nu - 2\int_0^{\tau_\nu} B_\nu(T) E_2(\tau_\nu - t_\nu)\, dt_\nu, \tag{2.8}$$

and the monochromatic flux may then be determined once the $\tau = \tau(T)$ relationship is specified. The integrated flux is then found from the expression

$$F(\tau_\nu) = \int_0^\infty F_\nu(\tau_\nu)\, d\nu, \tag{2.9}$$

and if the assumed $\tau = \tau(T)$ relationship is incorrect then the derived flux will also be incorrect.

If the $\tau = \tau(T)$ relationship is written in the form

$$T^4 = \tfrac{3}{4} T_e^4 [a + b\tau + cE_2(\tau) + dE_3(\tau)], \qquad (2.10)$$

(cf. equation 2.2) the coefficients a, b, c, and d may be found from the condition that the observed flux is reproduced by equation (2.8).

Swihart first constructed a standard model, a plane parallel atmosphere in radiative and mechanical equilibrium, by the above procedure, taking into account the uncertain blanketing effect by increasing the flux at all depths by approximately 10 per cent. He later (**17**) modified this model by introducing an assumed, plausible, convective transport in the lower layers (~1 per cent at $\tau = 1{\cdot}5$ increasing to 40 per cent at $\tau = 3{\cdot}0$). This had the effect of reproducing the desired flux rather more accurately than the standard model but increased

TABLE I

Solar atmospheric models

	Claas Model			Vitense Model			Swihart Model			
τ_0	θ	Log P_g	Log P_e	θ	Log P_g	Log P_e	τ	θ	Log P_g	Log P_e
0·01	1·022	3·92	0·09	1·072	3·95	0·10	0·01	1·098	3·93	−0·03
0·02	1·015	4·07	0·24	1·046	4·15	0·32	0·02	1·088	4·09	0·12
0·03	1·011	4·16	0·31	1·035	4·23	0·41	0·03	1·078	4·19	0·22
0·04	1·007	4·23	0·38	1·029	4·30	0·48	0·04	1·070	4·25	0·28
0·05	1·003	4·28	0·42	1·022	4·36	0·53	0·05	1·062	4·31	0·34
0·06	0·999	4·33	0·47	1·015		0·57	0·06	1·054	4·35	0·39
0·07				1·010	4·43	0·60	0·07	1·048	4·38	0·43
0·08	0·990	4·39	0·54	1·004		0·64	0·08	1·040	4·42	0·47
0·09				0·999		0·68	0·09	1·034	4·44	0·50
0·10	0·980	4·45	0·61	0·995	4·53	0·71	0·10	1·028	4·47	0·53
0·20	0·942	4·61	0·81	0·949	4·68	0·90	0·20	0·980	4·63	0·75
0·30	0·910	4·71	0·98	0·915	4·78	1·05	0·30	0·946	4·73	0·89
0·40	0·884	4·78	1·11	0·887	4·86	1·17	0·40	0·916	4·80	1·02
0·50	0·860	4·82	1·24	0·864	4·91	1·31	0·50	0·894	4·85	1·12
0·60	0·840	4·86	1·37	0·845	4·94	1·43	0·60	0·874	4·89	1·22
0·70				0·829	4·97	1·55	0·70	0·854	4·92	1·32
0·80	0·808	4·91	1·58	0·813	4·99	1·65	0·80	0·838	4·95	1·42
0·90				0·799	5·01	1·70	0·90	0·824	4·97	1·51
1·00	0·781	4·94	1·77	0·787	5·02	1·78	1·00	0·810	4·99	1·60
1·20	0·757	4·96	1·94	0·765	5·05	1·93	1·20	0·784	5·02	1·77
1·40	0·736	4·97	2·09	0·746	5·07	2·06	1·40	0·760	5·04	1·94
1·60	0·720	4·99	2·22	0·729		2·17	1·60	0·740	5·05	2·08
1·80	0·706	5·00	2·32	0·715	5·10	2·27	1·80	0·724	5·06	2·20
2·00	0·694	5·01	2·41	*0·702	5·10	2·40	2·00	0·710	5·07	2·30
2·20	*0·684	5·01	2·49	0·693	5·11	2·47	2·20	0·697	5·08	2·40
2·40	0·674	5·02	2·56	0·683	5·12	2·55	2·40	0·687	5·08	2·48
2·60	0·665	5·03	2·63	0·674	5·12	2·61	2·60	0·679	5·09	2·54
2·80	0·658	5·03	2·68	0·665	5·13	2·68	2·80	0·672	5·09	2·59
3·00	0·651	5·04	2·74	0·658	5·13	2·74	3·00	0·666	5·10	2·64
3·20	0·644	5·04	2·80	0·651	5·14	2·80	3·20	0·662	5·10	2·67
3·40	0·637	5·04	2·85	0·644	5·14	2·85	3·40	0·659	5·11	2·70
3·60	0·631	5·05	2·90	0·637	5·14	2·90	3·60	0·656	5·11	2·72
3·80	0·624	5·05	2·95	0·631	5·15	2·95	3·80	0·653	5·11	2·74
4·00	0·619	5·05	2·99	0·624	5·15	2·99	4·00	0·650	5·12	2·77
4·20	0·613	5·05	3·03				5·00	0·642	5·13	2·83
							6·00	0·632	5·14	2·92
							7·00	0·620	5·15	3·00

* Extension of model to greater depth by Lyttkens.

the divergence of the predicted limb-darkening results when compared with the observed limb-darkening. Swihart concluded that the actual convective transport could not be much larger than assumed in this model.

The model was recomputed with regular numerical interval in τ using the values of a, b, c and d obtained by Swihart. Tables of the first exponential integral function are available and functions of higher degree were calculated from the relationship

$$nE_{n+1}(\tau)=e^{-\tau}-\tau E_n(\tau).$$

The complete models are given in Table I.

3. *The nitrogen absorption lines.*—The electron configuration of the ground state of the nitrogen atom is $1s^2 2s^2 2p^3$. The electrons in addition to the closed shells, i.e. the equivalent electrons $2p^3$, give rise to possible total spin quantum numbers $S=\frac{1}{2}, \frac{3}{2}$ and therefore to multiplicities, $(2S+1)$, of doublets and quartets. By the Pauli exclusion principle the three equivalent electrons may give rise to the terms ^{2}P, ^{2}D, and ^{4}S only, and, as the term with the greatest multiplicity designates the lowest energy state, the ground state of the nitrogen atom is designated $1s^2 2s^2 2p^3\,{}^4S^0_{3/2}$. Here the subscript refers to the value of the inner quantum number J, and the superscript "o" refers to the fact that the term is odd, i.e. $\sum l_i$ is odd where the summation is extended over all the electrons of the atom. Excited states are obtained when one of the $2p$ electrons moves to a higher orbit; in addition a ^{4}P term is indicated where one electron moves from the $2s$ to the $2p$ orbit. The electron configurations, term designations, and energy levels of all the states of nitrogen are available in the publication *Atomic Energy Levels* (**13**) and all the relevant information is taken from this source.

Transitions between two atomic levels, producing a spectral line, are subject to the selection rules (for dipole radiation): total angular momentum $\Delta J=0, \pm 1$ with the restriction $J=0 \nrightarrow J=0$ forbidden; spin angular momentum $\Delta S=0$, i.e. only terms of equal multiplicity will combine; orbital angular momentum $\Delta L=0, \pm 1$. In addition for the electron making the quantum transition $\Delta l=\pm 1$, this may be interpreted as $\Delta(\sum l_i)=\pm 1$, i.e. even terms will combine with odd terms only, and odd terms with even terms only. Table II gives the possible multiplet transitions for nitrogen, together with their component lines, within the wave-length range of the present investigation.

The identification of the lines is based upon measurements made by Professor Edlén and supplied to the author by Dr B. Strömgren. The strongest Fraunhofer line, $\lambda=8680{\cdot}24$ A, is seen to have a considerable wave-length discrepancy when compared with the solar spectrum ($-0{\cdot}14$ A), thus placing the identification in some doubt. It will be seen later, however, that the omission of this line has no effect upon the abundance determinations. The excitation potentials refer to the lower level of the transition and have been corrected to correspond to an ionization potential of hydrogen of 13·595 volts (i.e. by multiplying the level by the factor 0·00012395).

The oscillator strengths f of the transitions in question can be shown, by the well-known analysis of Einstein, to be related to the strength of the spectral line S_1 by the equation

$$f=\frac{8}{3}\frac{\pi^2 mc}{he^2}\cdot\frac{1}{g_i\lambda}\cdot S_1 \qquad (3.1)$$

where m, c, e, and h have their usual significance, and g_i is the statistical weight

TABLE II

Nitrogen I

Ionization potential 14·54 volts

Config.	Desig.	J	Level cm^{-1}	Config.	Desig.	J	Level cm^{-1}
$2s^22p^3$	$2p^3\ ^4S^0$	$1\frac{1}{2}$	0	$2s^22p^2(^3P)3p$	$3p\ ^2S^0$	$\frac{1}{2}$	93582·3
$2s^22p^3$	$2p^3\ ^2D^0$	$2\frac{1}{2}$	19223	$2s^22p^2(^3P)3p$	$3p\ ^4D^0$	$\frac{1}{2}$	94772·2
		$1\frac{1}{2}$	19231			$1\frac{1}{2}$	94794·8
$2s^22p^3$	$2p^3\ ^2P^0$	$1\frac{1}{2}$	28840			$2\frac{1}{2}$	94832·1
		$\frac{1}{2}$				$3\frac{1}{2}$	94883·1
$2s^22p^2(^3P)3s$	$3s\ ^4P$	$\frac{1}{2}$	83285·5	$2s^22p^2(^3P)3p$	$3p\ ^4P^0$	$\frac{1}{2}$	95476·5
		$1\frac{1}{2}$	83319·3			$1\frac{1}{2}$	95494·9
		$2\frac{1}{2}$	83366·0			$2\frac{1}{2}$	95533·2
$2s^22p^2(^3P)3s$	$3s\ ^2P$	$\frac{1}{2}$	86131·4	$2s^22p^2(^3P)3p$	$3p\ ^4S^0$	$1\frac{1}{2}$	96751·7
		$1\frac{1}{2}$	86223·2	$2s^22p^2(^3P)3p$	$3p\ ^2D^0$	$1\frac{1}{2}$	96788·2
$2s2p^4$	$2p^4\ ^4P$	$2\frac{1}{2}$	88109·5			$2\frac{1}{2}$	96864·2
		$1\frac{1}{2}$	88153·4	$2s^22p^2(^3P)3p$	$3p\ ^2P^0$	$\frac{1}{2}$	97770·1
		$\frac{1}{2}$	88173·0			$1\frac{1}{2}$	97805·8
				N II($^3P^0$)	Limit	...	117345

Absorption lines

Multiplet Desig.	ΔJ	Laboratory Wave-length λ(A)	Laboratory Excit. Pot. (Volts)	Sun Sun − Lab. $\Delta\lambda$	Sun Identification
$3s^4P$–$3p^4S^0$	$\frac{1}{2}$–$1\frac{1}{2}$	7423·63	10·32	−0·12	Si Masked
	$1\frac{1}{2}$–$1\frac{1}{2}$	*7442·28*	10·33	−0·05	*Nitrogen*
	$2\frac{1}{2}$–$1\frac{1}{2}$	*7468·29*	10·33	−0·02	*Nitrogen*
$3s^4P$–$3p^4P^0$	$1\frac{1}{2}$–$2\frac{1}{2}$	8184·80	10·33	−0·02	Atmos. N
	$\frac{1}{2}$–$1\frac{1}{2}$	8187·95	10·32	−0·10	Atmos. N Masked
	$\frac{1}{2}$– $\frac{1}{2}$	8200·31	10·32	−0·32	Atmos. N
	$1\frac{1}{2}$–$1\frac{1}{2}$	8210·64	10·33	0·32	Atmos. N
	$2\frac{1}{2}$–$2\frac{1}{2}$	*8216·28*	10·33	0·02	*Nitrogen*
	$1\frac{1}{2}$– $\frac{1}{2}$	8223·07	10·33	−0·19	Atmos. N
	$2\frac{1}{2}$–$1\frac{1}{2}$	8242·34	10·33	0·02	Atmos. N
$3s^2P$–$3p^2P^0$	$\frac{1}{2}$–$1\frac{1}{2}$	8567·74	10·67	0·04	Fe
	$\frac{1}{2}$– $\frac{1}{2}$	8594·01	10·67		Absent
	$1\frac{1}{2}$–$1\frac{1}{2}$	*8629·24*	10·68	−0·08	*Nitrogen*
	$1\frac{1}{2}$– $\frac{1}{2}$	8655·88	10·68	0·17	Blended. Wing Ca
$3s^4P$–$3p^4D^0$	$2\frac{1}{2}$–$3\frac{1}{2}$	*8680·24*	10·33	−0·14	*Nitrogen*
	$1\frac{1}{2}$–$2\frac{1}{2}$	*8683·38*	10·33	0·00	*Nitrogen*
	$\frac{1}{2}$–$1\frac{1}{2}$	8686·13	10·32	0·24	Nitrogen Masked
	$\frac{1}{2}$– $\frac{1}{2}$	*8703·24*	10·32	−0·09	*Nitrogen*
	$1\frac{1}{2}$–$1\frac{1}{2}$	*8711·69*	10·33	−0·02	*Nitrogen*
	$2\frac{1}{2}$–$2\frac{1}{2}$	*8718·82*	10·33	−0·06	*Nitrogen*
	$1\frac{1}{2}$– $\frac{1}{2}$	8728·88	10·33	−0·28	Fe
	$2\frac{1}{2}$–$1\frac{1}{2}$	8747·35	10·33	0·09	Fe

of the lower level concerned in the transition. The statistical weight is equal to the degree of degeneracy, $(2J+1)$ of the level in question. Introducing the numerical constants in equation (3.1), expressing the wave-length λ in Angström units and S_1 in atomic units ($a_0^2e^2$, where a_0 is the radius of the first Bohr orbit) we have

$$f = \frac{3{\cdot}04 \times 10^2 S_1}{g_i \lambda}. \tag{3.2}$$

The line strengths S_1 may be expressed in the following form:

$$S_1 = S(M)S(L)\sigma^2, \tag{3.3}$$

where $S(M)$ is a factor which depends upon the particular multiplet concerned in the transition and $S(L)$ is a factor which depends upon the particular line of the multiplet, σ^2 is a function of the radial wave functions of the initial and final states of the active electron and upon the greater of the two azimuthal quantum numbers. $S(M)$ may be found from tables in two papers by Goldberg, the first (**6**) giving the relative strength of the multiplet and the second (**7**) a factor for the conversion of relative strengths to absolute strengths. $S(L)$ is obtained from Russell (**14**) where the line strength of a particular transition is expressed as a fraction of the sum of line strengths comprising the multiplet. An approximate evaluation of σ^2 has been made by Bates and Damgaard (**3**) for a large number of transitions in light elements and it is found that the value of σ^2 is the same for all multiplets of the $3s$–$3p$ transitions which are of interest in the present investigation. The oscillator strengths may therefore be calculated directly from equation (3.2).

The equivalent width W_λ of a spectral line is by definition the width of a perfectly black line, i.e. of rectangular profile, which, in the same region of the spectrum as the line itself, would absorb the same amount of energy from the continuum as does the spectral line, i.e.

$$W_\lambda = \int_{-\infty}^{+\infty} \frac{\Delta I_\nu}{I_\nu^c} d\lambda. \tag{3.4}$$

The nine nitrogen lines identified in Table II are measurable in the *Utrecht Photometric Atlas* (**11**). The nine lines, however, are faint and difficult to measure with accuracy (Table III).

TABLE III

Atomic parameters and equivalent widths

λ (A)	Transition $3s$–$3p$	$S(L)$	$S(M)$	a	σ^2	S_1	g_i	f	W_λ (mA)
7442·28	$^4P_{3/2}$–$^4S^0_{3/2}$	0·333	$2a$	2	9·76	13·00	4	0·133	3
7468·29	$^4P_{5/2}$–$^4S^0_{3/2}$	0·500	$2a$	2	9·76	19·52	6	0·132	3·5
8216·28	$^4P_{5/2}$–$^4P^0_{5/2}$	0·350	$6a$	2	9·76	40·99	6	0·253	6
8629·24	$^2P_{3/2}$–$^2P^0_{3/2}$	0·556	$3a$	2	9·76	32·56	4	0·287	4
8680·24	$^4P_{5/2}$–$^4D^0_{7/2}$	0·400	$10a$	2	9·76	78·08	6	0·456	17
8683·38	$^4P_{3/2}$–$^4D^0_{5/2}$	0·210	$10a$	2	9·76	40·99	4	0·359	7
8703·24	$^4P_{1/2}$–$^4D^0_{1/2}$	0·083	$10a$	2	9·76	16·20	2	0·284	5
8711·69	$^4P_{3/2}$–$^4D^0_{3/2}$	0·107	$10a$	2	9·76	20·89	4	0·182	4
8718·82	$^4P_{5/2}$–$^4D^0_{5/2}$	0·090	$10a$	2	9·76	17·57	6	0·102	4

4. *The method of weighting functions.*—We wish, initially, to consider the well-known method of weighting functions for the determination of solar atmospheric abundances from weak Fraunhofer lines. The relationship between the intensity of an absorption line and the structure of the solar atmosphere is simpler in the case of weak absorption lines than in the case of strong lines. For any given solar model we may assign a weight $g_\nu(\tau)$ to each elementary layer of the atmosphere which expresses the contribution of that layer to the emitted radiation, in any wave-length, either in the continuum or in the absorption line. For a faint line in pure absorption we have therefore

$$\frac{\Delta I_\nu}{I_\nu^c(0,\theta)} = \frac{I_\nu^c(0,\theta) - I_\nu(0,\theta)}{I_\nu^c(0,\theta)} = \int_0^\infty g_\nu(\tau)\, d\tau. \tag{4.1}$$

In his development of the theory of weighting functions Minnaert (**10**) obtained the form of the weighting function essentially in the following way.

The intensity in the continuum, at the centre of the solar disk, is given by (cf. equation (1.1))

$$I_\nu^c(0,0) = \int_0^\infty B_\nu(\tau) e^{-\tau_\nu}\, d\tau_\nu, \tag{4.2}$$

and the intensity in the line is

$$I_\nu(0,0) = \int_0^\infty B_\nu(\tau) e^{-t_\nu}\, dt_\nu. \tag{4.3}$$

The optical depths τ_ν and t_ν are related by

$$\frac{dt_\nu}{d\tau_\nu} = \frac{k_\nu + l_\nu}{k_\nu}, \quad \text{where } l_\nu \ll k_\nu, \tag{4.4}$$

i.e.

$$t_\nu = \tau_\nu + \int_0^{\tau_\nu} \frac{l_\nu}{k_\nu}\, d\tau_\nu. \tag{4.5}$$

We may write this in the form

$$t_\nu = \tau_\nu + \tau_l \quad \text{where} \quad \tau_l = \int_0^{\tau_\nu} \frac{l_\nu}{k_\nu}\, d\tau_\nu. \tag{4.6}$$

Equation (4.3) then becomes

$$\begin{aligned} I_\nu(0,0) &= \int_0^\infty B_\nu(\tau) e^{-(\tau_\nu+\tau_l)} \left(1 + \frac{l_\nu}{k_\nu}\right) d\tau_\nu \\ &= \int_0^\infty B_\nu(\tau) e^{-\tau_\nu}(1-\tau_l) \left(1 + \frac{l_\nu}{k_\nu}\right) d\tau_\nu \\ &\doteq \int_0^\infty B_\nu(\tau) e^{-\tau_\nu}\, d\tau_\nu - \int_0^\infty B_\nu(\tau) e^{-\tau_\nu} \left(\tau_l - \frac{l_\nu}{k_\nu}\right) d\tau_\nu, \end{aligned}$$

to the first order. The intensity dip in the continuum is therefore

$$\Delta I_\nu = I_\nu^c(0,0) - I_\nu(0,0) = \int_0^\infty B_\nu(\tau) e^{-\tau_\nu} \tau_l\, d\tau_\nu - \int_0^\infty B_\nu(\tau) e^{-\tau_\nu} \frac{l_\nu}{k_\nu}\, d\tau_\nu, \tag{4.7}$$

and transforming this equation by use of the relationship

$$\int_0^\infty y(\tau) z(\tau)\, d\tau = \int_0^\infty dz \int_\tau^\infty y\, d\tau,$$

we have

$$\begin{aligned} \Delta I_\nu &= \int_0^\infty d\tau_l \int_{\tau_\nu}^\infty B_\nu(\tau) e^{-\tau_\nu}\, d\tau_\nu - \int_0^\infty B_\nu(\tau) e^{-\tau_\nu}\, d\tau_l \\ &= \int_0^\infty \left[\int_{\tau_\nu}^\infty B_\nu(\tau) e^{-\tau_\nu}\, d\tau_\nu - B_\nu(\tau) e^{-\tau_\nu} \right] d\tau_l, \end{aligned} \tag{4.8}$$

an equation which was also obtained by Unsöld (**18**). Expanding the first term of equation (4.8) we have

$$\int_{\tau_\nu}^{\infty} B_\nu(\tau)e^{-\tau_\nu}d\tau_\nu = -\int_{\tau_\nu}^{\infty} B_\nu(\tau)d(e^{-\tau_\nu})$$
$$= -\left|B_\nu(\tau)e^{-\tau_\nu}\right|_{\tau_\nu}^{\infty} - \left|\frac{dB_\nu}{d\tau_\nu}e^{-\tau_\nu}\right|_{\tau_\nu}^{\infty} + \int_{\tau_\nu}^{\infty}\frac{d^2B_\nu}{d\tau_\nu^2}e^{-\tau_\nu}d\tau_\nu$$
$$= \left[B_\nu(\tau) + \frac{dB_\nu}{d\tau_\nu} + \frac{d^2B_\nu}{d\tau_\nu^2} + \ldots\right]e^{-\tau_\nu}.$$

Equation (4.8) then becomes

$$\Delta I_\nu = \int_0^{\infty}\left[\frac{dB_\nu}{d\tau_\nu} + \frac{d^2B_\nu}{d\tau_\nu^2} + \ldots\right]e^{-\tau_\nu}d\tau_l. \tag{4.9}$$

Similarly the intensity in the continuum is given by

$$I_\nu^c(0,0) = \int_0^{\infty} B_\nu(\tau)e^{-\tau_\nu}d\tau_\nu = -\int_0^{\infty} B_\nu(\tau)d(e^{-\tau_\nu})$$
$$= \left[B_\nu + \frac{dB_\nu}{d\tau_\nu} + \frac{d^2B_\nu}{d\tau_\nu^2} + \ldots\right]_{\tau_\nu=0}, \tag{4.10}$$

i.e.

$$\frac{\Delta I_\nu}{I_\nu^c(0,0)} = \frac{\int_0^{\infty}[B_\nu' + B_\nu'' + B_\nu''' + \ldots]e^{-\tau_\nu}d\tau_l}{[B_\nu + B_\nu' + B_\nu'' + \ldots]_{\tau_\nu=0}}. \tag{4.11}$$

Unsöld indicated how this integral may be evaluated assuming the Planck function to be an approximately linear function of optical depth. Minnaert ((**10**), note also (**12**)) improved upon this and considered the form of the Planck function as a power series, i.e.

$$B_\nu(\tau_\nu) = a_\nu + b_\nu\tau_\nu + c_\nu\tau_\nu^2 + d_\nu\tau_\nu^3 + e_\nu\tau_\nu^4, \tag{4.12}$$

giving

$$B_\nu'(\tau_\nu) = b_\nu + 2c_\nu\tau_\nu + 3d_\nu\tau_\nu^2 + 4e_\nu\tau_\nu^3$$
$$B_\nu''(\tau_\nu) = 2c_\nu + 6d_\nu\tau_\nu + 12e_\nu\tau_\nu^2$$
$$B_\nu'''(\tau_\nu) = 6d_\nu + 24e_\nu\tau_\nu$$
$$B_\nu''''(\tau_\nu) = 24e_\nu.$$

Introducing the following constants

$$\left.\begin{aligned} A_\nu &= b_\nu + 2c_\nu + 6d_\nu + 24e_\nu \\ B_\nu &= 2c_\nu + 6d_\nu + 24e_\nu \\ C_\nu &= 3d_\nu + 12e_\nu \\ D_\nu &= 4e_\nu \end{aligned}\right\} \tag{4.13}$$

and

$$N_\nu = a_\nu + b_\nu + 2c_\nu + 6d_\nu + 24e_\nu$$

equation (4.11) simplifies to the form

$$\frac{\Delta I_\nu}{I_\nu^c(0,0)} = \frac{\int_0^{\infty}[A_\nu + B_\nu\tau_\nu + C_\nu\tau_\nu^2 + \ldots]e^{-\tau_\nu}d\tau_l}{N_\nu} = \int_0^{\infty} g_\nu(\tau_\nu)d\tau_l. \tag{4.14}$$

It is clear therefore that a knowledge of the coefficients a_ν, b_ν, c_ν, d_ν etc. of the expansion representing the Planckian function is sufficient completely to evaluate the weighting function at any depth τ_ν. This information may be obtained from the observational investigation of the limb-darkening of the Sun.

4.1. *Limb-darkening.*—The intensity of radiation emitted by the solar atmosphere in the continuum at frequency ν, in a direction at an angle θ with the outward surface normal is given by

$$I_\nu^c(0,\theta)=\int_0^\infty B_\nu(\tau)e^{-\tau_\nu \sec\theta}\sec\theta\, d\tau_\nu. \tag{4.15}$$

This has a solution of the form

$$I_\nu^c(0,\theta)=A_\nu'+B_\nu'\cos\theta+C_\nu'\cos^2\theta+\ldots, \tag{4.16}$$

i.e. direct integration of equation (4.15) yields

$$\begin{aligned} I_\nu^c(0,\theta)&=\int_0^\infty B_\nu(\tau)e^{-\tau_\nu/\mu}\frac{d\tau_\nu}{\mu} \qquad \text{where} \qquad \mu=\cos\theta \\ &=-\int_0^\infty B_\nu(\tau)d(e^{-\tau_\nu/\mu}) \\ &=\left[B_\nu+\mu\frac{dB_\nu}{d\tau_\nu}+\mu^2\frac{d^2B_\nu}{d\tau_\nu^2}+\ldots\right]_{\tau_\nu=0}, \end{aligned} \tag{4.17}$$

which is of the same form as equation (4.16). Introducing the Planck function in the form given in equation (4.12), we have

$$I_\nu^c(0,\theta)=a_\nu+b_\nu\cos\theta+2c_\nu\cos^2\theta+\ldots. \tag{4.18}$$

Observations of $I_\nu^c(0,\theta)$ have been made by a large number of workers. The results obtained by Abbot and Raudenbusch have been most carefully analysed by Chalonge and Kourganoff (**4**), who, expressing $I_\nu^c(0,\theta)$ (or more exactly $\phi_\nu=I_\nu^c(0,\theta)/I_\nu^c(0,0)$) in the form of equation (4.16), obtained the values of the coefficients A_ν', B_ν', and C_ν' for a large range of wave-lengths.

From equations (4.16) and (4.18) we see that $A_\nu'=a_\nu$, $B_\nu'=b_\nu$, and $C_\nu'=2c_\nu$ etc., and therefore the constants of equation (4.14) may be evaluated and the value of the weighting function obtained at any depth τ_ν in the atmosphere.

An advantage of using the observational results of limb-darkening is that this minimizes the number of uncertain assumptions which are required to be made, e.g. no uncertain factors depending upon turbulence or the blanketing effect need be considered. The obvious disadvantage is that, from the nature of the observations made, the values of the coefficients will be accurate for only the outer layers of the atmosphere, and for large optical depths the method may be unreliable.

4.2. *Transition to the standard optical depth.*—In order to be able to compare calculations made in different regions of the spectrum it is advantageous to use one variable for the optical depth in all spectral regions. The optical depth τ_0 in wave-length $\lambda=5000$ A is chosen as the standard variable; this also facilitates numerical calculations since many of the model atmospheres are defined with $\tau_0=\tau_0(\theta)$ expressed in regular numerical interval. (In the case of the Swihart model however the temperature distribution is referred to the Rosseland mean optical depth $\tau=\tau(\theta)$ and, for this model only, all spectral regions are referred to this optical depth.)

In some particular wave-length λ, corresponding to frequency ν, equation (4.14) gives

$$\frac{\Delta I_\nu}{I_\nu^c(0,0)}=\int_0^\infty g_\nu(\tau_\nu)\,d\tau_l=\int_0^\infty g_\nu(\tau_0)\frac{l_\nu}{k_\nu}\,d\tau_\nu, \tag{4.19}$$

where

$$g_\nu(\tau_0)=g_\nu[\tau_\nu(\tau_0)]. \tag{4.20}$$

Equation (4.20) expresses the transition of the weighting function for wave-length $\lambda = x$, referred to optical depth τ_ν (i.e. in wave-length x), to the weighting function for $\lambda = x$ referred to optical depth τ_0 (i.e. in the standard wave-length $\lambda = 5000$ A). Corresponding values of τ_0 and τ_ν are easily calculated, since

$$\tau_0 = \int_0^{\tau_\nu} \frac{k_0}{k_\nu} d\tau_\nu, \tag{4.21}$$

and tables of the absorption coefficients $k_\nu = k_\nu(\theta, P_e)$ are available (Strömgren (**15**)). The weighting function may thus be expressed with τ_0 as depth variable and this function is designated $g_\nu(\tau_0)$. If, following Claas (**5**), we write

$$\frac{g_\nu(\tau_0)}{k_0} = h_\nu(\tau_0), \tag{4.22}$$

then equation (4.19) may be written in the form

$$\frac{\Delta I_\nu}{I_\nu^c(0,0)} = \int_0^\infty g_\nu(\tau_0) \frac{l_\nu}{k_\nu} \cdot \frac{k_\nu}{k_0} d\tau_0 = \int_0^\infty h_\nu(\tau_0) l_\nu d\tau_0. \tag{4.23}$$

4.3. *The line absorption coefficient l_ν.*—If x_ν is the selective absorption coefficient per absorbing atom, and N_i the number of absorbing atoms per cm^3, then $N_i/N_H m_H$ is the number of absorbing atoms per gram. That is, due to the overwhelming abundance of hydrogen in the solar atmosphere, it is assumed that the density of the atmospheric gas is $N_H m_H$ g cm^{-3}. The selective absorption coefficient per gram is therefore

$$l_\nu = \frac{N_i}{N_H m_H} x_\nu. \tag{4.24}$$

It has been established (e.g. Aller (**1**)) that the total absorption by an atom radiating as a classical dipole is given by

$$\int_{-\infty}^{+\infty} x_\nu \, . \, d\lambda = \frac{\pi e^2}{mc} \cdot \frac{\lambda^2}{c} \, . \tag{4.25}$$

Quantum theory however requires that the absorption of N_i atoms is the same as the absorption of $N_i f$ classical oscillators, i.e. equation (4.25) becomes

$$\int_{-\infty}^{+\infty} x_\nu \, . \, d\lambda = \frac{\pi e^2 \lambda^2}{mc^2} \, . \, f, \tag{4.26}$$

and we may therefore write

$$\int_{-\infty}^{+\infty} l_\nu \, d\lambda = \int_{-\infty}^{+\infty} \frac{N_i}{N_H m_H} x_\nu \, d\lambda = \frac{\pi e^2 \lambda^2}{mc^2} \cdot \frac{f}{m_H} \cdot \frac{N_i}{N_H} \, . \tag{4.27}$$

4.4. *Introduction of Boltzmann's law.*—The absorption line intensity depends not only on the particular atomic transition probability but also upon the number of atoms in the initial absorbing state, N_i. Boltzmann's equation expresses the number of atoms in absorbing state i, N_i, in terms of the number of atoms of the same element in all states n, i.e. the total number of atoms N:

$$\frac{N_i}{N} = \frac{g_i e^{-E_i/KT}}{\sum_n g_n e^{-E_n/KT}} = \frac{g_i e^{-E_i/KT}}{u} \, , \tag{4.28}$$

where g_n is the statistical weight of the level n, $u = \sum_n g_n e^{-E_n/KT}$ is the partition function of the element in question, and E_i is excitation energy of the level i. The population of a level may also be influenced by the perturbations produced by neighbouring particles; this however will be of importance only for states of large principal quantum number and these levels produce spectral lines in

the far infra-red, i.e. far beyond the wave-length range considered here. There is therefore no perturbation correction required for the population of the initial level in the present investigation. Claas (5) has obtained values of the partition function of nitrogen as a function of temperature and these values are used in the present discussion. The introduction of the parameter $\theta = 5040/T$ enables us to express the excitation potential directly in volts, for if E_i is the excitation us energy (in electron volts) then

$$\log_{10} e^{-E_i/KT} = -V\theta,$$

(V in volts) and equation (4.28) becomes

$$\frac{N_i}{N} = \frac{g_i \times 10^{-V\theta}}{u}. \tag{4.29}$$

4.5. *Determination of relative abundance.*—The equivalent width of a spectral line is expressed by

$$W_\lambda = \int_{-\infty}^{+\infty} \frac{\Delta I_\nu}{I} d\lambda.$$

Introducing equation (4.23) this becomes

$$W_\lambda = \int_{-\infty}^{+\infty} \int_0^\infty h_\nu(\tau_0) l_\nu \, d\tau_0 \, d\lambda, \tag{4.30}$$

$h_\nu(\tau_0)$ is of course practically constant over the width of the line and therefore by equation (4.27) we have

$$W_\lambda = \frac{\pi e^2 \lambda^2}{mc^2} \frac{f}{m_H} \int_0^\infty h_\nu(\tau_0) \frac{N_i}{N_H} \, d\tau_0. \tag{4.31}$$

If A is the relative abundance of nitrogen with respect to hydrogen, i.e. $A = N/N_H$ (at temperatures prevailing in the solar atmosphere the degree of ionization of nitrogen, I.P. = 14·54 volts, is very small indeed and we may consider all the nitrogen atoms to be neutral), we have then

$$\frac{N_i}{N_H} = \frac{N_i}{N} A. \tag{4.32}$$

Utilizing equations (4.29) and (4.32), equation (4.31) becomes

$$W_\lambda = \frac{\pi e^2 \lambda^2}{mc^2} \frac{f}{m_H} A g_i \int_0^\infty \frac{h_\nu(\tau_0) \times 10^{-V\theta}}{u} d\tau_0. \tag{4.33}$$

The numerical value of the constant $\pi e^2/mc^2 m_H$ is $5{\cdot}28 \times 10^{11}$; if however the equivalent width W_λ is expressed in mA and the wave-length λ in Angström units we have finally

$$W_\lambda = 5{\cdot}28 \times 10^6 . \lambda^2 f g_i A \int_0^\infty \frac{h_\nu(\tau_0) \times 10^{-V\theta}}{u} d\tau_0. \tag{4.34}$$

This equation expresses the equivalent width of the absorption line in terms of the weighting function, various other parameters, i.e. λ, f, g_i, V which are characteristic of the particular atomic transition, and the relative abundance of nitrogen. The weighting function may be calculated from the observed limb-darkening (Section 4.1), the parameters of the atomic transitions and the equivalent widths are known (Section 3), and hence the relative abundance may be determined.

4.6. *Numerical calculations.*—In the wave-length range under consideration, i.e. 7442–8719 A, it was found sufficiently accurate for the determination of the weighting function $g_\nu(\tau_\nu)$ to adopt the wave-length $\lambda = 8206$ A as representative of the range.

(*a*) $g_\nu(\tau_0)$. For $\lambda = 8206$ A the investigation of Chalonge and Kourganoff (**4**) gives the results

$$A_\nu' = a_\nu = 0{\cdot}501, \qquad B_\nu' = b_\nu = 0{\cdot}666, \qquad C_\nu' = 2c_\nu = -0{\cdot}172.$$

The weighting function $g_\nu(\tau_\nu) = (A_\nu + B_\nu\tau_\nu)e^{-\tau_\nu}/N_\nu$ may then be evaluated at any value of the optical depth τ_ν since

$$A_\nu = b_\nu + 2c_\nu = 0{\cdot}494, \qquad B_\nu = 2c_\nu = -0{\cdot}172, \qquad N_\nu = a_\nu + b_\nu + 2c_\nu = 0{\cdot}995.$$

Corresponding values of τ_ν ($\lambda = 8206$ A) and τ_0 ($\lambda = 5000$ A) are determined from equation (4.21) and hence the weighting function is determined for a large range of values of τ_0 with irregular interval. Interpolation in these results enables $g_\nu(\tau_0)$ to be obtained for a range of values of τ_0 with regular interval (see Fig. 1).

(*b*) $(Q) = \int_0^\infty \frac{h_\nu(\tau_0) \times 10^{-V\theta}}{u}\, d\tau_0$. The parameter $h_\nu(\tau_0) = g_\nu(\tau_0)/k_0$ is obtained from the results of Section 4.6 (*a*) and the values of $k_0 = k_0(\theta, P_e)$ obtained from tables provided by Dr B. Strömgren (unpublished). The excitation potentials V of the lines considered are listed in Table II, $\tau_0 = \tau_0(\theta)$ is determined by the model, and the nitrogen partition function u is obtained from Claas (**5**). The function $h_\nu(\tau_0) \times 10^{-V\theta}/u$ may then be calculated at regular intervals of τ_0 (see Fig. 1) and the integration (Q) determined. The values of (Q) obtained for the

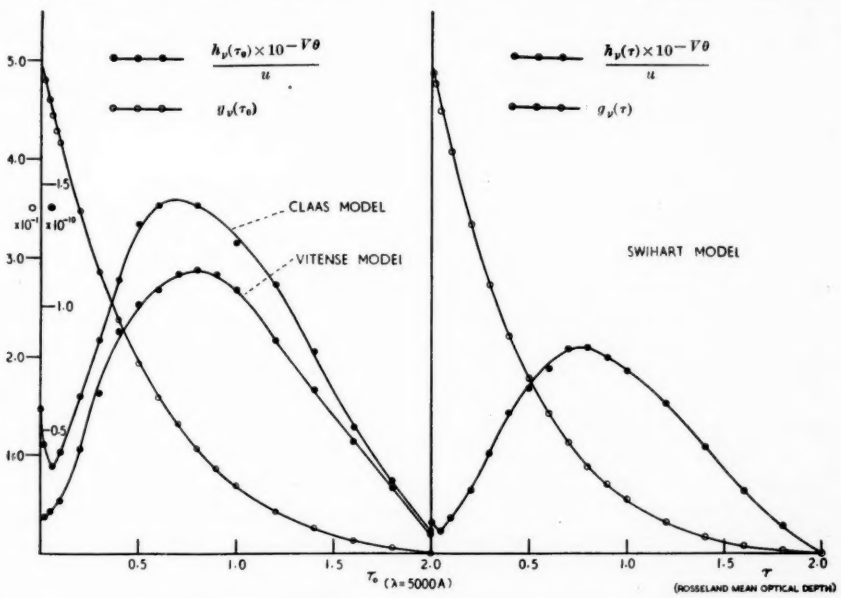

FIG. 1.—*The contribution to the total nitrogen absorption as a function of optical depth in the atmosphere by the method of weighting functions.* ($\theta = 10{\cdot}33$ volts ; ν refers to $\lambda = 8206$ A.)

excitation potentials of interest, for each of the models, are shown below:

TABLE IV

Model	(Q) 10·33 volts	(Q) 10·68 volts
Claas	$1{\cdot}768\times10^{-10}$	$0{\cdot}923\times10^{-10}$
Vitense	$1{\cdot}398\times10^{-10}$	$0{\cdot}728\times10^{-10}$
Swihart	$0{\cdot}921\times10^{-10}$	$0{\cdot}471\times10^{-10}$

(*c*) $(Y)=5{\cdot}28\times10^{6}.\lambda^{2}fg_{i}$. All the parameters are given in Table III. We may then calculate $W_{\lambda}/A=(Y)(Q)$ and hence determine the relative abundance A from each of the nine nitrogen lines, since

$$\log A=\log W_{\lambda_{\text{Obs.}}}-\log(Y)(Q).$$

The final results are given in Table V.

TABLE V

Nitrogen abundance by weighting function method

			$\log(Q)$			$\log A$		
λ	$\log W_{\lambda_{\text{Obs.}}}$	$\log(Y)$	Claas	Vitense	Swihart	Claas	Vitense	Swihart
7442·28	0·4771	14·1920	$\bar{1}\bar{0}{\cdot}2475$	$\bar{1}\bar{0}{\cdot}1456$	$\bar{1}\bar{1}{\cdot}9645$	$\bar{4}{\cdot}038$	$\bar{4}{\cdot}140$	$\bar{4}{\cdot}321$
7468·29	0·5441	14·3678	$\bar{1}\bar{0}{\cdot}2475$	$\bar{1}\bar{0}{\cdot}1456$	$\bar{1}\bar{1}{\cdot}9645$	$\bar{5}{\cdot}929$	$\bar{4}{\cdot}031$	$\bar{4}{\cdot}212$
8216·28	0·7782	14·7333	$\bar{1}\bar{0}{\cdot}2475$	$\bar{1}\bar{0}{\cdot}1456$	$\bar{1}\bar{1}{\cdot}9645$	$\bar{5}{\cdot}797$	$\bar{5}{\cdot}899$	$\bar{4}{\cdot}080$
8629·24	0·6021	14·6546	$\bar{1}\bar{1}{\cdot}9651$	$\bar{1}\bar{1}{\cdot}8622$	$\bar{1}\bar{1}{\cdot}6729$	$\bar{5}{\cdot}982$	$\bar{4}{\cdot}085$	$\bar{4}{\cdot}275$
8680·24	1·2304	15·0371	$\bar{1}\bar{0}{\cdot}2475$	$\bar{1}\bar{0}{\cdot}1456$	$\bar{1}\bar{1}{\cdot}9645$	$\bar{5}{\cdot}946$	$\bar{4}{\cdot}048$	$\bar{4}{\cdot}229$
8683·38	0·8451	14·7571	$\bar{1}\bar{0}{\cdot}2475$	$\bar{1}\bar{0}{\cdot}1456$	$\bar{1}\bar{1}{\cdot}9645$	$\bar{5}{\cdot}841$	$\bar{5}{\cdot}942$	$\bar{4}{\cdot}124$
8703·24	0·6990	14·3564	$\bar{1}\bar{0}{\cdot}2475$	$\bar{1}\bar{0}{\cdot}1456$	$\bar{1}\bar{1}{\cdot}9645$	$4{\cdot}095$	$4{\cdot}197$	$\bar{4}{\cdot}378$
8711·69	0·6021	14·4649	$\bar{1}\bar{0}{\cdot}2475$	$\bar{1}\bar{0}{\cdot}1456$	$\bar{1}\bar{1}{\cdot}9645$	$\bar{5}{\cdot}890$	$\bar{5}{\cdot}992$	$\bar{4}{\cdot}173$
8718·82	0·6021	14·3903	$\bar{1}\bar{0}{\cdot}2475$	$\bar{1}\bar{0}{\cdot}1456$	$\bar{1}\bar{1}{\cdot}9645$	$5{\cdot}964$	$4{\cdot}066$	$\bar{4}{\cdot}247$
					Mean $\log A=$	$\bar{5}{\cdot}942$	$\bar{4}{\cdot}044$	$\bar{4}{\cdot}227$

(on the basis $\log A_H=12{\cdot}00$)

Claas model	Vitense model	Swihart model
$\log A_N=7{\cdot}94$	$\log A_N=8{\cdot}04$	$\log A_N=8{\cdot}23$

The results show a substantially lower nitrogen abundance than those obtained by Unsöld (**19**) ($\log A_N=8{\cdot}61$) and by Hunaerts (**8**) ($\log A_N=9{\cdot}02$). The method of weighting functions is however subject to several uncertain factors which will be examined in Section 6. In the following section a second method for the determination of the nitrogen abundance is developed and, in Section 6, a comparison is made between this second method and the method of weighting functions.

5. ***The method utilizing the Planckian gradient.***—The purpose of the present section is to develop a method of determining the equivalent width of an absorption line as a function of the relative abundance of the element, the characteristic parameters of the particular atomic transition, and other factors which, in contrast with the method of weighting functions, are determined purely by the physical characteristics of the model solar atmosphere considered. In this method, suggested by Dr B. Strömgren, no recourse is made to the observational results of limb-darkening.

The intensity of radiation in the continuum, at the centre of the disk, is given by

$$I_\nu^c(0,0) = \int_0^\infty B_\nu(\tau) e^{-\tau_\nu} d\tau_\nu, \tag{5.1}$$

i.e.

$$\begin{aligned} I_\nu^c(0,0) &= -\int_0^\infty B_\nu(\tau) d(e^{-\tau_\nu}) \\ &= -\left| B_\nu(\tau) e^{-\tau_\nu} \right|_0^\infty + \int_0^\infty \frac{dB_\nu}{d\tau_\nu} e^{-\tau_\nu} d\tau_\nu \\ &= B_\nu(\tau)_{\tau_\nu=0} + \int_0^\infty \frac{dB_\nu}{d\tau_\nu} e^{-\tau_\nu} d\tau_\nu. \end{aligned} \tag{5.2}$$

Again the intensity in the line is

$$I_\nu(0,0) = \int_0^\infty B_\nu(\tau) e^{-t_\nu} dt_\nu, \tag{5.3}$$

where

$$t_\nu = \int_0^{\tau_\nu} \left(1 + \frac{l_\nu}{k_\nu}\right) d\tau_\nu = \tau_\nu + \tau_l, \tag{5.4}$$

and

$$\tau_l = \int_0^{\tau_\nu} \frac{l_\nu}{k_\nu} d\tau_\nu. \tag{5.5}$$

We may develop equation (5.3) in the following manner:

$$\begin{aligned} I_\nu(0,0) &= -\int_0^\infty B_\nu(\tau) d(e^{-t_\nu}) \\ &= -\left| B_\nu(\tau) e^{-t_\nu} \right|_0^\infty + \int_0^\infty \frac{dB_\nu}{dt_\nu} e^{-t_\nu} dt_\nu, \end{aligned}$$

and introducing equation (5.4) we have

$$\begin{aligned} I_\nu(0,0) &= B_\nu(\tau)_{t_\nu=0} + \int_0^\infty \frac{dB_\nu}{d\tau_\nu} e^{-(\tau_\nu+\tau_l)} d\tau_\nu \\ &= B_\nu(\tau)_{t_\nu=0} + \int_0^\infty \frac{dB_\nu}{d\tau_\nu} e^{-\tau_\nu} d\tau_\nu (1-\tau_l), \end{aligned}$$

to the first order, i.e.

$$I_\nu(0,0) = B_\nu(\tau)_{t_\nu=0} + \int_0^\infty \frac{dB_\nu}{d\tau_\nu} e^{-\tau_\nu} d\tau_\nu - \int_0^\infty \frac{dB_\nu}{d\tau_\nu} e^{-\tau_\nu} \tau_l d\tau_\nu. \tag{5.6}$$

From equations (5.2) and (5.6) we see that the dip in the continuum is

$$\Delta I_\nu = I_\nu^c(0,0) - I_\nu(0,0) = \int_0^\infty \frac{dB_\nu}{d\tau_\nu} e^{-\tau_\nu} \tau_l d\tau_\nu, \tag{5.7}$$

which, by equation (5.5), becomes

$$\Delta I_\nu = \int_0^\infty \frac{dB_\nu}{d\tau_\nu} e^{-\tau_\nu} \left[\int_0^{\tau_\nu} \frac{l_\nu}{k_\nu} d\tau_\nu \right] d\tau_\nu. \tag{5.8}$$

The equivalent width of the spectral line is therefore given by

$$W_\lambda = \int_{-\infty}^{+\infty} \frac{\Delta I_\nu}{I_\nu^c(0,0)} d\lambda = \int_{-\infty}^{+\infty} \frac{\int_0^\infty \frac{dB_\nu}{d\tau_\nu} e^{-\tau_\nu} \left[\int_0^{\tau_\nu} \frac{l_\nu}{k_\nu} d\tau_\nu \right] d\tau_\nu}{\int_0^\infty B_\nu(\tau) e^{-\tau_\nu} d\tau_\nu} d\lambda. \tag{5.9}$$

All factors, other than l_ν, are of course sensibly constant over the width of the line and therefore, utilizing the development of Section 4.3, equation (5.9) gives

$$W_\lambda = \frac{\int_0^\infty \frac{dB_\nu}{d\tau_\nu} e^{-\tau_\nu} \frac{\pi e^2 \lambda^2}{mc^2} \frac{f}{m_H} \left[\int_0^{\tau_\nu} \frac{N_i}{N_H k_\nu} d\tau_\nu \right] d\tau_\nu}{\int_0^\infty B_\nu(\tau) e^{-\tau_\nu} d\tau_\nu}. \qquad (5.10)$$

Since $N_i/N_H = (N_i/N)A$, where the relative abundance $A = N/N_H$, we may introduce Boltzmann's equation (cf. Section 4.4), i.e.

$$\frac{N_i}{N} = \frac{g_i \times 10^{-V\theta}}{u},$$

and obtain the equivalent width in the form

$$W_\lambda = \frac{\pi e^2 \lambda^2}{mc^2} \cdot \frac{f}{m_H} \cdot g_i \cdot A \frac{\int_0^\infty \frac{dB_\nu}{d\tau_\nu} e^{-\tau_\nu} \left[\int_0^{\tau_\nu} \frac{10^{-V\theta}}{uk_\nu} d\tau_\nu \right] d\tau_\nu}{\int_0^\infty B_\nu(\tau) e^{-\tau_\nu} d\tau_\nu}. \qquad (5.11)$$

For ease in numerical integration we again transpose the integral to a function of optical depth τ_0 in the standard wave-length $\lambda = 5000$ A by the relationship $d\tau_\nu = (k_\nu/k_0)\, d\tau_0$ (cf. Section 4.2). As in the method of weighting functions, if we express the equivalent width in mA and the wave-length in Angström units the value of the numerical constant is $5{\cdot}28 \times 10^6$, and the final form of the equation becomes

$$W_\lambda = 5{\cdot}28 \times 10^6 \lambda^2 f g_i A \frac{\int_0^\infty \frac{dB_\nu}{d\tau_0} e^{-\tau_\nu} \left[\int_0^{\tau_\nu(\tau_0)} \frac{10^{-V\theta}}{uk_0} d\tau_0 \right] d\tau_0.}{\int_0^\infty B_\nu(\tau) e^{-\tau_\nu} \frac{k_\nu}{k_0} d\tau_0}. \qquad (5.12)$$

For a given atomic transition (λ, f, g_i, V known) the equivalent width is therefore expressed as a function of the relative abundance A and the characteristic $\tau_0 = \tau_0(\theta)$ of the particular solar atmosphere under consideration.

5.1. *Numerical calculations.*—In the wave-length range under consideration, i.e. 7442–8719 A, it was again found to be sufficiently accurate for the determination of $k_\nu = k_\nu(\theta, P_e)$ and $B_\nu = B_\nu(\theta)$ to adopt the wave-length $\lambda = 8206$ A as representative of the range. Tables of the Planckian function and absorption coefficients were provided by Dr B. Strömgren (unpublished).

(*a*) $I(\tau_0) = \int_0^{\tau_\nu(\tau_0)} \frac{10^{-V\theta}}{uk_0} d\tau_0$. The excitation potentials V are given in Table II and values of the partition function $u = u(\theta)$ are taken from Claas (**5**). The value of the integrand was then computed for a large range of values of τ_0 with regular interval and the integration performed at each value of τ_0 throughout the atmosphere.

(*b*) $(Z) = \int_0^\infty \frac{dB_\nu}{d\tau_0} e^{-\tau_\nu} I(\tau_0)\, d\tau_0$. Since all the factors of the integrand are known as functions of the optical depth τ_0, the regular interval in τ_0 could be maintained thereby greatly facilitating the integration. For a given wave-length, in this case 8206 A, the Planck function is a function of temperature only, i.e. $B_\nu = B_\nu(\theta)$, and, as the atmospheric model provides $\tau_0 = \tau_0(\theta)$,

$$dB_\nu/d\tau_0 = (dB_\nu/d\theta)(d\theta/d\tau_0)$$

may be calculated in the following manner:

$$B_\nu = \frac{2h\nu^3}{c^2}(e^\alpha - 1)^{-1},$$

where

$$\alpha = \frac{h\nu}{KT} = \beta\theta,$$

i.e.

$$\frac{dB_\nu}{d\alpha} = -B_\nu e^\alpha (e^\alpha - 1)^{-1},$$

and

$$\frac{d\alpha}{d\theta} = \beta,$$

i.e.

$$\frac{dB_\nu}{d\theta} = \frac{dB_\nu}{d\alpha} \cdot \frac{d\alpha}{d\theta} = \frac{-\beta B_\nu}{(1 - e^{-\alpha})}$$

(the constant β has the value, for $\lambda = 8206$ A, $\beta = h\nu/KT\theta = 3{\cdot}4795$) and $d\theta/d\tau_0$ may be determined directly from the model. Values of the integrand obtained are illustrated in Fig. 2. It was found necessary to extrapolate graphically the integrand to zero at large optical depth; any reasonable change in the extrapolated values, however, produces little change in the result of the numerical integration.

(*c*) $I_\nu^c(0,0) = \int_0^\infty B_\nu(\tau)e^{-\tau_\nu}\frac{k_\nu}{k_0}d\tau_0$. Only in the case of the Swihart model is the atmosphere defined to sufficiently great depth to allow exact evaluation of the integral, graphical extrapolation of the integrand is necessary for the Claas and Vitense models, but again the numerical uncertainty is small (Fig. 2). The values obtained for these integrations are shown below.

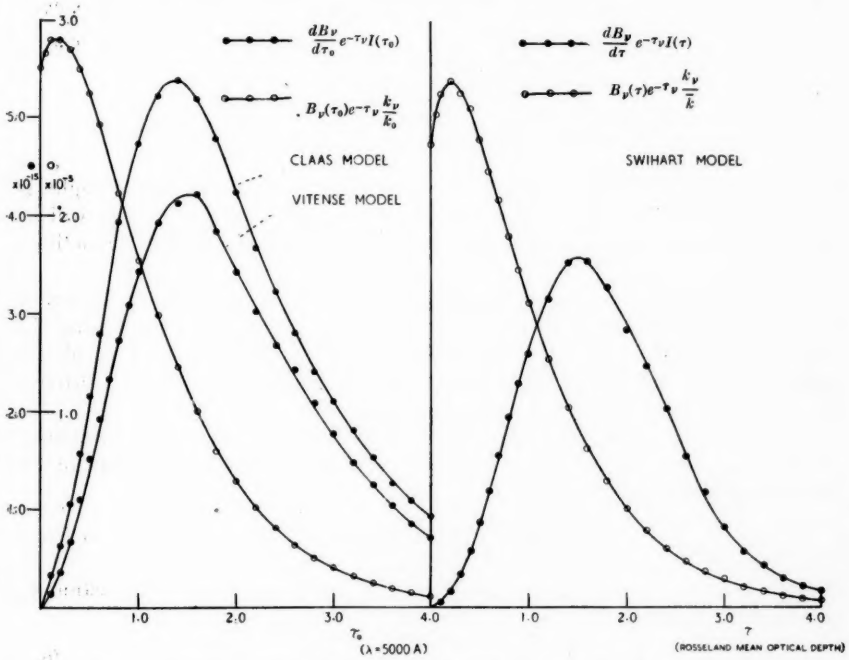

FIG. 2.—*The contribution to the total nitrogen absorption as a function of optical depth in the atmosphere by the Planckian Gradient method.* ($\theta = 10{\cdot}33$ *volts;* ν *refers to* $\lambda = 8206$ A.)

TABLE VI

Model	(Z) erg cm^{-2} sec^{-1}		$I^c_\nu(0, 0)$ erg cm^{-2} sec^{-1}
	10·33 volts	10·68 volts	
Claas	$124{\cdot}69 \times 10^{-16}$	$67{\cdot}60 \times 10^{-16}$	$4{\cdot}172 \times 10^{-5}$
Vitense	$96{\cdot}60 \times 10^{-16}$	$52{\cdot}41 \times 10^{-16}$	$4{\cdot}049 \times 10^{-5}$
Swihart	$65{\cdot}27 \times 10^{-16}$	$34{\cdot}44 \times 10^{-16}$	$3{\cdot}605 \times 10^{-5}$

(*d*) $(Y) = 5{\cdot}28 \times 10^6 \lambda^2 f g_i$. All the parameters are given in Table III. We may then calculate $W_\lambda/A = (Y)(Z)/I^c_\nu(0, 0)$ and hence determine the relative abundance A for each of the nine nitrogen lines since

$$\log A = \log W_{\lambda_{\text{Obs.}}} - \log (Y)(Z)/I^c_\nu(0, 0).$$

The final results are given in Table VII. These results show an appreciably

TABLE VII

Nitrogen abundance by Planckian gradient method

λ	$\log W_{\lambda_{\text{Obs.}}}$	$\log (Y)$	$\log (Z)/I^c_\nu(0, 0)$			$\log A$		
			Claas	Vitense	Swihart	Claas	Vitense	Swihart
7442·28	0·4771	14·1920	$\bar{1}0{\cdot}4755$	$\bar{1}0{\cdot}3777$	$\bar{1}0{\cdot}2579$	$\bar{5}{\cdot}810$	$\bar{5}{\cdot}907$	$\bar{4}{\cdot}027$
7468·29	0·5441	14·3678	$\bar{1}0{\cdot}4755$	$\bar{1}0{\cdot}3777$	$\bar{1}0{\cdot}2579$	$\bar{5}{\cdot}701$	$\bar{5}{\cdot}799$	$\bar{5}{\cdot}918$
8216·28	0·7782	14·7333	$\bar{1}0{\cdot}4755$	$\bar{1}0{\cdot}3777$	$\bar{1}0{\cdot}2579$	$\bar{5}{\cdot}569$	$\bar{5}{\cdot}667$	$\bar{5}{\cdot}787$
8629·24	0·6021	14·6546	$\bar{1}0{\cdot}2095$	$\bar{1}0{\cdot}1120$	$\bar{1}1{\cdot}9801$	$\bar{5}{\cdot}738$	$\bar{5}{\cdot}836$	$\bar{5}{\cdot}967$
8680·24	1·2304	15·0371	$\bar{1}0{\cdot}4755$	$\bar{1}0{\cdot}3777$	$\bar{1}0{\cdot}2579$	$\bar{5}{\cdot}718$	$\bar{5}{\cdot}816$	$\bar{5}{\cdot}935$
8683·38	0·8451	14·7571	$\bar{1}0{\cdot}4755$	$\bar{1}0{\cdot}3777$	$\bar{1}0{\cdot}2579$	$\bar{5}{\cdot}613$	$\bar{5}{\cdot}710$	$\bar{5}{\cdot}830$
8703·24	0·6990	14·3564	$\bar{1}0{\cdot}4755$	$\bar{1}0{\cdot}3777$	$\bar{1}0{\cdot}2579$	$\bar{5}{\cdot}867$	$\bar{5}{\cdot}965$	$\bar{4}{\cdot}085$
8711·69	0·6021	14·4649	$\bar{1}0{\cdot}4755$	$\bar{1}0{\cdot}3777$	$\bar{1}0{\cdot}2579$	$\bar{5}{\cdot}662$	$\bar{5}{\cdot}760$	$\bar{5}{\cdot}879$
8718·82	0·6021	14·3903	$\bar{1}0{\cdot}4755$	$\bar{1}0{\cdot}3777$	$\bar{1}0{\cdot}2579$	$\bar{5}{\cdot}736$	$\bar{5}{\cdot}834$	$\bar{5}{\cdot}954$
					Mean $\log A =$	$\bar{5}{\cdot}713$	$\bar{5}{\cdot}810$	$\bar{5}{\cdot}931$

(on the basis $\log A_H = 12{\cdot}00$)

Claas model	Vitense model	Swihart model
$\log A_N = 7{\cdot}71$	$\log A_N = 7{\cdot}81$	$\log A_N = 7{\cdot}93$

lower nitrogen abundance than that obtained by the previous method of weighting functions (cf. Table V). The reasons for this numerical discrepancy will be considered in the following section where a comparison between the two methods is made.

The accuracy of the results would obviously be increased if more detailed profiles of the faint nitrogen lines were available, as measurements using the *Utrecht Photometric Atlas* are difficult and rather uncertain. In spite of this difficulty it is pleasing to note (Table VII) that results for each of the nine nitrogen lines give only a small spread about the mean value.

6. *Comparison of methods used.*—In the Planckian gradient method (Section 5) it has been established that for a weak line in pure absorption the dip in the continuum is given by the equation

$$\Delta I_\nu = \int_0^\infty \frac{dB_\nu}{d\tau_\nu} e^{-\tau_\nu} \left[\int_0^{\tau_\nu} \frac{l_\nu}{k_\nu} d\tau_\nu \right] d\tau_\nu. \tag{6.1}$$

Minnaert, in the development of the theory of weighting functions (Section 4), obtained the equation

$$\Delta I_\nu = \int_0^\infty \left[\frac{dB_\nu}{d\tau_\nu} + \frac{d^2 B_\nu}{d\tau_\nu^2} + \ldots \right] e^{-\tau_\nu} \frac{l_\nu}{k_\nu} d\tau_\nu. \tag{6.2}$$

It has been found however that a large numerical discrepancy exists between the two methods, the former method using purely the characteristics of the model atmosphere, and the latter method utilizing the observational results of limb-darkening. We seek then to establish the identity of the two equations and then to consider the source of the numerical discrepancy

$$\begin{aligned}\Delta I_\nu &= \int_0^\infty \frac{dB_\nu}{d\tau_\nu} e^{-\tau_\nu}\left[\int_0^{\tau_\nu} \frac{l_\nu}{k_\nu} d\tau_\nu\right] d\tau_\nu = -\int_0^\infty \frac{dB_\nu}{d\tau_\nu}\left[\int_0^{\tau_\nu} \frac{l_\nu}{k_\nu} d\tau_\nu\right] d(e^{-\tau_\nu}) \\ &= -\left|\frac{dB_\nu}{d\tau_\nu}\left[\int_0^{\tau_\nu} \frac{l_\nu}{k_\nu} d\tau_\nu\right] e^{-\tau_\nu}\right|_0^\infty + \int_0^\infty \frac{dB_\nu}{d\tau_\nu}\frac{l_\nu}{k_\nu} e^{-\tau_\nu} d\tau_\nu \\ &\qquad + \int_0^\infty \frac{d^2B_\nu}{d\tau_\nu^2}\left[\int_0^\infty \frac{l_\nu}{k_\nu} d\tau_\nu\right] e^{-\tau_\nu} d\tau_\nu \\ &= \int_0^\infty \frac{dB_\nu}{d\tau_\nu}\frac{l_\nu}{k_\nu} e^{-\tau_\nu} d\tau_\nu + \int_0^\infty \frac{d^2B_\nu}{d\tau_\nu^2}\frac{l_\nu}{k_\nu} e^{-\tau_\nu} d\tau_\nu + \int_0^\infty \frac{d^3B_\nu}{d\tau_\nu^3}\left[\int_0^\infty \frac{l_\nu}{k_\nu} d\tau_\nu\right] e^{-\tau_\nu} d\tau_\nu \\ &= \int_0^\infty \left[\frac{dB_\nu}{d\tau_\nu} + \frac{d^2B_\nu}{d\tau_\nu^2} + \frac{d^3B_\nu}{d\tau_\nu^3} + \ldots\right] e^{-\tau_\nu} \frac{l_\nu}{k_\nu} d\tau_\nu. \end{aligned} \tag{6.3}$$

Again, in the establishment of equation (6.2) Minnaert obtained the equation (previously established by Unsöld)

$$\Delta I_\nu = \int_0^\infty \left[\int_{\tau_\nu}^\infty B_\nu e^{-\tau_\nu} d\tau_\nu - B_\nu e^{-\tau_\nu}\right] \frac{l_\nu}{k_\nu} d\tau_\nu \tag{6.4}$$

(see equation (4.8)); this, of course, should also reduce to the form (6.1), i.e.

$$\begin{aligned}\Delta I_\nu &= \int_0^\infty \left[-\left|B_\nu e^{-\tau_\nu}\right|_{\tau_\nu}^\infty + \int_{\tau_\nu}^\infty \frac{dB_\nu}{d\tau_\nu} e^{-\tau_\nu} d\tau_\nu - B_\nu e^{-\tau_\nu}\right] \frac{l_\nu}{k_\nu} d\tau_\nu \\ &= \int_0^\infty \left[\int_{\tau_\nu}^\infty \frac{dB_\nu}{d\tau_\nu} e^{-\tau_\nu} d\tau_\nu\right] \frac{l_\nu}{k_\nu} d\tau_\nu \\ &= \left|\left[\int_{\tau_\nu}^\infty \frac{dB_\nu}{d\tau_\nu} e^{-\tau_\nu} d\tau_\nu\right]\left[A + \int_0^{\tau_\nu} \frac{l_\nu}{k_\nu} d\tau_\nu\right]\right|_0^\infty + \int_0^\infty \frac{dB_\nu}{d\tau_\nu} e^{-\tau_\nu}\left[\int_0^{\tau_\nu} \frac{l_\nu}{k_\nu} d\tau_\nu\right] d\tau_\nu \\ &\qquad + A\int_0^\infty \frac{dB_\nu}{d\tau_\nu} e^{-\tau_\nu} d\tau_\nu \\ &= \int_0^\infty \frac{dB_\nu}{d\tau_\nu} e^{-\tau_\nu}\left[\int_0^{\tau_\nu} \frac{l_\nu}{k_\nu} d\tau_\nu\right] d\tau_\nu. \end{aligned} \tag{6.5}$$

The equations are equivalent. We must therefore look to the information used in the numerical integrations for the source of the numerical difference in the results obtained by the two methods.

Minnaert, in the method of weighting functions, considered the precise form of the Planckian function, i.e.

$$B_\nu(\tau_\nu) = a_\nu + b_\nu\tau_\nu + c_\nu\tau_\nu^2 + d_\nu\tau_\nu^3 + e_\nu\tau_\nu^4.$$

However, in introducing the observational results of Chalonge and Kourganoff only a_ν, b_ν and c_ν, i.e. the first three coefficients, could be determined. In effect the form of the Planckian function used is then

$$B_\nu(\tau_\nu) = a_\nu + b_\nu\tau_\nu + c_\nu\tau_\nu^2, \tag{6.6}$$

i.e.

$$B_\nu' = b_\nu + 2c_\nu\tau_\nu \tag{6.7}$$

and

$$B_\nu'' = 2c_\nu. \tag{6.8}$$

The equation (6.2), representing the dip in the continuum, therefore reduces to

$$\Delta I_\nu = \int_0^\infty \left(\frac{dB_\nu}{d\tau_\nu} + \frac{d^2 B_\nu}{d\tau_\nu^2} \right) e^{-\tau_\nu} \frac{l_\nu}{k_\nu} d\tau_\nu \tag{6.9}$$

$$= \int_0^\infty (b_\nu + 2c_\nu \tau_\nu + 2c_\nu) e^{-\tau_\nu} \frac{l_\nu}{k_\nu} d\tau_\nu. \tag{6.10}$$

It may easily be shown that for the special case of the Planckian function of the form (6.6) the equation (6.1), used in the method of the Planckian gradient, also reduces to the form (6.10). Minnaert has then assumed the first differential of the Planckian function to be a linear function of optical depth, and the coefficients b_ν and c_ν determining the differential are obtained from observational limb-darkening. The values of these coefficients are reliable only for the outer layers of the atmosphere and therefore linear extrapolation of the first differential to large optical depths (where the contribution of the undetermined coefficients d_ν and e_ν would be appreciable) is justifiable only if the contribution of the lower layers to the absorption is small. The weight of the deeper layers is in fact small for all elements of low ionization potential. For nitrogen however the weight of the deeper layers is large (maximum contribution at $\tau_0 \sim 1{\cdot}6$ and approximately 40 per cent of the total absorption originates at $\tau_0 > 2{\cdot}0$) due to the high ionization potential of the element. (See Fig. 2.)

In the case of the method of the Planckian gradient the precise form of the Planck function is used, i.e.

$$B_\nu(\theta) = \frac{2h\nu^3}{c^2} \frac{1}{(e^{h\nu/KT} - 1)},$$

the atmospheric model provides $\tau_\nu = \tau_\nu(\theta)$ and hence $dB_\nu/d\tau_\nu$ may be computed directly as a function of optical depth. The value of the first differential is therefore determined entirely by the temperature dependence on the optical depth, which is characteristic of each atmospheric model considered.

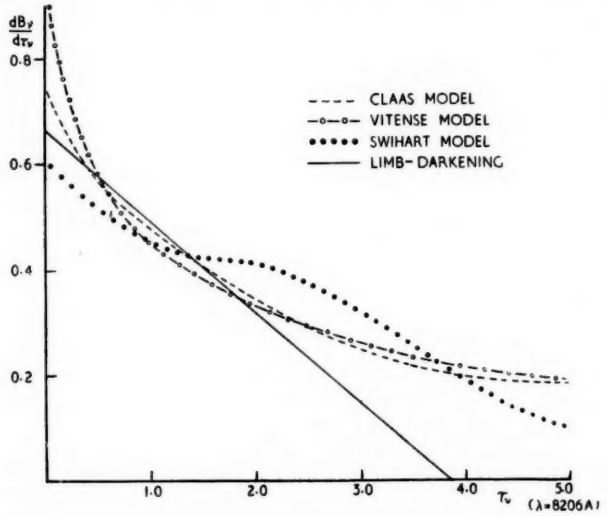

FIG. 3.—*Comparison between $dB_\nu/d\tau_\nu$ as predicted by the solar atmospheric models and as determined from observed limb-darkening results.*

A comparison is made in Fig. 3 between $dB_\nu/d\tau_\nu$ calculated in accordance with equation (6.7) and $dB_\nu/d\tau_\nu$ as predicted by the atmospheric models (in this latter case $dB_\nu/d\tau_\nu=(dB_\nu/d\tau_0)(k_0/k_\nu)$ and the values are then reduced to the same scale, $dB_\nu/d\tau_\nu \div I_\nu^c(0,0)$, used in the method of weighting functions). It is seen that there is quite close agreement in the upper layers, except immediately below the surface where the weight is small, and the difference is not important in the range $0<\tau_\nu<1{\cdot}5$. For $\tau_\nu>1{\cdot}5$, however, the difference is large and the divergence becomes important. It will be noted also that the method of weighting functions assumes the second differential constant, equation (6.8), and for $\lambda=8206$ A the limb-darkening results give $d^2B_\nu/d\tau_\nu{}^2=-0{\cdot}172$ and therefore equation (6.9) is equal to zero for $dB_\nu/d\tau_\nu=0{\cdot}172$, i.e. at approximately $\tau_\nu=2{\cdot}8$ ($\tau_0\simeq 2{\cdot}0$). By the method of weighting functions therefore, no contribution to the total absorption is possible below $\tau_0\simeq 2{\cdot}0$, while the method using the precise form of the Planck function shows that approximately 40 per cent of the total absorption, in the case of nitrogen, originates below this level.

It may be concluded that in cases where the absorption originates almost entirely in the uppermost layers, i.e. for elements of low ionization potential, the method of weighting functions may be used and may, in extreme cases, be superior to the method of the Planckian gradient (since the atmospheric models are rather uncertain very close to the surface). In the case of nitrogen, however, and in general for elements of high ionization potential, the weight of the deeper layers is large and the method of weighting functions is quite unreliable. Here the method of the Planckian gradient should be used. For these reasons, in the present investigation for nitrogen, the results obtained by the method of weighting functions are discarded.

Since now additional weight is placed upon the results of the Planckian gradient method it is obviously desirable to consider equations whereby these results may be checked. This is done in the following section.

7. *Equations for use in numerical checking*

(**A**) Reconsidering equations (5.3), (5.4) and (5.5) we see that we may write the intensity in the line in the form

$$\begin{aligned} I_\nu(0,0) &= \int_0^\infty B_\nu(\tau)\mathrm{e}^{-(\tau_\nu+\tau_l)}\left(1+\frac{l_\nu}{k_\nu}\right)d\tau_\nu \\ &= \int_0^\infty B_\nu(\tau)\mathrm{e}^{-\tau_\nu}[1-(1-\mathrm{e}^{-\tau_l})]\left(1+\frac{l_\nu}{k_\nu}\right)d\tau_\nu. \end{aligned} \tag{7.1}$$

Since the intensity in the continuum is given by

$$I_\nu^c(0,0)=\int_0^\infty B_\nu(\tau)\mathrm{e}^{-\tau_\nu}\,d\tau_\nu,$$

the dip in the continuum may be written

$$\Delta I_\nu = I_\nu^c(0,0)-I_\nu(0,0)=\int_0^\infty B_\nu(\tau)\mathrm{e}^{-\tau_\nu}\left[-\frac{l_\nu}{k_\nu}+(1-\mathrm{e}^{-\tau_l})\left(1+\frac{l_\nu}{k_\nu}\right)\right]d\tau_\nu. \tag{7.2}$$

From equation (5.5) we have

$$\tau_l=\int_0^{\tau_\nu}\frac{l_\nu}{k_\nu}\,d\tau_\nu,$$

and equation (7.2) becomes

$$\begin{aligned} \Delta I_\nu &= \int_0^\infty B_\nu(\tau)\mathrm{e}^{-\tau_\nu}\left[-\frac{l_\nu}{k_\nu}+\int_0^{\tau_\nu}\frac{l_\nu}{k_\nu}\left(1+\frac{l_\nu}{k_\nu}\right)d\tau_\nu\right]d\tau_\nu \\ &= \int_0^\infty B_\nu(\tau)\mathrm{e}^{-\tau_\nu}\left[-\frac{l_\nu}{k_\nu}+\int_0^{\tau_\nu}\frac{l_\nu}{k_\nu}\,d\tau_\nu\right]d\tau_\nu, \end{aligned} \tag{7.3}$$

to the first order. We now require to show this is in fact an alternative form of the equation used in the method of the Planckian gradient (equation (5.8)), i.e. equation (7.3) may be written

$$\begin{aligned}\Delta I_\nu &= -\int_0^\infty B_\nu(\tau)\left[-\frac{l_\nu}{k_\nu}+\int_0^{\tau_\nu}\frac{l_\nu}{k_\nu}\,d\tau_\nu\right]d(\mathrm{e}^{-\tau_\nu})\\ &= -\left|B_\nu\left[-\frac{l_\nu}{k_\nu}+\int_0^{\tau_\nu}\frac{l_\nu}{k_\nu}\,d\tau_\nu\right]\mathrm{e}^{-\tau_\nu}\right|_0^\infty+\int_0^\infty\frac{dB_\nu}{d\tau_\nu}\left[-\frac{l_\nu}{k_\nu}+\int_0^{\tau_\nu}\frac{l_\nu}{k_\nu}\,d\tau_\nu\right]\mathrm{e}^{-\tau_\nu}\,d\tau_\nu\\ &\qquad+\int_0^\infty B_\nu\left[\frac{l_\nu}{k_\nu}-\frac{d}{d\tau_\nu}\left(\frac{l_\nu}{k_\nu}\right)\right]\mathrm{e}^{-\tau_\nu}\,d\tau_\nu\\ &= -\left[B_\nu\frac{l_\nu}{k_\nu}\right]_{\tau_\nu=0}+\int_0^\infty\frac{dB_\nu}{d\tau_\nu}\left[-\frac{l_\nu}{k_\nu}+\int_0^{\tau_\nu}\frac{l_\nu}{k_\nu}\,d\tau_\nu\right]\mathrm{e}^{-\tau_\nu}\,d\tau_\nu\\ &\quad-\int_0^\infty B_\nu\frac{d}{d\tau_\nu}\left(\frac{l_\nu}{k_\nu}\right)\mathrm{e}^{-\tau_\nu}\,d\tau_\nu-\left|B_\nu\frac{l_\nu}{k_\nu}\mathrm{e}^{-\tau_\nu}\right|_0^\infty+\int_0^\infty\frac{dB_\nu}{d\tau_\nu}\frac{l_\nu}{k_\nu}\mathrm{e}^{-\tau_\nu}\,d\tau_\nu\\ &\qquad+\int_0^\infty B_\nu\frac{d}{d\tau_\nu}\left(\frac{l_\nu}{k_\nu}\right)\mathrm{e}^{-\tau_\nu}\,d\tau_\nu\\ &= \int_0^\infty\frac{dB_\nu}{d\tau_\nu}\left[\int_0^{\tau_\nu}\frac{l_\nu}{k_\nu}\,d\tau_\nu\right]e^{-\tau_\nu}\,d\tau_\nu. \qquad (7.4)\end{aligned}$$

An attempt was therefore made to use equation (7.3) as a numerical check on the accuracy of the computations made in the method of the Planckian gradient.

Comparing equations (5.9) and (5.12) we find

$$\int_0^{\tau_\nu(\tau_0)}\frac{l_\nu}{k_0}\,d\tau_0\propto\int_0^{\tau_\nu(\tau_0)}\frac{10^{-V\theta}}{uk_0}\,d\tau_0$$

and l_ν/k_ν is therefore easily obtained since $l_\nu/k_\nu=(l_\nu/k_0)(k_0/k_\nu)$, all other factors have been previously computed and hence equation (7.3) may be evaluated. A feature of the computations is the negative contribution to the absorption in the upper layers which subtracts from the "integrated" absorption in the lower layers. Here the contribution from the very deep layers is most important and it was found that the method could only be applied in the case of the Swihart model, which is defined to great depth. The equation (7.3) is moderately insensitive to small variations in the parameters and should provide a good numerical check for models defined to sufficiently great depth.

(B) Since the models of Vitense and Claas are not defined to sufficiently great depth to allow the application of equation (7.3) recourse was made to Unsöld's equation (equation (4.8))

$$\Delta I_\nu=\int_0^\infty\frac{l_\nu}{k_\nu}\left[\int_{\tau_\nu}^\infty B_\nu\mathrm{e}^{-\tau_\nu}\,d\tau_\nu-B_\nu\mathrm{e}^{-\tau_\nu}\right]d\tau_\nu. \qquad (7.5)$$

It has been established that this equation is equivalent (equation (6.5)) to the form (5.8) used in the method of the Planckian gradient. It was found however that the results obtained by equation (7.5) are extremely sensitive to small variations in the values of

$$\int_0^\infty B_\nu\mathrm{e}^{-\tau_\nu}\,d\tau_\nu \text{ and } \int_0^{\tau_\nu}B_\nu\mathrm{e}^{-\tau_\nu}\,d\tau_\nu.$$

The results obtained by the above methods are compared with the Planckian gradient results in the following table.

TABLE VIII

Model	Planckian Gradient method	Check (B) method	Check (A) method
Claas	$(Z) = 124{\cdot}7 \times 10^{-16}$	$126{\cdot}9 \times 10^{-16}$	...
Vitense	$(Z) = 96{\cdot}6 \times 10^{-16}$	$86{\cdot}8 \times 10^{-16}$	...
Swihart	$(Z) = 65{\cdot}3 \times 10^{-16}$	$64{\cdot}0 \times 10^{-16}$	$61{\cdot}8 \times 10^{-16}$

Equivalent width $W_\lambda = \text{const.}\ (Z)A$.

It must be emphasized however that only in the case of the Swihart model, where the model is defined to large depth, are the numerical results of the check methods reliable, and even in this case are not to be preferred to the Planckian gradient calculation (i.e. in the check **(B)** method the results are extremely sensitive to small variations in $\int B_\nu e^{-\tau_\nu} d\tau_\nu$, and the check **(A)** method shows an appreciable contribution even at very large depth). Again the apparently excellent agreement obtained for the Claas model can only be regarded as extremely fortuitous in that a reduction of 0·010 in the value of $\int_0^\infty B_\nu e^{-\tau_\nu} d\tau_\nu$, which is easily obtained by a reasonable variation in the extrapolation of Fig. 2, reduces the value of (Z) to approximately 108×10^{-16}. For the Vitense model the agreement is only moderate but here again a similar increase of 0·010 in $\int_0^\infty B_\nu e^{-\tau_\nu} d\tau_\nu$ increases the value of (Z) to approximately 102×10^{-16}. We may conclude therefore that, for the Swihart model, the agreement between the Planckian gradient result and the results obtained by the check methods is very good. For the Claas and Vitense models the Planckian gradient results are well within the degree of error possible in the results of the check methods.

8. *Discussion of results.*—The method of weighting functions developed by Unsöld and Minnaert leads to the results, for the nitrogen abundance, shown in Table V. The method of the Planckian gradient developed in the present paper leads to the substantially lower values of the nitrogen abundance (Table VII):

Claas model	Vitense model	Swihart model
$\log A_N = 7{\cdot}71$	$\log A_N = 7{\cdot}81$	$\log A_N = 7{\cdot}93$

(on the basis $\log A_H = 12{\cdot}00$)

The comparison of the two methods, as presented in Section 6, leads to an argument which, in the opinion of the author, is sufficiently in favour of the method of the Planckian gradient, in the case of nitrogen, to necessitate the exclusion of the results obtained by the method of weighting functions.

Although the above results indicate that the derived nitrogen abundance is moderately insensitive to the atmospheric model chosen, we would require, in estimating the most probable value of $\log A_N$, some measure of the reliability of each of the models. This will be considered in a subsequent paper.

(i) *Previous determinations.*—Hunaerts (**8**), in 1950, determined the abundance of nitrogen from measured intensities of rotational lines in the NH molecular band and obtained the value $\log A_N = 9{\cdot}02$. The molecular abundance has first to be determined by a curve of growth method and this requires a knowledge of the oscillator strengths of the molecular transitions. A great deal of doubt however still exists with regard to these f-values, and Hunaerts points out that

the values adopted may be incorrect by appreciable factors. The atomic abundance may now be determined by consideration of the dissociation equilibrium, but here additional uncertainties arise due to the inadequate data concerning the dissociation energies. Hunaerts concludes that the estimated atomic abundance is very uncertain.

Unsöld (**19**), in 1948, in an extensive analysis of the solar atmosphere, obtained the value $\log A_N = 8{\cdot}61$ by a curve of growth method. Slightly low values of ionization potential were adopted for the five lines considered although the error introduced is probably slight. The method does however suffer from the fact that the detailed structure of the atmosphere is not considered and an idealized atmosphere is assumed.

(ii) *Comments.*—A major source of uncertainty in the abundance calculations is the measurement of the equivalent widths of the weak nitrogen lines as presented in the *Utrecht Photometric Atlas.* However, since the nitrogen abundance, as determined for each of the nine lines, shows only a small spread about the mean value (Table VII), it is probable that this restriction is not too severe. When more definite measurements become available, simple recalculation in Table VII will provide any necessary correction in the final estimate of the nitrogen abundance.

The hydrogen/metal ratio, $\mathscr{A}$, in each of the models has been taken to be $\log \mathscr{A} = 3{\cdot}8$. This is probably rather low and a value of 3·90 or 3·95 may be a better estimate. Further, the helium abundance in the atmosphere has been ignored but, as shown by Claas (**5**), abundance determinations will be rather insensitive to this factor.

It may be considered to be a disadvantage of the method of the Planckian gradient that no recourse is made to the accurate determinations of the limb-darkening of the Sun, and that consequently great stress is placed upon the accuracy of the theoretical model. It must be pointed out however that the Claas and Vitense models are themselves based upon the observed limb-darkening results in the regions where these results are most reliable. The Swihart model however is more at variance with the limb-darkening results.

The author would like to thank Dr B. Strömgren for suggesting this problem and for the time he most generously spent in many helpful and stimulating conversations during the author's visits to the Yerkes Observatory. The author is also indebted to Dr Swihart for permission to utilize his results in advance of his own publications and to Professor C. W. Allen for the interest he has shown in the progress of this research.

Department of Theoretical Physics,
The University,
Manchester 13 :
1958 *April.*

References

(1) Aller, L., *Astrophysics*, Vol. 1 (New York : Ronald Press Co.), 1953.
(2) Barbier, D., *Ann. d'Astrophys.*, **9**, 173, 1946.
(3) Bates, D. R. and Damgaard, A., *Phil. Trans.*, **242**, A, 101, 1949.
(4) Chalonge, D. and Kourganoff, V., *Ann. d'Astrophys.*, **9**, 69, 1946.
(5) Claas, W. J., *Rech. Obs. Utrecht*, **12**, 13, 1951.
(6) Goldberg, L., *Ap. J.*, **82**, 1, 1935.
(7) Goldberg, L., *Ap. J.*, **84**, 11, 1936.

(8) Hunaerts, J., *Trans. I.A.U.*, **7**, 462, 1950.
(9) Lyttkens, E., Uppsala University, communicated by B. Strömgren.
(10) Minnaert, M., *Zs. f. Astrophys.*, **12**, 313, 1936.
(11) Minnaert, M., Mulders, G. F. W. and Houtgast, J., *Photometric Atlas of the Solar Spectrum*, Utrecht, 1940.
(12) Minnaert, M., *B.A.N.*, **10**, 339, 1948.
(13) Moore, C. E., *Atomic Energy Levels*, Nat. Bur. Std., Circ. No. 467, 1948.
(14) Russell, H. N., *Ap. J.*, **83**, 129, 1936.
(15) Strömgren, B., *Pub. Medd. København Obs.*, **138**, 1944.
(16) Swihart, T. L., *Ap. J.*, **123**, 139, 1956.
(17) Swihart, T. L., *Ap. J.*, **123**, 143, 1956.
(18) Unsöld, A., *Zs. f. Astrophys.*, **4**, 339, 1932.
(19) Unsöld, A., *Zs. f. Astrophys.*, **24**, 306, 1948.
(20) Vitense, E., *Zs. f. Astrophys.*, **34**, 209, 1954.

EXCITATION TEMPERATURES FOR THE CN EMISSION FROM THE LOW CHROMOSPHERE

D. V. Thomas

(Received 1958 May 2)

Summary

Microphotometer tracings have been made of the region of the CN 3883 A band system, which is a prominent feature of the flash spectrogram obtained by Redman at the 1952 eclipse. The CN bands are seriously affected by blending, but enough unaffected lines have been found to enable the rotational intensity distribution in the 0–0 band to be measured at three heights below about 400 km. Self absorption is important, particularly at the band heads, and its effects have been estimated. The measurements indicate a negative excitation temperature gradient, the temperature at about 400 km being $\simeq 4500°$, and the value of the gradient uncertain. However, the CN emission may not be inconsistent with the positive kinetic temperature gradient of de Jager's most recent chromospheric model, if departures from local thermodynamical equilibrium and the imperfection of the observational data are taken into account.

---

1. *Introduction.*—Until quite recently it was thought that there was strong evidence both for a high ($\sim 30\,000°$K) and a low ($< 10\,000°$K) kinetic temperature for the low chromosphere. The conflicting evidence has been summarized and discussed by van de Hulst (1953). While a low temperature is now generally accepted, its exact value and gradient are still uncertain. One of the most prominent features of the flash spectrogram obtained by Redman at the total eclipse of 1952 February 25 is the 3883 A band system of cyanogen. In principle, these bands supply an excellent means for obtaining accurate temperatures, as the relative intensities of the lines composing the bands and of the bands themselves depend strongly on the temperature. However, in practice, measurements of the intensity of the CN emission in the flash spectrum yield directly only the relative populations of different energy levels of the molecule, and hence an effective excitation temperature. The corresponding kinetic temperature is then a matter of interpretation in terms of the physical conditions assumed to exist in the chromosphere.

Determinations of molecular excitation temperatures in the low chromosphere have already been published by Blackwell (1955), Pecker and Athay (1955) and Parker (1955). Using Redman's 1940 eclipse spectrogram (Redman 1942) Blackwell measured lines of the weak 4216 A CN and 4300 A CH bands, neglecting the band heads. Pecker and Athay's discussion is confined to the 3883 A CN band head on the High Altitude Observatory's 1952 slitless spectrograms, and is open to serious criticism. Parker, working with the Mount Wilson 75-ft spectrograph outside eclipse, had the advantage of a high resolution, but needed to employ a difficult correction for the contribution of photospheric radiation (both scattered and direct) to the intensities of the Swan C_2 bands. These authors' results are

discussed in the light of the present work in Section 7. The excitation temperatures determined in this paper are based upon the largest dispersion slit spectrogram yet obtained at an eclipse. In the analysis, both band heads and individual lines have been considered and allowance has been made for self-absorption.

2. *Observational material.*—Only the essential details of the instrument used and the procedure followed at the 1952 eclipse need be noted here, as a full account has already been given by Redman (1953, 1955). The slit spectrograph employed a 15000 lines per inch 6-in concave grating of 21-ft radius of curvature in a Wadsworth mounting. The resulting dispersion in the wave-length range 3400 A to 4100 A was 2·4 A/mm. The instrumental profile was determined at the eclipse site by means of a mercury isotope lamp. The excellent flash spectrogram used in the present work was obtained during an exposure of 1·5 sec immediately preceding third contact, the coelostat being rated to follow the Moon. An attempted relative intensity calibration on the eclipse plate itself was unsuccessful. Four photospheric spectrograms were therefore obtained on another plate from the same batch with a Hilger rhodium-on-quartz step wedge in front of the slit. The two plates were processed identically and may be assumed to possess the same characteristics. The transmission factors of the step wedge were determined at the National Physical Laboratory.

A portion of the flash spectrogram in the region of the principal CN band heads is reproduced in Plate 7. The variation in intensity perpendicular to the direction of the dispersion is due partly to irregularities on the limb of the Moon and dust on the jaws of the slit, partly to the fact that positions along the slit represent, in some measure, heights above the photosphere, and partly to the spicular structure of the chromosphere. Initially, it is sufficient to denote positions along the slit by the arbitrary system of "levels" indicated in Plate 7, as the analysis of each level is independent. Only when correlating the results from different levels is it necessary to know even their relative heights, which are easily obtained. The determination of the actual effective chromospheric heights is a difficult problem, but they are necessary only for the final interpretation of the results. During the exposure the slit, following the Moon, scans the chromosphere at a rate of about 400 chromospheric km/sec. The "seeing" was estimated by Redman to be 2″, corresponding to 1400 chromospheric km. As a result, the recorded emission originates in varying proportions from slices right through the chromosphere, covering a range of about 2000 km of the chromosphere and the (occulted) photosphere. A geometrical determination of effective heights is therefore impossible. Redman and Suemoto (1954), in their study of the metal lines in this spectrogram, compared the relative intensities of some prominent lines with their relative intensities on the slitless spectrograms obtained by Houtgast (1953) at the same eclipse. In this way they estimated that Levels 1, 2 and 3 correspond to heights < 50 km, < 100 km and $\simeq 600$ km, respectively. According to Houtgast the intensity gradient in the chromosphere is much steeper for the CN 3883 A band head than it is for the metal lines. The effective heights of the CN emission must therefore be somewhat less than the above figures. The adopted heights for the three levels, of which an analysis has subseqently been made, are: Level $1 \simeq 0$ km; Level $2 \simeq 50$ km; Level $3 \simeq 400$ km.

In order to obtain the intensities of the CN lines in the flash spectrum, tracings of Levels 1, 2 and 3 were made with the Cambridge Observatories' recording densitometer. Levels 2a and 3a proved to be unsuitable because of the weakness

of the CN lines and Levels 1a and 1b because of their high background intensities. The characteristic curve of the plate was obtained from tracings made across the step wedge spectra, no change with wave-length being detectable. A mean characteristic curve for the microphotometer tracings was then derived, the range of measurable intensities being represented by 100 units on an arbitrary relative intensity scale. Fluctuations in the dark current and clear glass transmission, etc., produce an estimated maximum error of ± 2 units in intensities obtained from this mean curve. The microphotometer tracings were reduced to direct intensities at the Dominion Astrophysical Observatory, B.C., using the Beals (1944) intensitometer. The completed records have an amplitude of 10 in., corresponding to 100 units on the above scale. At various points they were checked with a point-by-point reduction and found to be very satisfactory. The record of Level 1 in the region of the CN 0–0 band head is reproduced in Fig. 1.

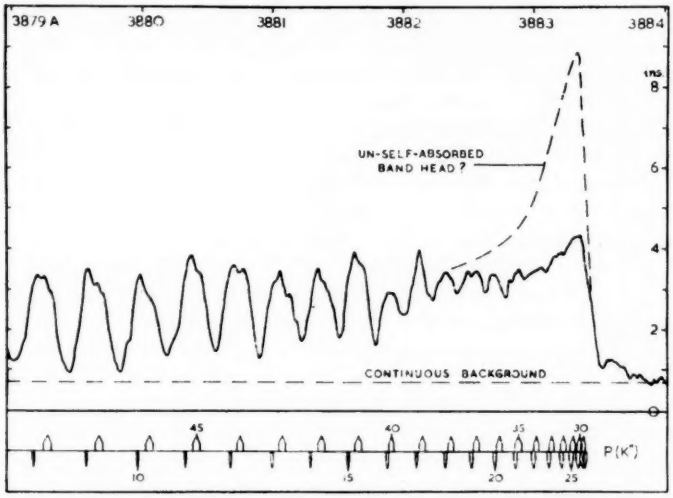

FIG. 1.—*Reproduction of the region of the* CN 0–0 *band head on the direct intensity record of Level* 1. *Theoretical positions of individual lines are indicated below.*

From measurements of the positions of 75 sharp lines, whose identifications and wave-lengths were obtained from the Revised Rowland Table of photospheric wave-lengths (St John 1928), the dispersion of the plate was found to be linear over the range covered by the CN bands. The same lines were identified on the intensity records, the dispersion obtained from their measured positions being 82·86 mm/A, showing the magnification of the records over the plate to be just less than 200 times. The maximum error in the position of a line on the records was estimated to be ± 4 mm ($\pm 0{\cdot}05$ A).

3. *The ultra-violet CN bands.*—The ultra-violet bands of cyanogen arise from the transition between the $X\,^2\Sigma^+$ and $B\,^2\Sigma^+$ electronic states of the CN molecule. The sequence $\Delta v = 0$ forms a series of bands degraded towards the violet with its head at 3883 A, the head of the 0–0 band. In $^2\Sigma$ electronic states the rotational levels with quantum number K are split into two components

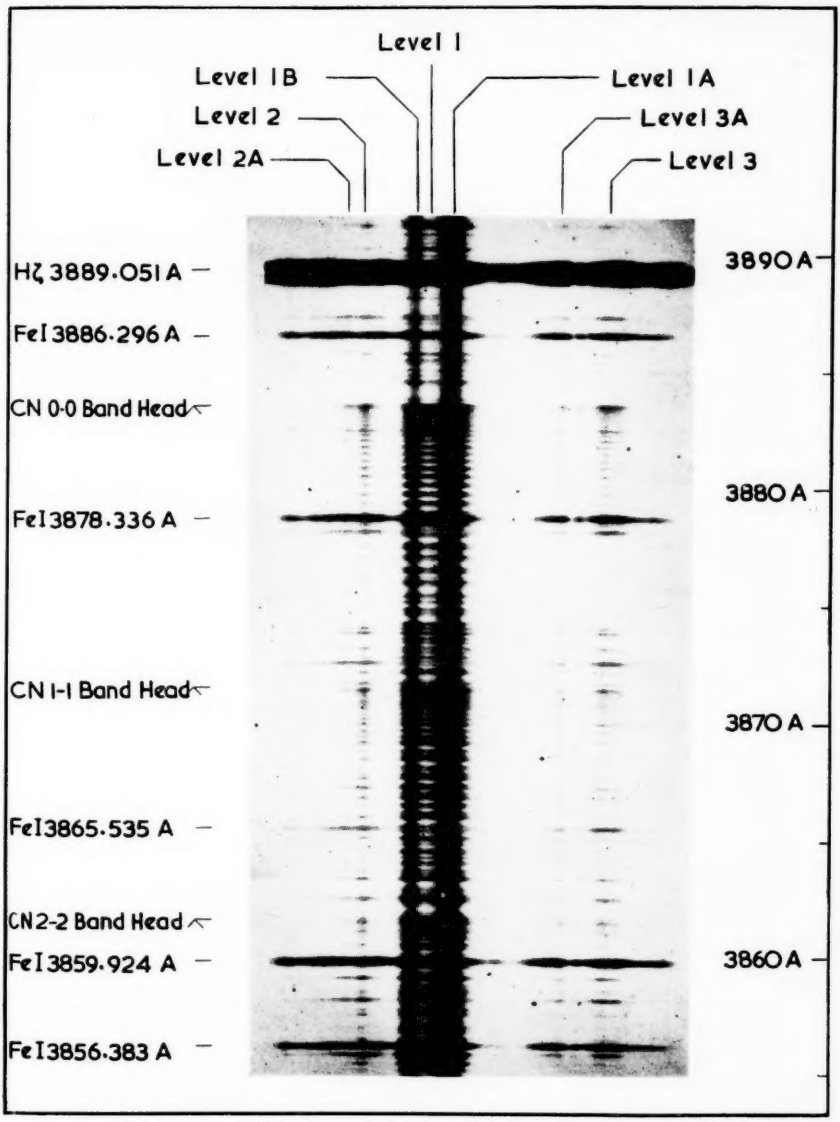

The region of the principal CN *band heads in Redman's* 1952 *eclipse spectrogram. Enlargement* ×9 *(approx.).*

with quantum numbers $J = K \pm \frac{1}{2}$. As a result of the selection rules $\Delta K = \pm 1$, $\Delta J = 0, \pm 1$, a $^2\Sigma$–$^2\Sigma$ band consists of a doublet P branch, a doublet R branch, and two satellite P-form and R-form Q branches. The satellite branches are very much less intense than the P and R branches, so the CN bands are often treated as $^1\Sigma$–$^1\Sigma$ bands ($J = K$), each P and R branch doublet being considered as a single line at the centre of the doublet. The relations governing the wave-numbers of the individual lines in a $^1\Sigma$–$^1\Sigma$ band are given in the standard texts (e.g. Herzberg 1950). The P and R branch relations may be expressed as one equation with the " running number "m as argument:

$$\sigma(m) = A + Bm + Cm^2 + Dm^3 + Em^4 + \ldots, \tag{3.1}$$

$$\left.\begin{aligned} &\text{where for the } P \text{ branch} \quad m = -K'', \\ &\text{and for the } R \text{ branch} \quad m = K'' + 1, \end{aligned}\right\} \tag{3.2}$$

and the constants $A \ldots E$ are easily determined functions of the rotational constants of the molecule. The most recent rotational constants, due to Douglas and Routly (1955), have been adopted. The values of the constants are such that for the most important bands of the 3883 A band system, $\sigma(m)$ is a minimum at $m \simeq -30$, so that a band head is formed in the P branches near P (30).

The most extensive laboratory measurements of the CN 3883 A band system are still those made by Uhler and Patterson (1915). There is no systematic difference between their wave-lengths and those recently published by Weinard (1955): as the random differences are generally less than 0·005 A, which is only one-tenth of the possible error in the intensity records, the accuracy of the published wave-lengths is more than sufficient for the purpose of identifying CN lines on the records.

For each of the 0–0 ... 4–4 bands, the gap corresponding to the forbidden line $P(0)$ has been detected, so the quantum numbering of the R branches, and the P branches as far as the band heads, is simply obtained by following the regular series of lines. The numbering of the returning portions of the 0–0 and 1–1 P branches has been obtained by Smit-Miessen and Spier (1942); they compared Uhler and Patterson's measures with values computed from equation (3.1), whose coefficients were determined from the wave-numbers of lines already indentified. The identifications have been confirmed by computing the coefficients in (3.1) independently from Douglas and Routly's band constants. The P branches of the other bands are too greatly obscured in the flash spectrum for identifications to be necessary.

The positions of all Uhler and Patterson's lines whose quantum numbering had been determined were marked on the intensity records. The general concentration of lines in the ultraviolet region of the flash spectrum is so great that even the Rowland table of *photospheric* wave-lengths does not contain them all. It cannot be determined with certainty, therefore, that any particular CN line is unblended. For this reason, and also because of the irregularities in the dispersion of the records, certain identification of lines on the records as CN lines is not possible.

4. *Intensity distribution in CN bands in emission.*—As the flash spectrum does not possess an absolute intensity calibration, the present work is concerned only with the relative intensities of the lines emitted as a result of the transition $B\,^2\Sigma \rightarrow X\,^2\Sigma$ at any particular temperature. Assuming a Boltzmann distribution

of molecules amongst the energy states corresponding to an excitation temperature T, the relative intensities of lines emitted as a result of transitions from the levels (v', K') of the upper state to the levels (v'', K'') of the lower state are given by

$$I_{v'K'-v''K''} = C\sigma^4_{v'K'-v''K''} P_{v'-v''} \exp\left\{G'(v')\frac{hc}{kT}\right\} S_{K'-K''} \exp\left\{-F'_{v'}(K')\frac{hc}{kT}\right\}, \tag{4.1}$$

where C = a constant determined by the transition, the temperature and the total number of molecules,

$\sigma_{v'K'-v''K''}$ = the wave-number of the line,

$P_{v'-v''}$ = the vibrational transition probability,

$S_{K'-K''}$ = the rotational line strength, and

$G'(v'), F'_{v'}(K')$ = the vibrational and rotational term values of the upper state, dependent upon the band constants. The relative intensities of the rotational lines in a band of the $\Delta v = 0$ sequence are therefore given by

$$I_{K'-K''} = \text{constant}\ \sigma^4_{K'-K''} S_{K'-K''} \exp\left\{F'_v(K')\frac{hc}{kT}\right\}. \tag{4.2}$$

The line strengths for the various branches of $^2\Sigma$–$^2\Sigma$ and $^1\Sigma$–$^1\Sigma$ bands have been derived by Mulliken (1927). When $K' \geqslant 5$, the intensities of the satellite Q branches of a $^2\Sigma$–$^2\Sigma$ band are negligible, and the combined intensity of the two components of a P or R branch doublet differs by less than 1 per cent from the intensity of the corresponding singlet in a $^1\Sigma$–$^1\Sigma$ band. The intensities of the CN lines are therefore given to a sufficient approximation by (4.2), where $S_{K'-K''}$ now represents the line strengths for $^1\Sigma$–$^1\Sigma$ bands, i.e.

$$\left.\begin{aligned} &\text{for the } P \text{ branch } && S_{K'-K''} = 2(K'+1) \\ &\text{and for the } R \text{ branch } && S_{K'-K''} = 2K', \end{aligned}\right\} \tag{4.3}$$

and $\sigma_{K'-K''}$ and $F_v'(K')$ now refer to the centres of the doublets.

A useful modification of (4.2) is obtained by taking logarithms:

$$\ln\left\{\frac{I_{K'-K''}}{\sigma^4 S_{K'-K''}}\right\} = \text{constant} - F_v'(K')\frac{hc}{k}\cdot\frac{1}{T}. \tag{4.4}$$

Plotting $\ln\{I_{K'-K''}/\sigma^4 S_{K'-K''}\}$ against $F_v'(K')hc/k$, where the I's are measured intensities, a least-squares method yields the slope $-1/T$ of the straight line relation, and hence the temperature directly.

The relative intensities of homologous lines in the v–v and 0–0 bands can be obtained from (4.1). Taking $F_v'(K') = F_0'(K')$ and substituting the wave-numbers of the respective band origins for those of the individual lines (these approximations are justified by the lower accuracy of the measures subsequently made on the 1–1 ... 4–4 bands and the uncertainties in the values of the vibrational transition probabilities), the relation simplifies to

$$\frac{I(v, K)}{I(0, K)} = \frac{\sigma^4_{v-v}}{\sigma^4_{0-0}}\cdot\frac{P_{v-v}}{P_{0-0}}\cdot\frac{\exp\{-G'(v)hc/kT\}}{\exp\{-G'(0)hc/kT\}}. \tag{4.5}$$

The transition probabilities adopted are those computed by Pillow (1953). The small differences between these and the more recent laboratory values of Floyd and King (1955) have no significant effect on intensities calculated from (4.5).

5. *Determination of effective excitation temperatures*

5.1. *Preliminary estimates.*—As the CN lines are strongest on the intensity records of Level 1, this level was selected for preliminary measurements. An immediate difficulty is the presence of a continuous background caused partly by the continuous radiation from the chromosphere itself, and partly by scattered photospheric radiation from the first traces of a Baily's bead (see Redman 1955). The background is distorted in many places by the overlapping of large numbers of faint lines and the wings of strong lines, and by errors in the photometric reductions. Superimposed upon it are fluctuations due to the photographic grain and dust on the plate. Photometric errors due to the use of a mean characteristic curve in the reduction to direct intensity can be reduced by drawing the apparent rather than the mean continuous background, assuming it to vary smoothly between those regions of the spectrum apparently not enhanced by overlapping weak lines. The background was determined separately for two limiting cases: the lowest possible background, which assumes that the major small-scale irregularities are weak lines, and the highest possible background, which assumes that these irregularities are all " noise ". An analysis based on an estimation of the exact position of the background has no advantage over an interpolation between the results obtained from the two limiting cases considered.

It appears from the intensity records of Level 1 (Fig. 1) that the 0–0 band head is probably affected by self-absorption; the peak intensity of the band head is very little greater than the peak intensities of the pairs of lines nearby. The simplest method of obtaining a preliminary estimate of the temperature therefore appeared to be to find the distribution of intensities amongst the rotational lines of the 0–0 band and make use of (4.2). The intensities of all the lines in positions where 0–0 band lines were predicted were measured with a planimeter, assuming the lowest possible background for this preliminary determination. The total area of each P branch *pair* (formed by the near coincidence of lines of the proceeding and returning portions of the P branch) and the total intensity of the band head, in three sections, were also measured. The best method of representing the measures graphically is that adopted in Fig. 2, the abscissa of which is a linear scale in the running number m reflected at $m = -28$, the head of the P branch. This makes possible the representation of the intensities of the P branch pairs, since the nearly coincident components of the pairs appear as exactly coincident in the figure. From $m \simeq -21$ to -35 the separation of the individual components of the doublets is of the same order as that of the doublets themslves (see Fig. 1), so the band head would not exhibit the "pair" formation even with complete resolution of the lines. However, as it is only possible to measure the total intensity of the band head, the representation is not rendered invalid, and it is convenient for comparing measured and theoretical intensity distributions.

No account was taken of possible blends, so the intensities in Fig. 2 are in effect maximum intensities. As perturbed lines were omitted, the plotted points should all lie on or above (for unblended and blended lines, respectively) the intensity distribution curve for the appropriate temperature. The intensity curves for three temperatures, calculated by means of (4.2), are drawn in Fig. 2 to scales such that all the plotted points lie on or above the curves. Comparing the three curves with the measured intensities, it appears that very few of the measured lines are unblended. The distribution for 7000° fits the measures best but requires considerable self-absorption at the band head. The conclusion that the band head is depressed by self-absorption can be avoided by assuming a

temperature of 10000°, but this would necessitate large blending corrections for all the strong lines and no correction at all for a number of weak lines. The effective rotational temperature therefore appears to be in the region of 7000°, not as high as 10000°, and probably not as low as 4000°.

An approximate blending correction to the measured intensities was derived from consideration of the average intensities of lines immediately to the red of the 0–0 band head. However, the corrected intensities merely confirm the indication of Fig. 2 of a rotational temperature in the region of 7000°.

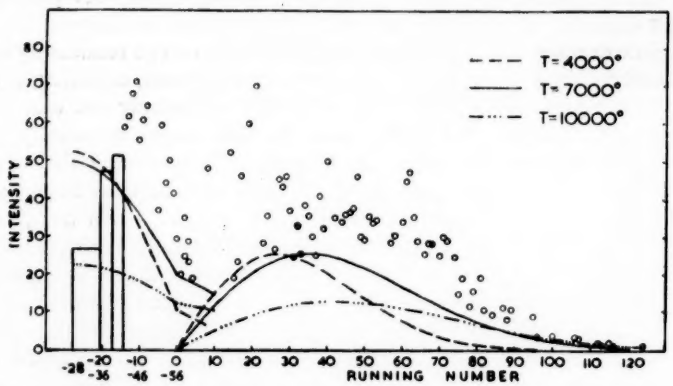

FIG. 2.—CN 0–0 *band, Level* 1*: uncorrected line areas (assuming lowest continuous background). In this and subsequent figures the points "* o *" represent the areas (= intensities) of the corresponding lines or "pairs" of lines. The area of each rectangle equals the total area (= total intensity) of the corresponding group of unresolved lines.*

Because of the suspected depression of at least the 0–0 band head by self-absorption, it would be unwise to attempt to obtain an estimate of the effective vibrational temperature by comparing the intensities of the band heads. The *P* branches are badly obscured, but the intensities of lines in the *R* branches of the various bands may be compared, utilising the relations (4.2) and (4.5). The areas of all the lines in positions where the *R* branch lines of the 1–1 ... 4–4 bands had been predicted were therefore measured, no attempt being made to allow for blends. The measured intensities were plotted on diagrams of running number versus intensity, together with the intensity distributions corresponding to those already drawn in Fig. 2 for the 0–0 band. While the 7000° curves agree best with the measures, neither the curves for 4000° nor those for 10000° violate the condition that all the measured points should lie on or above the curves.

5.2. *Computed CN line profiles.*—It is not possible to deduce reliable CN line profiles from the intensity records because all the CN lines are unresolved doublets and only a very few appear to be free from blends. However, it is possible to compute profiles for an assumed temperature and turbulence of the emitting gas, knowing the characteristics of the recording apparatus. It may safely be assumed that the effects of collision and radiation damping are negligible for all except the strongest chromospheric lines. The emitted CN line with wavelength λ_0 will therefore have a Doppler profile with equation

$$I(\lambda) = C \exp\left\{ -\left(\frac{\mu}{2RT} + \frac{1}{\xi_0^2}\right)\frac{c^2}{\lambda_0^2}(\lambda - \lambda_0)^2 \right\}, \qquad (5.1)$$

where μ is the molecular weight, T is the kinetic temperature, and the probability

of a molecule having a turbulent velocity in the line of sight between ξ and $\xi + d\xi$ is proportional to $\exp\{-\xi^2/\xi_0^2\}d\xi$. A half-width of 0·073 A was obtained for all CN lines on computing the profile (5.1) with the following assumptions: the kinetic temperature equal to the estimated effective excitation temperature, i.e. 7000°, a turbulence $\xi_0 = 2{\cdot}7$ km/sec, as determined by Redman and Suemoto (1954) from metal lines at the identical Level 1, λ_0 constant for all CN lines.

The effect of the apparatus function of the spectrograph and the width of the microphotometer slit on the emitted line profile was determined by the method of Voigt functions described by van de Hulst and Reesinck (1947). The resulting computed profile of a CN line on the intensity records of Level 1 has a half-width of 8·9 mm (0·11 A). The variation in the computed profile with wave-length is negligible for the wave-length range covered by the CN bands. The total variation in the computed half-width, due to an assumed probable error of $\pm 0{\cdot}5$ km/sec in the adopted ξ_0 and to a temperature range of $\pm 3000°$ about the adopted 7000°, is less than ± 10 per cent. The computed CN line profiles are thus relatively insensitive to the adopted kinetic temperature, and can be used to determine the intensities of the CN lines on the records more accurately.

5.3. *Effective excitation temperature of Level* 1.—For the reasons pointed out earlier, the predicted line positions may be in error by ± 4 mm, and the fact that the majority of CN lines are affected by blending means that in most cases the exact line positions cannot be determined more accurately by inspection. Thus in each case lines having the computed profiles were constructed within ± 4 mm of the predicted position such that the resulting line intensity was the maximum possible consistent with the feature on the intensity record (the two components of the doublets were taken to have equal intensities). For those doublets unresolved by Uhler and Patterson, theoretical doublet separations were obtained from a diagram of the separations of the resolved doublets plotted against the rotational quantum number K'': the mean curve through the plotted points was extrapolated back to $K'' = 0$ in accordance with the relations governing the splitting of the rotational energy levels (Mulliken 1930).

As the half-widths of all the CN lines are the same, their intensities are proportional to their central intensities. Hence the height of the central ordinate of either component of a constructed doublet may be used instead of its area as a measure of its intensity. The intensities of the constructed lines of the 0–0 band are plotted in Fig. 3 (heavily blended lines are omitted). Individual lines could not be constructed in the unresolved portion of the band head, so its previously measured area was converted to the new intensity units by determining the area of a standard line profile.

The intensities in Fig. 3 are once again maximum intensities, apart from six lines (two of these constituting a P branch pair) which appear to be unblended and whose intensities may therefore be considered accurate. A least-squares solution of a plot of $\ln\{I/\sigma^4 K'\}$ versus $F_0'(K')hc/k$ for the three accurate R branch lines $R(14)$, $R(49)$ and $R(74)$, gives $T = 7300°$. The probable error, $\pm 200°$, does not give such a good idea of the likely maximum or minimum temperatures as the scatter $\pm 500°$, obtained by assuming each pair of points in turn to be correct. The computed temperature distributions for 7300° and 7800°, shown in Fig. 3, fit the R branch intensities almost equally well, but the band head again appears to be depressed by self-absorption.

Comparing the corresponding computed intensity distributions in the 1–1 ... 4–4 bands with the measured intensities of the constructed *R* branch lines, there appears to be no appreciable difference between the agreement for 7300° and 7800°, which is good in each case. Thus there is no detectable difference between the effective rotational and vibrational temperatures.

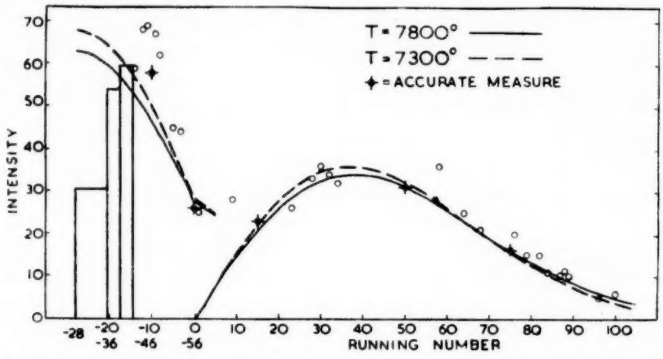

FIG. 3.—CN o–o *band, Level* 1: *intensities of constructed lines (assuming lowest continuous background).*

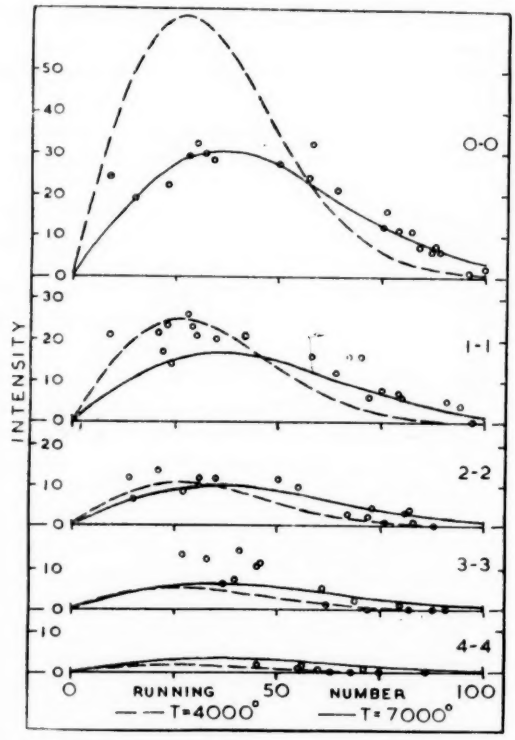

FIG. 4.—CN *R branches, Level* 1: *intensities of constructed lines (assuming highest continuous background).*

The effect of changing the assumed height of the continuous background was investigated by repeating the above procedure with the highest possible background level previously determined. A diagram similar to Fig. 3 was obtained, with $T = 7000°$ and a small probable error. The measures of the R branches are plotted in Fig. 4, from which it is clear that a vibrational temperature of 7000° requires intensities significantly in excess of the measured intensities for the 2–2, 3–3, and especially the 4–4 band. There are several possible explanations of this. First, there may be a considerable difference between the vibrational and rotational temperatures, but this should not be inferred from the above evidence alone. Secondly, if the assumed continuous background is too high then the intensities of the weaker lines and bands will have been reduced systematically, compared with the intensities of the stronger lines. Thirdly, if the continuous background has been correctly drawn then the vibrational–rotational temperature must be less than 7000°. In this case, the measured intensities of the 0–0 band must either all be too great because of blending, which seems unlikely, or the intensities of the strongest lines, in addition to the band heads, must be depressed by self-absorption. The theoretical intensity distributions for 4000°, drawn in Fig. 4, indicate that even such a low temperature as this might be possible if self-absorption is assumed to be sufficiently great.

It is clear from these results that the maximum possible excitation temperature for Level 1 is 7800°, obtained on the assumption of the lowest possible continuous background. Raising the continuous background level necessitates a progressive lowering of the excitation temperature and an increase in effects which must be attributed to self-absorption. A reliable estimate of the continuous background level and quantitative knowledge of the effects of self-absorption are therefore required to fix the excitation temperature accurately.

5.4. *Effective rotational temperatures of Levels* 2 *and* 3.—The absence of a detectable continuous background on the intensity records of Levels 2 and 3 is a considerable advantage, but because of the weakness of the CN lines, errors

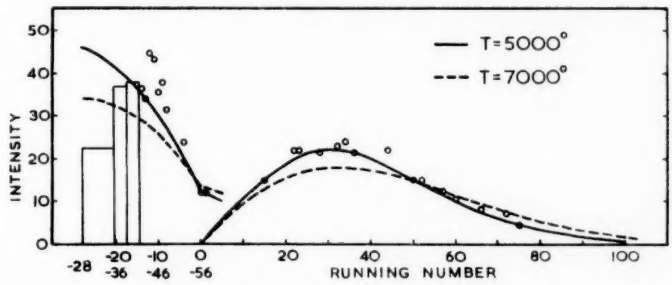

FIG. 5.—CN 0–0 *band, Level* 2: *intensities of constructed lines.*

in the photometry are proportionally greater. To minimise such errors, the zero intensity in the vicinity of each line was estimated from the original tracings. The line profile appropriate to Level 2 was then computed and the procedure followed for Level 1 employed to obtain the measured intensities in Fig. 5. The close agreement with a rotational temperature of 5000° is possibly fortuitous, as the band head exhibits a deficiency, probably due to self-absorption. However,

the intensity distribution for 7000° demonstrates that a temperature as high as this is most unlikely. The lines with $m > 75$ are too weak to be detected on the records, as are all the lines of the 3–3 and 4–4 R branches. A few lines of the 1–1 and 2–2 bands are measurable, but not enough for a vibrational temperature to be obtained.

The CN lines at Level 3 are so weak that it was not feasible to construct line profiles, so the procedure used to obtain a preliminary temperature for Level 1 from the 0–0 band had to be adopted. No attempt was made to detect lines in other bands. The measured intensities, converted to central ordinate intensity units, are plotted in Fig. 6 together with theoretical intensity distributions for 4000°, 5000° and 7000°. The measured intensities are maximum intensities, so a temperature of 4500° ± 500° seems most likely and 7000° unreasonably high. As in the cases of Levels 1 and 2 there are indications that self-absorption affects the band head.

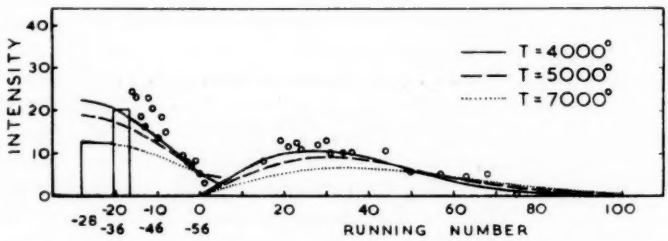

FIG. 6.—CN 0–0 *band, Level 3: measured intensities (uncorrected line areas).*

6. *Self-absorption.—Prima facie* evidence for the presence of self-absorption in the flash spectrum is provided by the conspicuous reversal of intensity in the centres of many lines of quite moderate intensity, some of which can be seen in Plate 7. However, it must be emphasized that self-reversal can only occur where there is a negative excitation temperature gradient, whereas self-absorption is inseparable from line emission by a gas in local thermodynamical equilibrium (L.T.E.), although in an optically thin layer (by definition) its effects are negligible. The theoretical treatment of self-reversal is a difficult problem, but fortunately it is not directly observed in the CN lines, so it may be assumed initially that the chromospheric CN is in L.T.E. at a single temperature. Even so, a new approach to the problem of self-absorption is necessary because, while previous work has been concerned with the profiles or equivalent widths of single lines, the CN bands consist of doublets with varying separations and unresolved groups of lines.

In the absence of self-absorption, the "ideal" emitted intensity of each component of a particular CN doublet will be given by the relations quoted in Section 4. Each component will have a profile given by (5.1), and the total line profile will depend on the doublet separation. Self-absorption will modify the profile of the emitted line. The intensity records show the emitted self-absorbed line broadened by the known apparatus function, but unchanged in total intensity. In principle, therefore, the "ideal" intensity of each component of a CN doublet can be deduced from the intensity records if the relation between "ideal" and "self-absorbed" intensity is known. The "ideal" intensity of emission from

a cylinder of the chromosphere in L.T.E. at a temperature T is

$$I_\nu' = B_\nu(T)\tau_\nu \tag{6.1}$$

where $B_\nu(T)$ is the Planck function and τ_ν is the optical thickness of the cylinder at the frequency ν. Taking self-absorption into account, the intensity of emission from the same cylinder is

$$I_\nu = B_\nu(T)\{1 - \exp(-\tau_\nu)\} \tag{6.2}$$

(see, e.g. Unsöld 1955). Hence the "self-absorbed" intensity is related to the "ideal" intensity by the equation

$$I_\nu = B_\nu(T)\{1 - \exp[-I_\nu'/B_\nu(T)]\}. \tag{6.3}$$

Two difficulties prevent the straightforward application of these principles. First, the intensity records do not have an absolute intensity calibration, so $B_\nu(T)$ in (6.3) is not known in terms of the relative intensity units adopted. Secondly, the removal of the effect of the apparatus is a practical impossibility in the case of a band head, and even in the simpler case of an unresolved doublet it would require mechanical integration, as the instrumentally broadened self-absorbed profile is not a Voigt function. However, if a value for the temperature is assumed, a theoretical CN band can be computed completely using the appropriate intensity relations of Section 4 and either measured or calculated wavelengths. Assuming a value for the Planck function, the corresponding self-absorbed band can be completely computed using (6.3). The areas of the observed lines and line groups on the intensity records (with due allowance for blends) should be equal to the areas of the corresponding computed lines, provided the assumptions regarding temperature and Planck constant are correct and the scale of the computed band has been correctly chosen. Hence, by trial and error, it should be possible to determine (approximately) whether the CN emission is in accordance with a chromosphere in L.T.E. and, if it is, to find the value of the corresponding absolute intensity scale of the records and the effective excitation temperature. This procedure was applied to the CN 0–0 band at Levels 1, 2 and 3.

In order to compute a theoretical band it is necessary to know the frequencies of the lines in the unresolved portions of the band head. These have been calculated by Smit-Miessen and Spier (1942), and their values have been adopted for the whole of the P branch. Doublet separations were obtained as described in Section 5.3. A rotational temperature of 4500° was adopted, this being the temperature previously derived for Level 3, where self-absorption must be least, and also the temperature obtained by Hunaerts (1947) from photospheric CN. The turbulence adopted was that appropriate to Level 1. The computed band need not be very accurate because the intensity records are subject to errors of many kinds already mentioned. It is therefore justifiable to take the positions of the lines correct only to the nearest millimetre (0·012 A) on the records, considerably reducing the labour involved in the computations. Portions of the approximate band profile were computed in a comparatively short time. The portions selected were the band head as far as the 3878 A Fe I line, a region which appears to be comparatively free from blends, the line P (56) which is also well observed, and those R-branch lines having theoretical doublet separations of an integral number of millimetres. The computed band, on an arbitrary intensity scale, is shown in Fig. 7.

To construct a corresponding self-absorbed band, it is necessary to assume a value for the Planck function in the intensity units of Fig. 7*. From (6.3) it is obvious that if, at the band head, $B_H \gg I_H'$, there will be hardly any self-absorption, while considerable self-absorption requires $B_H < I_H'$, giving B_H not much greater than I_H. As a first estimate, B_H was taken to be 100 units

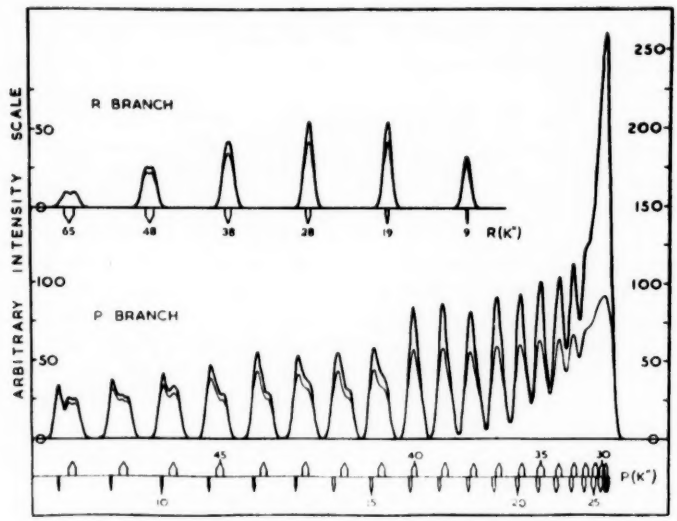

FIG. 7.—*Effect of self-absorption on the computed* CN 0–0 *band profile.* ($T = 4500°$; $\tau_H = 2{\cdot}63$).

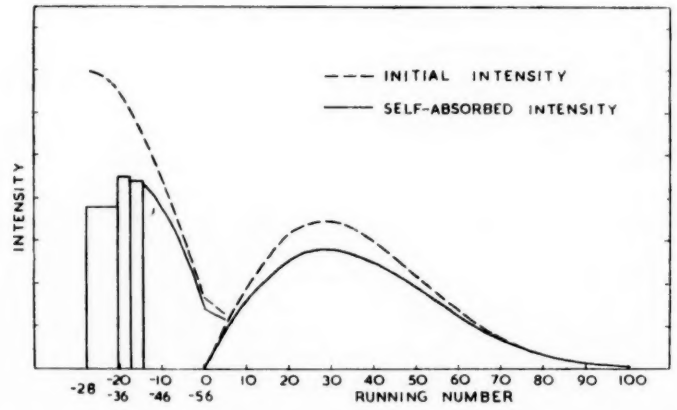

FIG. 8.—*Effect of self-absorption on the intensity distribution in the computed* CN 0–0 *band.* ($T = 4500°$; $\tau_H = 2{\cdot}63$).

* Because the intensity gradient in the chromosphere depends on the emitting element, the effective height and absolute intensity scale of the Level 1 spectrum are not the same for all elements. Hence, when considering the CN emission, it is incorrect to assume that the Planck function is approximately equal to the peak intensities of strongly self-absorbed lines such as Hζ.

on the intensity scale of Fig. 7; this is equivalent to assuming the optical depth at the band head to be $\tau_H = 2{\cdot}63$. The corresponding self-absorbed band in Fig. 7 was then computed.

The intensities of corresponding lines in the "ideal" and self-absorbed bands were obtained from their areas, and the intensity distributions plotted in Fig. 8. A quick glance at Figs. 2, 3 and 5 shows that the computed self-absorption produces an effect at least of the right order. While the self-absorption at the band head amounts to nearly 50 per cent, the intensity distribution in the self-absorbed *R* branch corresponds very closely to a rotational temperature of 4800°. This indicates that whatever the true temperature, unless self-absorption at the band head is very much greater than 50 per cent (i.e. $\tau_H \gg 2{\cdot}6$), the rotational temperature obtained from the *R* branch neglecting self-absorption will not be very much too high. On this account, agreement of the measured intensity distribution at Level 1 with the self-absorbed band computed for an assumed temperature of 4500° would not be expected—indeed, it was found to be quite impossible to reconcile the two, whatever value of τ_H was adopted. Unless the assumption of L.T.E. is seriously incorrect, either the emission from Level 1 is due to an atmosphere at a uniform higher temperature or there is a negative excitation temperature gradient. The lower temperatures already obtained for the higher levels show that the latter alternative is probably correct. Thus it was not considered worth while undertaking a further computation of the band for a higher temperature.

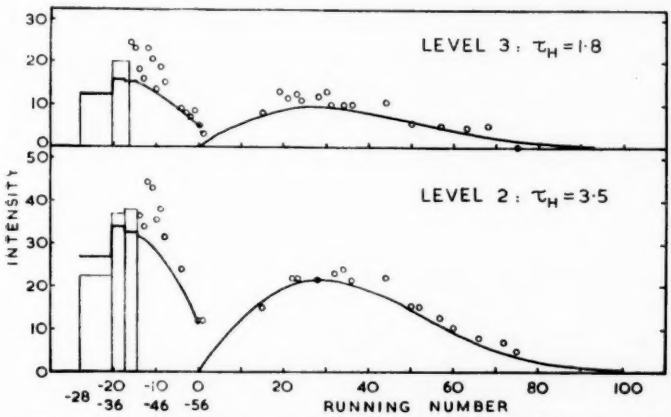

FIG. 9.—CN 0–0 *band, Levels 2 and 3: comparison of computed self-absorbed intensity distributions* ($T = 4500°$) *with measured intensities.*

Several different values of τ_H were also tried to obtain the best possible agreement between the computed self-absorbed intensity distribution and the measured distribution at Levels 2 and 3. The best fits, obtained with $\tau_H = 3{\cdot}5$ and 1·8 respectively, are shown in Fig. 9. The good agreement in the case of Level 3, when allowance is made for possible blends, shows that the CN 0–0 band on the intensity records is consistent with L.T.E. and a temperature of 4500°. The actual value of τ_H is not critical; for a range of τ_H from 1·5 to 2·5 there is

little variation in the resulting agreement, so small errors in the computed band profile will have little effect upon the result. Such errors will arise from the inaccuracy of the adopted line positions and the use of the Level 1 profile (the true Level 3 profile is wider because of the increase of turbulence with height detected by Redman and Suemoto).

For Level 2 the agreement is satisfactory except in the immediate vicinity of the band head. Again the value of τ_H between 3 and 4 is not critical, so the discrepancy at the band head cannot be ascribed to experimental errors. The CN emission from Level 2 may therefore correspond to a uniform temperature somewhat higher than 4500°, or there may be a negative excitation temperature gradient. The latter possibility seems the more likely, in view of the temperature of 4500° now established for Level 3.

7. *Discussion and conclusions.*—Correlating the results for the three levels studied it appears that, assuming L.T.E. and taking self-absorption fully into account, a definite excitation temperature can be ascribed only to Level 3. The CN spectrum is in agreement with an excitation temperature $\simeq 4500°$ at an effective height $\simeq 400$ km. The results obtained from Levels 1 and 2 can be interpreted as indicating a negative excitation temperature gradient, the temperature being greater than about 4500° at an effective height $\simeq 50$ km, and less than about 7000° at an effective height $\simeq 0$ km. The value of the temperature gradient cannot be determined without detailed consideration of the emission and absorption by an optically thick chromosphere with a negative temperature and density gradient—a problem which has not yet been attempted.

The excitation temperatures obtained above may be compared with those obtained by the authors mentioned in Section 1. The agreement with Parker's rotational temperature of $4600° \pm 400°$ for an estimated effective height < 500 km, is very satisfactory. Blackwell's temperatures of between 5000° and 7500° refer to an effective height of 1500 km and cannot be directly compared with the present results.

Superficially, Pecker and Athay's rotational temperature $\simeq 4500°$ at an effective height of 100 km appears to be in good agreement with the present results, but detailed examination of their paper reveals otherwise. Pecker and Athay's results are based on an analysis of the region between the 0–0 band head and the 3878 A Fe I line on slitless spectrograms. The resolution and dispersion are greatly inferior to those of Redman's spectrogram, and the region consequently presents an irregular and unresolved profile. The "rotational temperature" was determined from the peak intensities of the irregularities in the profile, the peaks being identified with the lines of the proceeding portion of the *P* branch. This procedure cannot be justified. In the absence of self-absorption, the observed band profile depends on the following factors: (1) the relative intensities (defining the effective rotational temperature) of the lines of both the proceeding and returning portions of the *P* branch, the latter being just as important as the former; (2) the separation of the lines, which decreases towards the band head; (3) the separation of the individual components of the doublets, which increases with increasing $|m|$; (4) the emitted line profile; (5) the instrumental profile. With a wide instrumental profile, such as that effective in producing Pecker and Athay's spectra, the combination of these five factors results in a band profile with peaks which cannot be identified, either in position or intensity, with the low *m*-number lines. This is clearly demonstrated by Fig. 10, which is identical

with the computed "ideal" band in Fig. 7, except that the line profile is rectangular and equal in width to that assumed by Pecker and Athay. If their assumptions and results are correct, the band profile in Fig. 10 must be almost identical with that of their eclipse spectrograms.

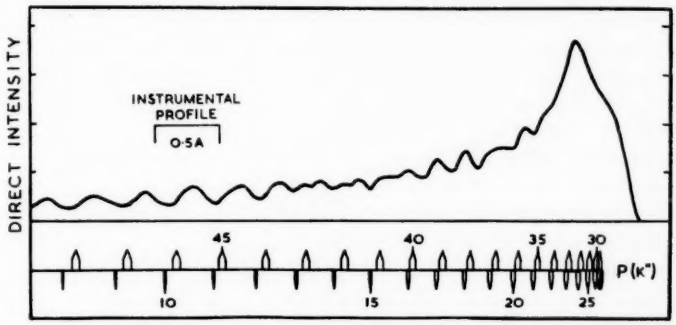

FIG. 10.—*Computed* CN 0–0 *band profile* ($T=4500°$), *smoothed by a wide instrumental profile.*

An attempt was made to determine the rotational temperature from Fig. 10, following exactly the procedure adopted by Pecker and Athay: the result was a negative temperature. The correct conclusion to be drawn from their data is that the region of the 0–0 band head exhibits an intensity distribution which is very far from being in accord with a rotational temperature of 4500°, when self-absorption is neglected. It would appear that self-absorption affects the band profile to just such an extent that Pecker and Athay's wrong analysis, quite fortuitously, gives approximately the right answer.

The above discussion does not, of itself, invalidate Pecker and Athay's detection of a positive temperature gradient from their spectrograms. However, this was deduced from an increase in the observed general slope of the band profile, an effect which will be produced by the certain decrease of self-absorption with height. Their measures do not necessarily indicate a positive temperature gradient*.

If strict L.T.E. holds throughout the regions considered, as assumed in the discussion of self-absorption, then the approximate excitation temperatures for the CN emission must be equated to the kinetic temperature at each height. There must therefore be a negative kinetic temperature gradient in the chromosphere, the temperature being defined as $\simeq 4500°$ at a height $\simeq 400$ km, with the value of the gradient uncertain. However, de Jager's (1957) most recent and reliable chromospheric model requires a *positive* kinetic temperature gradient, although the temperature of 4650° at 400 km agrees very well with the above results. Pagel (1956) has also obtained a positive temperature gradient, his temperatures being somewhat higher than de Jager's, due to the neglect of

* Pecker, in a private communication, has subsequently expressed a general agreement with these criticisms, but he has suggested that the observed band profile could be caused by the mixing of radiation from *optically thin* layers at different temperatures. However, although temperature inhomogeneities may well be present they could not alone explain the band profiles in Redman's spectrogram.

turbulence. It is clear that an analysis of the CN emission based upon L.T.E. and the general run of de Jager's kinetic temperatures will lead to a negative excitation temperature gradient contradicting the original assumptions. Thus, the hypothesis of L.T.E. is not self-consistent and must be abandoned.

The opposite extreme to purely thermal emission would be a chromospheric spectrum which is simply the scattered photospheric spectrum. At first sight, the 0–0 band head at zero height would appear to support such a hypothesis, as it is almost exactly the mirror image of the band head in the Utrecht Atlas (Minnaert, Mulders and Houtgast 1940). However, Hunaerts' (1947) rotational temperature for the 0–0 *R* branch in the Utrecht Atlas is $4464° \pm 117°$, which does not agree with the $\simeq 7000°$ deduced originally for zero height. In any case, if all the photospheric light were scattered by the bottom layers of the chromosphere, there would be none left to account for the spectrum at greater heights.

An intermediate possibility, first suggested privately by Pagel, is that most of the CN absorption might occur in the chromosphere. The bottom layers would then be excited by dilute radiation from the photosphere with a colour temperature of 6700° (Canavaggia and Chalonge 1946), which would determine the distribution of molecules amongst the various rotational and vibrational levels of the upper electronic state. With the formation of absorption lines in the lowest layers, the exciting radiation would be quickly depleted at the vital frequencies, so that ultimately the absorption spectrum of the centre of the disk would be controlled by the kinetic temperature (assumed to be $\simeq 4500°$ at heights above 100 km). The excitation temperature of the emission from these heights would be the same as the kinetic temperature, i.e. $\simeq 4500°$. The intensity distribution of the emission from zero height would correspond to an excitation temperature of 6700°, but would be modified by absorption by the cooler overlying layers. Also, if appreciable absorption at the band heads already existed in the high photosphere, the rotational levels $20 \lesssim K' \lesssim 35$ would be under-populated and the emission from these levels would be depleted. The final result would be an apparent excitation temperature $\simeq 7000°$ with depressed band heads, as observed.

An insurmountable difficulty, which prevents the adoption of the above explanation, is that the tangential optical depths in the chromosphere, being of the order 1 for strong lines, are altogether too small to account for the radial optical depths in the photospheric spectrum, which must also be of the order 1. The bulk of the CN absorption therefore takes place in the photosphere. A complete evaluation of the CN emission and absorption should start in the low photosphere, before any CN molecules have been formed, and progress upwards with the kinetic temperature, density, pressure, and partial pressure of CN all varying: excitation both by radiation and collisions must be considered. Such an analysis cannot be attempted at present.

The interpretations attempted or suggested above all assume implicitly that the recorded CN emission can be attributed to a certain effective height or range of heights in the chromosphere. It has already been pointed out (Section 6) that the effective height of any level depends on the intensity gradient of the line considered. The variation of self-absorption with "ideal" line intensity and with chromospheric height produces a steeper intensity gradient for weak lines than for strong lines of the same element. Hence, the CN band heads must refer to a greater effective height than the weak lines, and the absolute intensity scales for each must also be different. A comparison of the intensities of CN lines therefore

has little meaning, except as a rough approximation. It would be difficult to assess the magnitude of the effects of these considerations upon the present work. However, it is clear that the result must be a depression of the intensities of the band heads and the strong lines relative to those of the weak lines at the same level. Thus the chromospheric CN emission may not be inconsistent with de Jager's kinetic temperatures if departures from L.T.E. and the imperfection of the observational data are taken into account.

If the experimental and analytical difficulties could be overcome, the CN bands would yield a wealth of information about the transition region between the photosphere and the chromosphere. Ideally, one would like to have spectrograms of the mottles, and the regions between them, from the centre of the disk to the limb—also high-resolution flash spectra with absolute intensity calibrations, taken in the best possible observing conditions (from balloons or rockets, perhaps). It is unlikely that such data will be available in the near future. In the meantime, it is doubtful if much further progress can be made with the interpretation of solar CN spectra.

8. *Acknowledgments.*—It is a pleasure to acknowledge the encouragement and advice received from my supervisor, Dr D. E. Blackwell, who first suggested this investigation. I am greatly indebted to Professor R. O. Redman for the use of his spectrograms and for much unpublished information about the exposures and the eclipse apparatus, to Dr R. M. Petrie and Dr K. O. Wright of the Dominion Astrophysical Observatory for transforming the microphotometer tracings to direct intensity records, and to Dr B. E. Pagel for discussions on the interpretation of the results. I would also like to express my gratitude to the Department of Scientific and Industrial Research for a Maintenance Award during the course of this work, which was performed at the Cambridge Observatories as part of the requirements for the Ph.D. degree of the University. I am grateful to the Astronomer Royal for permission to use the facilities of the Royal Greenwich Observatory for the preparation of this paper.

Royal Greenwich Observatory,
Herstmonceux Castle,
Sussex:

1958 *April.*

References

Beals, C. E., 1944, *J. Roy. Ast. Soc. Canada.*, **38**, 65.
Beer, A. (Ed.), 1955, *Vistas in Astronomy*, Vol. I (London, Pergamon Press).
Blackwell, D. E., 1955, *cf.* Beer (1955), p. 726.
Canavaggia, R., and Chalonge, D., 1946, *Ann. d'Astrophys.*, **9**, 143.
Douglas, A. E., and Routly, P. M., 1955, *Ap. J. Supplement*, **1**, (No. 9), 295.
Floyd, A. L., and King, R. B., 1955, *J. Opt. Soc. America.*, **45**, 249.
Herzberg, G., 1950, *Spectra of Diatomic Molecules*, 2nd Ed. (New York, D. Van Nostrand Co.).
Houtgast, J., 1953, *Accademia Nazionale dei Lincei, Convegno Volta*, **11**, 68.
Hulst, H. C. van de, 1953, *cf.* Kuiper (1953), p. 222.
Hulst, H. C. van de and Reesinck, J. J. M., 1947, *Ap. J.*, **106**, 121.
Hunaerts, J., 1947, *Ann. d'Astrophys.*, **10**, 237.
Jager, C. de., 1957, *Bull. Ast. Inst. Ned.*, **13**, 275.
Kuiper, G. P. (Ed.), 1953, *The Sun* (Chicago, at the University Press).
Minnaert, M., Mulders, G. F. W., and Houtgast, J., 1940, *Photometric Atlas of the Solar Spectrum* (Amsterdam, Schnabel).

Mulliken, R. S., 1927, *Phys. Rev.*, **30**, 138, 785 ; 1930, *Rev. Mod. Phys.*, **2**, 60.
Pagel, B. E., 1956, *M.N.*, **116**, 608.
Parker, J. M., 1955, *Ap. J.*, **121**, 731.
Pecker, J. -C., and Athay, R. G., 1955, *Ap. J.*, **121**, 391.
Pillow, M. E., 1953, *Proc. Phys. Soc.* A, **66**, 737.
Redman, R. O., 1942, *M.N.*, **102**, 134; 1953, *Accademia Nazionale dei Lincei, Convegno Volta*, **11**, 72; 1955, *cf.* Beer, (1955), p. 731.
Redman, R. O., and Suemoto, Z., 1954, *M.N.*, **114**, 524.
Smit-Miessen, M. M. and Spier, J. L., 1942, *Physica*, **9**, 597.
St. John, C. E., and others, 1928, *Revision of Rowland's Preliminary Table of Solar Spectrum Wave-lengths* (Washington, Carnegie Institution).
Uhler, H. S., and Patterson, R. A., 1915, *Ap. J.*, **42**, 434.
Unsöld, A., 1955, *Physik der Sternatmosphären*, 2nd Ed. (Berlin, Springer), p. 627.
Weinard, J., 1955, *Ann. d'Astrophys.*, **18**, 334.

THE HYDROGEN RECOMBINATION SPECTRUM

A. Burgess

(Communicated by M. J. Seaton)

(Received 1958 May 27)

Summary

The radiative capture-cascade equations for hydrogen are solved, taking explicit account of the orbital angular momentum degeneracy of the atomic levels. All (n, l) levels with $n < 13$ are considered, together with the continuum.

The method of steepest descents is used to obtain asymptotic expansions of hydrogen dipole matrix elements involving the quantum number l explicitly, and other methods are also employed to obtain useful approximate expressions. Hydrogen photo-ionization cross-sections are tabulated for all (n, l) levels with $n < 13$, and recombination coefficients are given for electron temperatures $T_e = 10^4$ and 2×10^4 °K.

The cascade equations are solved for both case A and case B and $T_e = 10^4$ and 2×10^4 °K. The separate l levels for a given n are very far from being populated in proportion to their statistical weights. The present calculations give, for both case A and case B, Balmer decrements similar to those obtained by Baker and Menzel for case B.

The observed Balmer decrements of six planetary nebulae, when corrected for reddening, are in good agreement with the calculated decrements.

---

1. *Introduction.*—Considerable effort has already been devoted to the calculation of the statistical equilibrium produced in an assembly of hydrogen atoms by processes of radiative capture and cascade (see Baker and Menzel (**1**)). The calculated relative line intensities produced by such an assembly may be compared with relative intensities observed in gaseous nebulae. Even when the observed intensities are corrected for space reddening, calculations and observations may not agree, due to the effect of neglected physical processes, such as collisions in hot dense nebulae and line absorption in optically thick nebulae. In attempting to assess the possible importance of such processes it is important to consider the accuracy of the capture-cascade calculations. Previous work has not taken proper account of the orbital angular momentum degeneracy of the hydrogen atom. Let N_{nl} be the number density of hydrogen atoms in quantum states nl and put $N_n = \sum_l N_{nl}$. Previous workers have implicitly assumed N_{nl} to be proportional to the statistical weight $(2l+1)$, giving

$$N_{nl} = \frac{2l+1}{n^2} N_n. \qquad (1)$$

This relation will be satisfied in thermodynamic equilibrium but may not be satisfied when there are appreciable departures from thermodynamic equilibrium. The main purpose of the present work is to make calculations in which (1) is not assumed. Some of the results obtained will be used in further calculations for non-hydrogenic atoms and ions.

2. *The equilibrium equations.*—Consider, first, case A of Baker and Menzel. It is assumed that an optically thin nebula surrounds a central star. Ground state hydrogen atoms are ionized by stellar radiation. Due to the effectiveness of Coulomb collisions, the free electrons will have a Maxwellian velocity distribution corresponding to a kinetic temperature T_e (see Bohm and Aller (**2**)). It is assumed that the excited states of hydrogen are populated by radiative capture and by cascade from higher levels. One neglects the possibility of excited states being populated by absorption of stellar Lyman line radiation or by absorption of radiation produced in the nebula. The excited states are depopulated by cascade to lower states, the radiation field being considered sufficiently dilute to enable one to neglect absorption of radiation by atoms in excited states. On equating the number of atoms entering any excited state to the number leaving, one obtains for each level with $n \geqslant 2$

$$\alpha_j N_e^2 + \sum_{j'>j} N_{j'} A_{j'j} = N_j \sum_{j''<j} A_{jj''}, \tag{2}$$

where j stands for the quantum numbers (n, l), $j' < j$ implying $n' < n$. The number of atoms in state j is denoted by N_j, the Einstein coefficient for the $j' \rightarrow j$ transition by $A_{j'j}$ and the recombination coefficient for level j by α_j. The electron density N_e is assumed equal to the proton density.

Consider, next, case B of Baker and Menzel, which applies to nebulae which are very opaque to Lyman line radiation. One takes account of the nebular radiation field by supposing that a transition from level n to level 1 with emission of a Lyman quantum is counterbalanced by the reverse transition $1 \rightarrow n$ as the Lyman quantum is reabsorbed. Thus for case B, in the summation on the right of equation (2), n'' takes the values 2, 3, $(n-1)$, and (2) is valid only for $n > 2$. One assumes negligible flux of stellar Lyman line radiation.

In case A the population of the ground state, N_1, is determined by balancing the ionization rate against the total rate of capture on to all levels. The population of the $2s$ state is determined on equating the number entering $2s$ by capture and cascade to the number leaving $2s$ by $2s \rightarrow 1s$ transitions with two-quantum emission (**3**)* plus the number of collisionally induced $2s \rightarrow 2p$ transitions followed by Ly_α emission (**4**).

If it were assumed for case B that all Lyman radiation produced in the nebula, both line and continuous, was subsequently re-absorbed, then N_1 would be determined by equating the rate of ionization from the ground state by absorption of stellar radiation, to the rate of capture onto all levels with $n \geqslant 2$. These extreme assumptions cannot, however, be correct since no mechanism for depopulating $2p$ is included. If only radiative processes were considered, the $2p$ population would become so large that absorption of Balmer quanta would be important. In practice depopulation of $2p$ results from the fact that some Ly_α quanta do in fact escape and from the fact that $2p \rightarrow 2s$ collisional transitions may be followed by $2s \rightarrow 1s$ transitions with two-quantum emission. Whether or not case B conditions are ever closely approached in practice can be decided only by solving the Ly_α transfer problem and by allowing for collisional effects.

Assuming that in equation (2) all the α_j and $A_{jj'}$ are known, we see that an exact solution of the problem would involve the solution of an infinite set of simultaneous equations. Baker and Menzel (**1**), while ignoring the l degeneracy of the levels, solve for an infinite number of levels. In this paper the effect of

* See also end of Section 6.

allowing for the separate l states is investigated by taking into account all (n, l) states with $n \leqslant 12$ plus the continuum. We solve for both case A and case B for $T_e = 10\,000$ °K and 20 000 °K.

3. *Computation of recombination coefficients and transition probabilities.*—The Einstein coefficient for the spontaneous transition $j \rightarrow j'$ may be put into the form

$$A_{jj'} = 4\pi^2\nu^3 \left(\frac{8\pi\alpha a_0^2}{3c^2}\right) \frac{\max(l, l')}{2l+1} |\rho(nl, n'l')|^2, \tag{3}$$

where

$$\alpha = \frac{2\pi e^2}{ch} = \text{fine structure constant},$$

$$a_0 = \frac{\hbar^2}{me^2} = \text{Bohr radius}$$

and where

$$\rho(nl, n'l') = \int_0^\infty P(nl, r)\, r\, P(n'l', r)\, dr \tag{4}$$

is the dipole moment matrix element (in atomic units), $P(nl, r)$ and $P(n'l', r)$ being the normalized wave functions of the (n, l) and (n, l') states respectively.

Green, Rush and Chandler (**6**) have compiled extensive tables of $|\rho|^2$. These cover all the bound–bound transitions needed in this work.

The recombination coefficient is given by

$$\alpha_j = \frac{1}{c^2}\left(\frac{2}{\pi}\right)^{1/2} (mkT_e)^{-3/2} 2(2l+1) e^{I_j/kT_e} \int_{I_j}^\infty a_j(\nu)(h\nu)^2 e^{-h\nu/kT_e}\, d(h\nu), \tag{5}$$

where $I_j = h\nu_0 =$ energy of level j, $h\nu =$ energy of emitted photon, and $a_j(\nu)$ is the photo-ionization cross-section which, for the hydrogen atom, may be put into the form

$$a_j(\nu) = \left(\frac{8\pi\alpha}{3}\right) \frac{a_0^2}{2n^2} \left(\frac{\nu}{\nu_0}\right) \frac{1}{(2l+1)} [l|\sigma(nl, k^2 l-1)|^2 + (l+1)|\sigma(nl, k^2 l+1)|^2], \tag{6}$$

where

$$\sigma(nl, k^2 l \pm 1) = \int_0^\infty P(nl, r)\, r\, F(k^2 l \pm 1, r)\, dr \tag{7}$$

is the dipole moment matrix element between the bound state (n, l) and the free electron state $(k^2, l \pm 1)$, k^2 being the energy of the ejected electron (in units of 13·60 eV in all subsequent formulae). The normalization of the free wave function $F(k^2 l \pm 1, r)$ is such that it has asymptotic amplitude $k^{-1/2}$.

Thus in order to determine the α_{nl} we require a knowledge of the matrix elements $\sigma(nl, k^2 l \pm 1)$ over a sufficient range of k^2 to complete the integration in equation (5).

Exact analytic expressions for $\sigma(nl, k^2 l \pm 1)$ have been given by Gordon (**6**), but since these are highly complicated, except in certain special cases, and since a large number of such matrix elements is required, simpler approximate expressions were sought. To this end, formulae obtained in connection with other work on the derivation of an approximate general formula for the photo-ionization cross-sections of atoms other than hydrogen (Burgess and Seaton (**7**)) were found very useful.

At the threshold ($k^2 = 0$), σ and the rate of change of σ with k^2 are given by moderately simple expressions.

As a first approximation, for small k, it is found that σ may be represented by

$$\sigma(nl, k^2 l \pm 1) = \sigma(nl, \text{o}l+1)\left(\frac{\nu_0}{\nu}\right)^{\beta(nl,l\pm1)}, \tag{8}$$

where β is determined from $\partial\sigma/\partial k^2|_{k^2=0}$. Substituting this into (6) gives

$$a_{nl}(\nu) = \left(\frac{8\pi\alpha}{3}\right)\frac{{a_0}^2}{2n^2(2l+1)}\left[l|\sigma(nl, \text{o}l-1)|^2\left(\frac{\nu_0}{\nu}\right)^{\gamma(nl,l-1)} + (l+1)|\sigma(nl, \text{o}l+1)|^2\left(\frac{\nu_0}{\nu}\right)^{\gamma(nl,l+1)}\right]. \tag{9}$$

Burgess and Seaton (7) obtain

$$\sigma(nl, \text{o}l') = \left[\frac{2\pi}{(n+l)!\,(n-l-1)!}\right]^{1/2} 2^{n+l'} n^{l'+2} \text{e}^{-2n}\frac{(n+l'+2)!}{(2l'+1)!}\sum_{t=0}^{n-l-1} q_t F_t(n, l') \tag{10}$$

and

$$\gamma(nl, l') = 2\beta - 1 = \frac{\sum_{t=0}^{n-l-1} p_t K_t}{3(l'+1)\sum_{t=0}^{n-l-1} q_t F_t(n, l')} - \frac{l'(l'+1)(2l'+1)}{6n^2} - 1, \tag{11}$$

where $F_t(n, l')$ is the confluent hypergeometric function

$${}_1F_1(l'-n+t-1, 2l'+2; 2n)$$

and where $q_0 = 1$

$$q_t = \frac{l(l+1)-(n-t)(n-t+1)}{2t(n+l'-t+3)}\, q_{t-1}, \qquad (t \geqslant 1),$$

$$p_t = (l'+n-t+4)(l'+n-t+3)q_t,$$

$$K_t = F_{t-1}(n, l') + \frac{[l'(l'+1)-n(l'-n+t-2)]}{(l'+1)(2l'+3)}\, F_{t-1}(n, l'+1).$$

All the functions $F_t(n, l')$ required were generated by first computing $F_{n-1}(n, l')$ and $F_{n-2}(n, l')$ from the series defining the confluent hypergeometric function

$${}_1F_1(\alpha, \beta; z) = 1 + \frac{\alpha}{\beta}\frac{z}{1!} + \frac{\alpha(\alpha+1)}{\beta(\beta+1)}\frac{z^2}{2!} + \ldots$$

and then using the recurrence relation

$$(l'+n-t+3)F_{t-1}(l', n) + 2(t-2)F_t(l', n) - (l'-n+t-1)F_{t+1}(l', n) = 0.$$

Table I gives $|\sigma(nl, \text{o}l')|$ and $\gamma(nl, l')$ for all levels with $n \leqslant 12$.

Substituting (9) into (5) gives

$$'\alpha_{nl} = \left(\frac{2}{\pi}\right)^{1/2}\left(\frac{8\pi\alpha {a_0}^2}{3c^2}\right)\left(\frac{kT_e}{m}\right)^{3/2} f_j(T_e), \tag{12}$$

where

$$f_j(T_e) = \frac{\text{e}^{x_n}}{n^2}\left[l{\sigma_{l-1}}^2(x_n)^{\gamma_l - 1}E_{l-1}(x_n) + (l+1){\sigma_{l+1}}^2(x_n)^{\gamma_{l+1}}E_{l+1}(x_n)\right]. \tag{13}$$

$\sigma_{l\pm1}$ denotes $\sigma(nl, \text{o}l\pm1)$, $\gamma_{l\pm1}$ denotes $\gamma(nl, l\pm1)$, and $E_{l\pm1}(x_n)$ is given by the incomplete Γ-function

$$E_{l\pm1}(x_n) = \int_{x_n}^{\infty} \xi^{2-\gamma_{l\pm1}}\text{e}^{-\xi}\, d\xi, \tag{14}$$

where $x_n = I_n/kT_e$.

Putting $10^4 t = T_e\,°\text{K}$ and substituting for the constants involved gives

$$x_n = \frac{15{\cdot}788}{tn^2}. \tag{15}$$

TABLE I

$|\sigma(nl, ol')|/n^2$ *and* $\gamma(nl, l')$

n	l	l'	$\lvert\sigma\rvert/n^2$	γ	n	l	l'	$\lvert\sigma\rvert/n^2$	γ	n	l	l'	$\lvert\sigma\rvert/n^2$	γ
1	0	1	2·7139	2·6667	8	0	1	1·3551	2·1039	10	9	8	0·01553	5·6267
2	0	1	2·0777	2·0833		1	0	0·8638	2·3333		9	10	0·3107	5·8167
	1	0	0·5998	2·3333		1	2	1·5847	2·1082	11	0	1	1·2491	2·1375
	1	2	2·3991	3·0833		2	1	0·6440	2·5481		1	0	0·8704	2·3333
3	0	1	1·8080	2·0317		2	3	1·7569	2·2142		1	2	1·4306	2·1137
	1	0	0·7305	2·3333		3	2	0·4546	2·8292		2	1	0·6952	2·4955
	1	2	2·1916	2·4444		3	4	1·8244	2·4446		2	3	1·5847	2·1498
	2	1	0·3267	2·8889		4	3	0·2989	3·1860		3	2	0·5377	2·7000
	2	3	1·9602	3·4444		4	5	1·7401	2·8246		3	4	1·6891	2·2568
4	0	1	1·6504	2·0390		5	4	0·17777	3·6357		4	3	0·4006	2·9499
	1	0	0·7920	2·3333		5	6	1·4765	3·3820		4	5	1·7201	2·4469
	1	2	2·0009	2·2431		6	5	0·09027	4·2012		5	4	0·2852	3·2515
	2	1	0·4493	2·7470		6	7	1·0504	4·1458		5	6	1·6568	2·7342
	2	3	2·0538	2·7917		7	6	0·03390	4·9115		6	5	0·1915	3·6155
	3	2	0·19406	3·3542		7	8	0·5425	5·1458		6	7	1·4884	3·1329
	3	4	1·5525	3·7917	9	0	1	1·3140	2·1165		7	6	0·1189	4·0546
5	0	1	1·5438	2·0560		1	0	0·8678	2·3333		7	8	1·2217	3·6582
	1	0	0·8255	2·3333		1	2	1·5249	2·1077		8	7	0·06612	4·5835
	1	2	1·8561	2·1632		2	1	0·6654	2·5267		8	9	0·8868	4·3258
	2	1	0·5259	2·6657		2	3	1·6922	2·1826		9	8	0·03103	5·2188
	2	3	1·9949	2·5006		3	2	0·4879	2·7760		9	10	0·5365	5·1515
	3	2	0·2902	3·1333		3	4	1·7800	2·3581		10	9	0·01064	5·9780
	3	4	1·8136	3·1333		4	3	0·3386	3·0877		10	11	0·23413	6·1515
	4	3	0·12090	3·7733		4	5	1·7515	2·6538	12	0	1	1·2226	2·1464
	4	5	1·2090	4·1333		5	4	0·2185	3·4739		1	0	0·8700	2·3333
6	0	1	1·4653	2·0735		5	6	1·5801	3·0912		1	2	1·3925	2·1178
	1	0	0·8451	2·3333		6	5	0·1270	3·9520		2	1	0·7057	2·4840
	1	2	1·7447	2·1285		6	7	1·2653	3·6927		2	3	1·5399	2·1413
	2	1	0·5783	2·6129		7	6	0·06279	4·5432		3	2	0·5566	2·6715
	2	3	1·9115	2·3502		7	8	0·8476	4·4815		3	4	1·6467	2·2264
	3	2	0·3599	2·9944		8	7	0·02284	5·2716		4	3	0·4251	2·8988
	3	4	1·8714	2·7821		8	9	0·4112	5·4815		4	5	1·6935	2·3824
	4	3	0·19313	3·5000	10	0	1	1·2792	2·1277		5	4	0·3126	3·1716
	4	5	1·5450	3·4722		1	0	0·8698	2·3333		5	6	1·6622	2·6208
	5	4	0·07764	4·1667		1	2	1·4743	2·1089		6	5	0·2193	3·4966
	5	6	0·9317	4·4722		2	1	0·6820	2·5097		6	7	1·5412	2·9537
7	0	1	1·4043	2·0897		2	3	1·6351	2·1625		7	6	0·14484	3·8851
	1	0	0·8568	2·3333		3	2	0·5152	2·7339		7	8	1·3308	3·3936
	1	2	1·6564	2·1136		3	4	1·7339	2·2986		8	7	0·08824	4·3482
	2	1	0·6160	2·5758		4	3	0·3721	3·0110		8	9	1·0484	3·9533
	2	3	1·8303	2·2652		4	5	1·7413	2·5339		9	8	0·04802	4·8998
	3	2	0·4129	2·8990		5	4	0·2540	3·3497		9	10	0·7293	4·6464
	3	4	1·8604	2·5751		5	6	1·6334	2·8851		10	9	0·02199	5·5542
	4	3	0·2512	3·3170		6	5	0·16077	3·7634		10	11	0·4222	5·4861
	4	5	1·6862	3·0776		6	7	1·4022	3·3702		11	10	0·007337	6·3264
	5	4	0·13112	3·8544		7	6	0·09140	4·2678		11	12	0·17608	6·4861
	5	6	1·2850	3·8095		7	8	1·0664	4·0076					
	6	5	0·05091	4·5442		8	7	0·04401	4·8821					
	6	7	0·7128	4·8095		8	9	0·6771	4·8167					

The computation of the incomplete Γ-functions for the two electron temperatures considered ($t = 1, 2$) was tedious; tables given by K. Pearson (**8**) were found to be useful for some ranges of γ, but resort also had to be made to series of the form

$$\int_x^\infty \xi^{-p} e^{-\xi}\, d\xi = e^{-x} x^{-p} \left[\frac{x}{p-1} - \frac{x^2}{(p-1)(p-2)} + \frac{x^3}{(p-1)(p-2)(p-3)} - \cdots \right].$$

We consider now the accuracy of the α_{nl} resulting from the use of the approximate expression (9) for the variation of the photo-ionization cross-section with energy. Several checks may be made.

First, the sum over l of the recombination coefficient α_{nl} for a given n should correspond to the recombination coefficient given by Baker and Menzel (**1**). On simplification this requirement gives

$$t^3 \sum_l f_{nl}(T_e) = \frac{16}{\sqrt{3}} \left(\frac{Rch}{k 10^4} \right)^3 \frac{\bar{g}}{n^3} [-E_i(-x_n)] e^{x_n} = 36\,360\, \frac{\bar{g}}{n^3} [-E_i(-x_n)] e^{x_n}. \quad (16)$$

This was checked, and it was found that for n less than about 5, the agreement was satisfactory, but as n increases $\sum_l f_{nl}(T_e)$ tends to become too large.

TABLE II

$t^{3/2} f_{nl}(t)$ $\quad (t = 10^{-4} T_e)$

n	l	$t^{3/2} f_{nl}(t)$ $t=1$	$t=2$	n	l	$t^{3/2} f_{nl}(t)$ $t=1$	$t=2$	n	l	$t^{3/2} f_{nl}(t)$ $t=1$	$t=2$
1	0	1757	1183	7	5	9·16	3·30	10	7	1·79	0·586
2	0	261	178·3		6	2·23	0·854		8	0·560	0·183
	1	600	362	8	0	6·11	3·92		9	0·111	0·0406
3	0	87·3	59·1		1	15·3	8·70	11	0	2·49	1·56
	1	227	137·7		2	22·3	11·7		1	5·95	3·26
	2	193	101·4		3	23·3	10·9		2	8·85	4·60
4	0	40·5	27·1		4	17·6	7·16		3	10·2	5·00
	1	107·6	64·8		5	9·57	3·47		4	9·42	4·18
	2	121	63·2		6	3·62	1·23		5	6·91	2·74
	3	61·9	28·6		7	0·787	0·298		6	4·09	1·44
5	0	22·2	14·7	9	0	4·39	2·79		7	1·97	0·637
	1	58·8	34·9		1	10·84	6·07		8	0·767	0·240
	2	74·5	38·9		2	16·0	8·37		9	0·226	0·0710
	3	55·0	24·9		3	17·4	8·30		10	0·0435	0·0158
	4	19·9	8·40		4	14·3	6·07	12	0	1·94	1·22
6	0	13·54	8·86		5	8·88	3·34		1	4·45	2·49
	1	35·2	20·7		6	4·18	1·43		2	6·78	3·52
	2	47·8	24·9		7	1·43	0·473		3	8·05	3·91
	3	41·8	18·8		8	0·289	0·107		4	7·63	3·43
	4	22·8	9·03	10	0	3·27	2·07		5	5·99	2·42
	5	6·52	2·62		1	7·90	4·39		6	3·80	1·38
7	0	8·85	5·73		2	11·8	6·13		7	2·04	0·666
	1	22·6	13·06		3	13·4	6·40		8	0·919	0·280
	2	32·1	16·8		4	11·65	5·05		9	0·339	0·101
	3	31·4	14·2		5	7·94	3·05		10	0·0936	0·0289
	4	20·8	8·22		6	4·27	1·47		11	0·0175	0·00632

Secondly, for $l = n - 1$ the exact expressions for $\sigma(nl, k^2 l \pm 1)$ become particularly simple (see Appendix), and numerical integration in equation (5) is straightforward. This was carried out for all the $(n, n-1)$ levels considered, and for both electron temperatures.

Thirdly, for l small ($=0, 1, 2$), much more accurate expressions for $\sigma(nl, k^2 l \pm 1)$ are given by Burgess and Seaton (**7**). These are of the form

$$\frac{1}{n^2}\sigma(nl, k^2 l') = G(nl, l')[1 + n^2k^2]^{-\gamma'(nl,l')} \cos \pi \left[n + \chi(nl, l') + \alpha(l, l') \left(\frac{nk^2}{1 + nk^2} \right) + \beta(l, l') \left(\frac{n^2k^2}{1 + n^2k^2} \right) \right], \quad (17)$$

where $G(nl, l')$, $\gamma'(nl, l')$, $\chi(nl, l')$, $\alpha(l, l')$ and $\beta(l, l')$ are tabulated. In addition, the method of steepest descents was applied to the exact expressions for $\sigma(nl, k^2 l')$ in order to obtain asymptotic expansions valid for large n, small k and small l (see Appendix, equations (A 18) and (A 19)).

These formulae were used to obtain α_j accurately by numerical integration for $l = 0, 1, 2$ and for selected values of n. Thus by comparing these results with those obtained from equation (12), the errors in the $f_{nl}(T_e)$ were known, for a given n, for $l = 0, 1, 2$ and $n - 1$. For l lying between these values, the errors in the $f_{nl}(T_e)$ were estimated by interpolation, at the same time ensuring that equation (16) is satisfied. It should be noted that the greatest contribution to the summation on the left-hand side of equation (16) comes from the region of intermediate l, over which we have to interpolate, hence the condition (16) is sensitive to any error in the interpolation.

Table II gives the values of $t^{3/2} f_{nl}(T_e)$ after correcting in this way. For $l \leqslant 2$ they should be correct to within 1 per cent and for other cases the error should never exceed about 5 per cent.

4. *Solution of cascade equations.*—Equations (2) may be put into a form more convenient for solution by relating the populations of the levels to those which would hold if the system were in thermodynamic equilibrium. We therefore put

$$N_j = N_e^2 (2l + 1) \left[\frac{2\pi mkT_e}{h^2} \right]^{-3/2} e^{x_n} b(n, l), \quad (18)$$

where, for thermodynamic equilibrium, $b(n, l) = 1$, and equation (18) reduces to the Saha equation for the system.

Substituting equations (3), (12), and (18) into (2) we obtain, after simplifying,

$$\frac{1}{\pi}\left(\frac{kT_e}{I_1}\right)^3 f_j(T_e) + \sum_{j' > j} (2l' + 1) e^{x_{j'}} b(j') K_{j'j} = (2l + 1) e^{x_j} b(j) \sum_{j'' > l} K_{jj''}, \quad (19)$$

where

$$K_{jj'} = \frac{\max(l, l')}{(2l + 1)} |\rho|^2 \left(\frac{1}{n'^2} - \frac{1}{n^2} \right)^3.$$

Defining $\phi_j = (2l + 1) e^{x_j} b(j)$ we have finally

$$0{\cdot}8089 \times 10^{-4}\, t^3 f_j(T_e) + \sum_{j' > j} \phi_{j'} K_{j'j} = \phi_j \sum_{j'' < j} K_{jj''}. \quad (20)$$

Equations (20) were solved for ϕ_j, starting with the highest levels ($n = 12$), and working down through the levels one by one. The values of $b(j)$ obtained are given in Table III.

TABLE III

(*a*) Case A, $T_e = 10^4$ °K

$n \backslash l$	$b(n, l)$							
	0	1	2	3	4	5	6	7
2		0·00357						
3	0·594	0·0248	0·0618					
4	0·802	0·0487	0·123	0·156				
5	0·949	0·0665	0·168	0·246	0·189			
6	1·045	0·0780	0·198	0·305	0·295	0·158		
7	1·11	0·0855	0·218	0·348	0·367	0·262	0·107	
8	1·16	0·0899	0·230	0·375	0·418	0·334	0·189	0·0628

(*b*) Case A, $T_e = 2 \times 10^4$

$n \backslash l$	$b(n, l)$							
	0	1	2	3	4	5	6	7
2		0·0394						
3	2·68	0·0976	0·194					
4	2·46	0·133	0·279	0·299				
5	2·42	0·151	0·327	0·407	0·281			
6	2·40	0·161	0·356	0·469	0·396	0·203		
7	2·38	0·164	0·375	0·517	0·473	0·304	0·125	
8	2·38	0·163	0·386	0·556	0·539	0·381	0·200	0·0703

(*c*) Case B, $T_e = 10^4$

$n \backslash l$	$b(n, l)$			
	0	1	2	$l \geqslant 3$
3	0·947	0·215	0·0624	
4	1·06	0·307	0·125	
5	1·13	0·367	0·170	As in
6	1·18	0·402	0·201	Case A
7	1·21	0·422	0·221	
8	1·23	0·432	0·233	

(*d*) Case B, $T_e = 2 \times 10^4$

$n \backslash l$	$b(n, l)$			
	0	1	2	$l \geqslant 3$
3	4·09	0·846	0·197	
4	3·14	0·837	0·283	
5	2·82	0·836	0·332	As in
6	2·66	0·829	0·361	Case A
7	2·56	0·809	0·380	
8	2·49	0·785	0·389	

5. *Results and discussion.*—The first point of interest in the results given in Table III is that they show that the separate l levels for a given n are far from being populated according to their statistical weights, as is assumed in Baker and Menzel's treatment; if this were true then the $b(n, l)$ would be independent of l. In particular we note that for case A the p levels are grossly under-populated relative to the other levels, this depopulation being due to the fact that the probability of the transition $np \rightarrow 1s$ is very large.

The question arises as to how much the $b(n, l)$ are in error due to the neglect of all bound levels above $n = 12$. Let $b_N(j)$ be calculated neglecting levels with $n > N$. Results for $b_{12}(n)$, calculated neglecting l-degeneracy, are compared with the $b_\infty(n)$ of Baker and Menzel in Table IV. Values of $b_{14}(n)$ calculated by Baker and Menzel for case B, $t = 2$, are also included.

For case A it is seen that, as would be expected, $b_{12}(n) < b_\infty(n)$ for all n and that the effect on $b(n)$ due to neglecting the higher levels decreases as n becomes smaller. For case B however this is not the case; we see that $b_{12} < b_{14}$ for all n, but that for $n < 6$, $b_\infty(n)$ is less than both $b_{12}(n)$ and $b_{14}(n)$. This cannot be correct, both on physical grounds and from the form of the equations actually used by Baker and Menzel. Thus in equation (18) of Menzel and Baker (9), all the terms in the summations are positive, and neglecting all levels above say

TABLE IV

	Case A				Case B				
n	$T_e = 10^4$		$T_e = 2 \times 10^4$		$T_e = 10^4$		$T_e = 2 \times 10^4$		
	$b_{12}(n)$	$b_\infty(n)$	$b_{12}(n)$	$b_\infty(n)$	$b_{12}(n)$	$b_\infty(n)$	$b_{12}(n)$	$b_{14}(n)$	$b_\infty(n)$
2	0·00378		0·0456						
3	·0362	0·0393	·137	0·146	0·108	0·089	0·401	0·420	0·330
4	·0869	·0961	·215	·233	·183	·166	·448	·466	·404
5	·136	·150	·272	·296	·245	·233	·487	·510	·460
6	·176	·202	·312	·350	·290	·296	·512	·538	·512
7	·207	·242	·339	·391	·321	·341	·525	·558	·550
8	·231	·277	·358	·422	·342	·379	·530	·568	·577
9	·248	·311	·369	·448	·353	·417	·525	·570	·600
10	·258	·340	·372	·470	·356	·448	·513	·565	·620
11	·261	·359	·366	·488	·348	...	·489	...	...
12	0·250	0·376	0·344	0·503	0·321	...	0·443	...	...

TABLE V

(*a*) Case A, $T_e = 10^4$ °K

	$b'(n, l)$									
$n \backslash l$	0	1	2	3	4	5	6	7	8	9
2		0·00386								
3	0·647	0·0270	0·0674							
4	0·882	0·0536	0·135	0·172						
5	1·06	0·0745	0·188	0·276	0·212					
6	1·19	0·0889	0·226	0·348	0·336	0·180				
7	1·30	0·100	0·225	0·407	0·429	0·307	0·125			
8	1·39	0·108	0·276	0·450	0·502	0·401	0·227	0·0754		
9	1·48	0·115	0·296	0·487	0·563	0·480	0·309	0·145	0·0415	
10	1·60	0·122	0·317	0·529	0·627	0·560	0·387	0·209	0·0842	0·0216

(*b*) Case A, $T_e = 2 \times 10^4$

	$b'(n, l)$									
$n \backslash l$	0	1	2	3	4	5	6	7	8	9
2		0·0414								
3	2·84	0·103	0·206							
4	2·66	0·144	0·301	0·323						
5	2·66	0·166	0·360	0·448	0·309					
6	2·69	0·180	0·399	0·525	0·444	0·227				
7	2·74	0·189	0·431	0·595	0·544	0·350	0·144			
8	2·81	0·192	0·455	0·656	0·636	0·450	0·236	0·0830		
9	2·88	0·198	0·472	0·706	0·726	0·545	0·320	0·144	0·0445	
10	2·99	0·202	0·486	0·747	0·801	0·633	0·392	0·199	0·0799	0·0227

(*c*) Case B, $T_e = 10^4$

	$b'(n, l)$			
$n \backslash l$	0	1	2	$l \geqslant 3$
3	1·03	0·234	0·0680	
4	1·16	0·338	0·137	
5	1·27	0·411	0·191	
6	1·34	0·458	0·229	As in
7	1·41	0·494	0·259	Case A
8	1·47	0·518	0·280	
9	1·54	0·541	0·298	
10	1·63	0·568	0·319	

(*d*) Case B, $T_e = 2 \times 10^4$

	$b'(n, l)$			
$n \backslash l$	0	1	2	$l \geqslant 3$
3	4·34	0·897	0·209	
4	3·39	0·904	0·306	
5	3·10	0·920	0·365	
6	2·98	0·928	0·404	As in
7	2·94	0·930	0·437	Case A
8	2·94	0·926	0·459	
9	2·98	0·933	0·476	
10	3·04	0·939	0·489	

$n = 12$ simply involves cutting off all summations at that point. Hence it would appear that for case B, the $b_\infty(n)$ calculated by Baker and Menzel must be in error. The method by which they extrapolate from a finite to an infinite number of levels seems to be the most probable source of error.

A rather rough correction for the omitted higher levels can be made to the $b(n, l)$ by multiplying by the ratio $C_n = b_\infty(n)/b_{12}(n)$. Table V gives the values of $b'(n, l) = C_n b(n, l)$ obtained. These figures are probably not very accurate for n and l large, especially since for case B the $b_\infty(n)$ are in error, so that it was necessary to assume the ratio C_n to be the same as in case A. However, for moderately small n, the errors should not be more than about 5 per cent. Such accuracy should be sufficient for most astrophysical applications.

An exact solution of the problem taking into account all excited levels would be very difficult, not merely because an infinite number of levels must be considered, but also because of the fact that, as n increases, at some stage transitions due to collisions must become important. That this is so may be seen from the fact that we must have continuity between the highly excited bound states and the continuum of positive energy states. Thermodynamic equilibrium prevails for the continuum states because energy transfer due to collisions is much more important than transfer due to radiative processes (Bohm and Aller (**2**)). Thus as n increases we must reach some stage where $b(n, l) = 1$, due to the collisional redistribution of excited atoms between states of different n and of different l. It should be noted that the observations of Aller, Bowen and Minkowski (**10**) on NGC 7027 confirm that such effects probably occur among the highly excited states of He^+. Menzel and Baker do in fact show that their $b_n \to 1$ as $n \to \infty$. but this is merely a consequence of the fact that they have taken $b = 1$ for the continuum and that the population of a given line is influenced by the population of the levels above it. Their b_n tends to unity too slowly as n tends to infinity.

Consider a nebula which is optically thin (case A) and for which T_e is too small for collisional excitation from the ground state to be important. The probability of Ly_α emission by an atom in the $2p$ state is $6{\cdot}25 \times 10^8$ sec^{-1} and, for an electron density $N_e = 10^4$ cm^{-3}, the probability of a collisional $2p \to 2s$ transition is only $1{\cdot}7$ sec^{-1} (**4**). Probabilities of collisional $nl \to nl'$ transition have not been calculated for $n > 2$, but it may be expected that for small n such processes will also have probabilities much smaller than radiative transition probabilities. This is the situation assumed in the present calculations. As n increases, the first collisional effect may be that $nl \to nl'$ transitions become important and that the method of calculation used by Baker and Menzel will be more nearly correct. It may be only at still larger values of n that collisional transitions between energy levels become important.

6. *Astrophysical applications.*—The main astrophysical interest in this problem lies in the spectrum emitted by the system.

The energy emitted per cm^3 per second in transitions $j \to j'$ is given by

$$E_{jj'} = N_j h\nu A_{jj'}.$$

From equations (3) and (18) we have

$$E_{jj'} = N_e^2 [2\pi mkT_e]^{-3/2} 4\pi^2 \left(\frac{8\pi\alpha a_0^2}{3c^2}\right) (Rhc)^4 \left(\frac{1}{n'^2} - \frac{1}{n^2}\right) (2l+1) e^{x_n} b(n, l) K_{jj'},$$

where R is the Rydberg wave number ($= 109\,737$ cm^{-1}).

This gives $E_{jj'} = 2{\cdot}417 \times 10^{-23} \frac{N_e^2}{t^{3/2}} \left(\frac{1}{n'^2} - \frac{1}{n^2}\right) \phi_j K_{jj'}$ erg cm^{-3} sec^{-1}.

Hence the intensity of a line $n \to n'$ is given by

$$I_{nn'} = 2{\cdot}417 \times 10^{-23} \frac{N_e^2}{t^{3/2}} \sum_{ll'} \left(\frac{1}{n'^2} - \frac{1}{n^2}\right) \phi_j K_{jj'}. \qquad (21)$$

Of particular interest are the intensities I_{n2} of the Balmer lines. As is customary, the relative intensities of the lines referred to H_β as unity were calculated, and the values of $\mathscr{I}_n = I_{n2}/I_{42}$ are given in Table VI, where the results obtained by Baker and Menzel are also given, for comparison. In order to be able to obtain the absolute intensities, the absolute intensity I_{42} of the H_β line is given in Table VII. An alternative way of expressing the absolute intensity of the H_β line is by giving the effective value of b_4 for the $4 \to 2$ transition, i.e.

$$b_4 = \frac{\sum_{ll'} (2l+1) b(4l) A_{4l2l'}}{\sum_{ll'} (2l+1) A_{4l2l'}} .$$

The values of this quantity are also given in Table VII together with the values of b_4 obtained by Baker and Menzel. It should be noticed that Baker and Menzel's values are consistently lower.

Also of interest are the relative intensities of the Paschen and Balmer lines I_{n3}/I_{n2}, which we denote by $(P/B)^{(nl)}$. These are given in Table VIII, together with the Paschen–Balmer ratios obtained if the l degeneracy of the levels is ignored (denoted by $(P/B)^{(n)}$). It should be noted that $(P/B)^{(n)} = (A_{n3}\nu_{n3})/(A_{n2}\nu_{n2})$ is independent of electron temperature and of whether case A or case B applies. This is not the case for $(P/B)^{(nl)}$, as is seen from the table.

In comparing calculated and observed Balmer decrements the first step is to correct the observed decrements for interstellar reddening (Berman (**11**)). It has been shown by Aller (**12**) that the corrected observed decrements for Balmer lines other than H_α are in satisfactory agreement with Baker and Menzel's case B calculations. The present calculations give decrements which, for both cases and both temperatures, are similar to the Baker and Menzel case B results and are therefore in agreement with the observations of Aller (**12**). In more recent spectrophotometric work, (**10**) and (**13**), H_α intensities have also been obtained. Let $I_0(\lambda)$ denote the observed intensities and $I_T(\lambda)$ the intensities corrected for reddening. Then

$$\log I_T(\lambda) = \log I_0(\lambda) + cf(\lambda),$$

where $f(\lambda)$ is given in Table IX, the values being taken from Fig. 2 of the paper by Whitford (**14**). The units of $f(\lambda)$ are chosen such that $f(\lambda) = 0$ for the wave-length of the H_β line and $f(\infty) = -1$. For any given nebula we define B to be the factor by which the observed absolute H_β intensity must be multiplied in order to correct for interstellar absorption. With the units adopted for $f(\lambda)$ we then have $c = \log B$. The observed intensities for six nebulae*, (**10**, **13**), have been corrected for reddening by calculating c assuming the ratios $I_T(H_\gamma)/I_T(H_\beta) = 0{\cdot}50$ and $I_T(H_\delta)/I_T(H_\beta) = 0{\cdot}285$ (see Table VI) and adopting

* We consider all objects for which H_α, H_β, H_γ and H_δ intensities were measured either by Aller, Bowen and Minkowski or by Minkowski and Aller, with the exception of NGC 1535, for which the correction for atmospheric extinction appears to be uncertain.

TABLE VI

Relative Balmer intensities

n	Case A				Case B			
	$T_e = 10^4$		$T_e = 2 \times 10^4$		$T_e = 10^4$		$T_e = 2 \times 10^4$	
	$\mathcal{J}_n$	Baker and Menzel	$\mathcal{J}_n$	Baker and Menzel	$\mathcal{J}_n$	Baker and Menzel	$\mathcal{J}_n$	Baker and Menzel
3	2·48	1·915	2·36	1·984	2·62	2·50	2·53	2·59
4	1	1	1	1	1	1	1	1
5	0·501	0·576	0·510	0·560	0·489	0·51	0·493	0·50
6	0·288	0·374	0·296	0·353	0·276	0·31	0·280	0·30
7	0·181	0·255	0·188	0·236	0·172	0·206	0·174	0·192
8	0·122	0·182	0·128	0·165	0·114	0·143	0·117	0·130

TABLE VII

Absolute intensity of H_β

	$\frac{I_{42}}{N_e^2} \times 10^{26}$	$\bar{b}_4$	b_4 (Baker and Menzel)
Case A, $T_e = 10^4$	8·08	0·132	0·0961
Case A, $T_e = 2 \times 10^4$	4·12	0·312	0·233
Case B, $T_e = 10^4$	12·24	0·200	0·166
Case B, $T_e = 2 \times 10^4$	6·52	0·494	0·404

TABLE VIII

Paschen–Balmer ratios

$(P/B)^{(nl)}$

n	Case A		Case B		$(P/B)^{(n)}$
	$T_e = 10^4$	$T_e = 2 \times 10^4$	$T_e = 10^4$	$T_e = 2 \times 10^4$	
4	0·343	0·297	0·260	0·224	0·277
5	·399	·350	·311	·273	·294
6	·414	·369	·329	·294	·300
7	·424	·382	·340	·307	·302
8	·430	·394	·347	·319	·304
9	·432	·403	·351	·327	·304
10	·435	·409	·354	·334	·305
11	·437	·415	·356	·339	·305
12	0·439	0·417	0·359	0·342	0·305

the mean of the two values of c obtained. It should be noted that the observed H_α/H_β ratio is not used in estimating the reddening correction. Table X gives

TABLE IX

Corrections for interstellar absorption

λ	$f(\lambda)$	λ	$f(\lambda)$	λ	$f(\lambda)$	λ	$f(\lambda)$	λ	$f(\lambda)$
3200	+0·447	4400	+0·122	5400	−0·128	6600	−0·358	7800	−0·526
3400	+0·395	4600	+0·068	5600	−0·171	6800	−0·390	8000	−0·549
3600	+0·342	4800	+0·016	5800	−0·212	7000	−0·420	...	...
3800	+0·288	4861	0·000	6000	−0·251	7200	−0·449	∞	−1·000
4000	+0·233	5000	−0·035	6200	−0·288	7400	−0·476	...	...
4200	+0·177	5200	−0·083	6400	−0·324	7600	−0·502	...	...

TABLE X

Observed Balmer decrements corrected for reddening

	NGC 7027	NGC 7662	NGC 2392	NGC 2022	IC 351	J 320	Mean observed	Theory
H_α	2·38	2·78	3·19	1·75	2·94	2·27	2·55	2·36–2·62
H_β	1·00	1·00	1·00	1·00	1·00	1·00	1·00	1·00
H_γ	0·49	0·50	0·47	0·52	0·52	0·48	0·50	0·50
H_δ	0·29	0·28	0·31	0·27	0·27	0·30	0·29	$0·28_5$
B	17·4	2·6	1·6	4·9	1·6	1·8	...	...
	(16·6)	(2·9)	(2·1)	(3·5)	(1·9)	$(1·6_5)$	...	...

the corrected intensities and the H_β extinction corrections B. The mean corrected observed H_α/H_β ratio is seen to be in satisfactory agreement with theory. Also given, in parentheses, are the values of B obtained if we now also assume the ratio $I_T(H_\alpha)/I_T(H_\beta)=2·50$ to calculate a third value of c, and the average over the three values of c is taken.

When an extinction correction similar to that of Table X is adopted, it is found by Aller and Minkowski (**15**) that the observed Paschen intensities for NGC 7027 are too weak. With the present results for $(P/B)^{(nl)}$ the discrepancy would be somewhat increased. This discrepancy may be due to physical conditions being different from those assumed in the theory, but, as pointed out by Aller and Minkowski, it may be a consequence of the underlying continuum having been drawn too high.

The contribution to the continuous spectrum of a nebula due to 2-quantum emission from the $2s$ state (see Spitzer and Greenstein (**3**) and Seaton (**4**)) is proportional to the quantity

$$X=\frac{\text{No. of atoms arriving on } 2s \text{ state}}{\text{No. of recombinations on all levels with } n\geqslant 2}.$$

TABLE XI

	T_e	X
Case A	10^4	0·13
	2×10^4	0·15
Case B	10^4	0·34
	2×10^4	0·37

Spitzer and Greenstein, using case B, estimate that X must lie between 0·30 and 0·35 and adopt a mean value of 0·32. The present calculations enable a more precise estimate of X to be made. The results are shown in Table XI.

Acknowledgments.—I would like to express my sincere thanks to Dr M. J. Seaton for his constant guidance in this work, and to Dr L. C. Green for his kindness in sending the results of his computations prior to publication. The present work was carried out during the tenure of a Ministry of Education scholarship.

Appendix

Asymptotic expansions for dipole moment matrix elements.—Menzel and Pekeris (**16**) have used the method of steepest descents to obtain asymptotic expansions of the dipole matrix elements for bound–bound, bound–free and free–free transitions in hydrogen, in all cases, no account being taken of the l degeneracy of the levels, i.e. all expressions were implicitly averaged over the azimuthal quantum numbers of the initial and final states. In this appendix we apply the method to the matrix elements of transitions involving the quantum number l explicitly.

We consider first, transitions between bound states, later generalizing to bound–free and free–free transitions.

For the transition $(n,l)\rightarrow(n',l+1)$ we have, in atomic units (Gordon (**6**))

$$\rho(nl,n'l+1)=\frac{(-1)^{n-l-1}}{4(2l+1)!}\sqrt{\frac{(n'+l+1)!\,(n+l)!}{(n'-l-2)!\,(n-l-1)!}}\left(\frac{4nn'}{(n'-n)^2}\right)^{l+2}\left(\frac{n'-n}{n'+n}\right)^{n'+n}y \tag{A 1}$$

where

$$y={}_2F_1\left(l+2-n',l+1-n;2l+2;\frac{-4nn'}{(n'-n)^2}\right)-\left(\frac{n'-n}{n'+n}\right)^2{}_2F_1\left(l-n',l+1-n;2l+2;\frac{-4nn'}{(n'-n)^2}\right). \tag{A 2}$$

From the relation

$${}_2F_1(a,b;c;x)=(1-x)^{c-a-b}{}_2F_1(c-a,c-b;c;x)$$

we have

$$y=\left(\frac{n'+n}{n'-n}\right)^{2(n'+n)}Y,$$

where, writing $x=-4nn'/(n'-n)^2$,

$$Y=\left(\frac{n'-n}{n'+n}\right)^2{}_2F_1(l+n',l+1+n;2l+2;x)-{}_2F_1(l+2+n',l+1+n;2l+2;x). \tag{A 3}$$

Now, for $a\geqslant 1$ and $1\leqslant c\leqslant a$ we have, for a, b, c, integers,

$$\begin{aligned}{}_2F_1(a,b;c;x)&=\frac{\Gamma(b-c+1)\Gamma(c)}{\Gamma(b)\Gamma(a)}\frac{d^{a-1}}{dx^{a-1}}\left[x^{a-c}(1-x)^{c-b-1}\right]\\&=\frac{\Gamma(b-c+1)\Gamma(c)}{\Gamma(b)}\frac{1}{2\pi i}\oint_{t=x}\frac{t^{a-c}}{(t-x)^a(1-t)^{b+1-c}}\,dt\\&=\frac{\Gamma(b-c+1)\Gamma(c)}{\Gamma(b)}\frac{1}{2\pi i}\oint\frac{(1-z)^{a-c}}{(1-x-z)^a z^{b+1-c}}\,dz,\end{aligned} \tag{A 4}$$

the path of integration in the z-plane being a negative loop enclosing $z=(1-x)$

but not $z=0$, since $b+1>c$ in the hypergeometric functions required. Since $a\geqslant c$ the contour may enclose $z=1$ if necessary.

Also, since we always have $b>0$, the integral in (A 4) vanishes over a circle of infinite radius. Thus the above contour may be deformed into a positive loop enclosing $z=0$ but not $z=1-x$.

Substituting (A 4) into (A 3) and putting $\beta=(n'+n)/(n'-n)$, $\alpha=n/n'$, we obtain

$$Y=\frac{(n-l-1)!\,(2l+1)!}{(n+l)!}\left(\frac{\beta^2-1}{\beta^2}\right)\frac{1}{2\pi i}\oint\frac{(1-z)^{n'-l-2}(\beta^2-z^2)}{z^{n-l-2}(\beta^2-z)^{n'+l+2}}\,dz. \qquad (A\,5)$$

Putting this into a form suitable for applying the method of steepest descents (see Copson (**17**) or Erdelyi (**18**)),

$$Y=\frac{(n-l-1)!\,(2l+1)!}{(n+l)!}\left(\frac{\beta^2-1}{\beta^2}\right)\frac{1}{2\pi i}\oint\left[\frac{z^l(\beta^2-z^2)}{(1-z)^{l+2}(\beta^2-z)^{l+2}}\right]\times e^{-n\{\ln z-(1/\alpha)\ln[(1-z)/(\beta^2-z)]\}}\,dz. \qquad (A\,6)$$

Writing $f(z)=\ln z-(1/\alpha)\ln[(1-z)/(\beta^2-z)]$, we have $df/dz=0$ when $z=-\beta$. At this point $f(-\beta)=i\pi+(1+1/\alpha)\ln\beta$.

The paths of steepest ascent and descent starting at $z=-\beta$ are given by putting the imaginary part of $f(z)$ equal to $i\pi$. Writing $z=\rho e^{i\theta}$, this gives

$$\alpha(\theta-\pi)=\arg\left[\frac{1-\rho e^{i\theta}}{\beta^2-\rho e^{i\theta}}\right], \qquad (A\,7)$$

i.e.

$$\rho=\frac{1}{2}\left[(\beta^2+1)\cos\theta+\frac{(\beta^2-1)\sin\theta}{\tan(\alpha\pi-\alpha\theta)}\right]\pm\frac{1}{2}\left\{\left[(\beta^2+1)\cos\theta+\frac{(\beta^2-1)\sin\theta}{\tan(\alpha\pi-\alpha\theta)}\right]^2-4\beta^2\right\}^{1/2}. \qquad (A\,8)$$

Equation (A 8) defines two loops, symmetrical about the real axis, one starting at $z=-\beta$ and ending at $z=1$, the other starting at $z=-\beta$ and ending at β^2. The negative real axis is also a solution of (A 7). These contours are shown in Fig. 1.

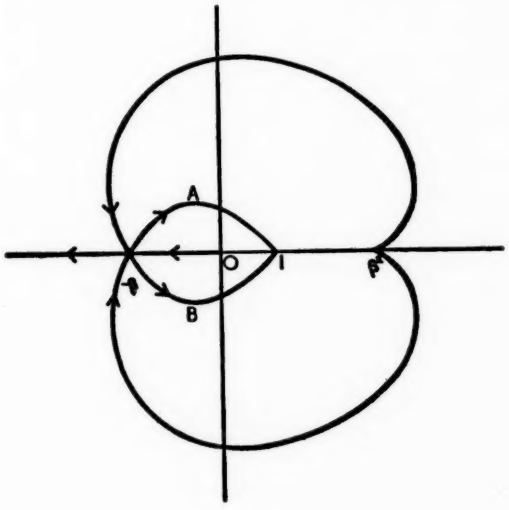

FIG. 1.

Defining

$$\tau(z)=f(z)-i\pi-\left(1+\frac{1}{\alpha}\right)\ln\beta \qquad (A\,9)$$

we see that $\tau(-\beta)=0$, and that $\tau(z)$ is real along the paths defined above.

The required paths of steepest *descent* are those along which $\tau(z)$ is a monotonic increasing function. To determine these, we expand τ as a power series in $u\equiv(z+\beta)$, obtaining

$$p^3/12\equiv\frac{-\tau}{1-\alpha^2}=\frac{1}{12}\left(\frac{u}{\beta}\right)^3+\frac{1}{8}\left(\frac{u}{\beta}\right)^4+\left(\frac{11+\alpha^2}{80}\right)\left(\frac{u}{\beta}\right)^5+\left(\frac{13+3\alpha^2}{96}\right)\left(\frac{u}{\beta}\right)^6$$
$$+\left(\frac{57+22\alpha^2+\alpha^4}{448}\right)\left(\frac{u}{\beta}\right)^7+\ldots. \qquad (A\,10)$$

When $|u|$ is small,

$$\frac{u}{\beta}\simeq\left(\frac{12}{1-\alpha^2}\right)^{1/3}(-\tau)^{1/3},$$

hence if τ is positive $\arg u\simeq-\frac{1}{3}\pi,\ \frac{1}{3}\pi,\ \pi$ and if τ is negative $\arg u\simeq-\frac{2}{3}\pi,\ 0,\ \frac{2}{3}\pi$. Thus the directions along which $\tau(z)$ increases are as shown by the arrows in Fig. 1.

We see that a suitable steepest descent contour is given by B − A; also, this path encloses $z=0$ but not $z=1-x$ $(=\beta^2)$, as required.

Equation (A 6) may now be written

$$Y=\frac{(n-l-1)!\,(2l+1)!\,(\beta^2-1)}{(n+l)!}\frac{e^{-in\pi}}{2\pi i}$$
$$\times\int_0^\infty\left[\frac{z^{l+1}}{(1-z)^{l+1}(\beta^2-z)^{l+1}}\left(\frac{\beta-z}{\beta+z}\right)\right]_A^B e^{-n\tau}\,d\tau. \qquad (A\,11)$$

Now, inversion of the series (A 10) gives

$$\frac{u}{\beta}=p\left[1-\frac{p}{2}+\frac{1}{5}\left(1-\frac{\alpha^2}{4}\right)p-\frac{3}{40}(1-\tfrac{2}{3}\alpha^2)p^3+\left(\frac{73-74\alpha^2+3\alpha^4}{2800}\right)p^4+\ldots\right]. \qquad (A\,12)$$

Also,

$$\left[\frac{z^{l+1}}{(1-z)^{l+1}(\beta^2-z)^{l+1}}\left(\frac{\beta-z}{\beta+z}\right)\right]=\left(\frac{u-\beta}{(\beta+1-u)(\beta^2-\beta-u)}\right)^{l+1}\left(\frac{2\beta-u}{u}\right)$$
$$=\frac{(-1)^{l+1}}{(\beta+1)^{2l+2}}\left[2\beta u^{-1}-1-\frac{2(l+1)}{(\beta+1)^2}u-\frac{(l+1)}{\beta(\beta+1)^2}u^2\right.$$
$$\left.-(l+1)\frac{(\beta_2+1-\beta l)}{\beta^2(\beta+1)^4}u^3+\ldots\right].$$

Hence, noting that

$$[p^m]_B^A=\left(\frac{12\tau}{1-\alpha^2}\right)^{m/3}\left(-i\sin\frac{m\pi}{3}\right),$$

we have

$$\left[\frac{z^{l+1}}{(1-z)^{l+1}(\beta^2-z)^{l+1}}\left(\frac{\beta-z}{\beta+z}\right)\right]_A^B=\frac{(-1)^{l+1}i\sqrt{3}}{(\beta+1)^{2l+2}}\left\{\frac{2}{12^{1/3}}\left(\frac{1-\alpha^2}{\tau}\right)^{1/3}\right.$$
$$\left.+\frac{12^{1/3}}{10}[4+5l-\alpha^2(5l+6)]\left(\frac{\tau}{1-\alpha^2}\right)^{1/3}+O(\tau)\right\}. \qquad (A\,13)$$

Substituting (A 13) into (A 11) gives

$$Y=(-1)^{l+1}e^{-in\pi}\frac{\sqrt{(3)}\Gamma(\frac{2}{3})}{\pi}\frac{(n-l-1)!\,(2l+1)!}{(n+l)!}\frac{(\beta-1)\beta^{-(n'+n+2)}}{(\beta+1)^{2l+1}}\left(\frac{1-\alpha^2}{12n^2}\right)^{1/3}$$
$$\times\left\{1+\frac{12^{2/3}}{30}\frac{\Gamma(\frac{4}{3})}{\Gamma(\frac{5}{3})}\frac{[4+5l-\alpha^2(5l+6)]}{(1-\alpha^2)^{2/3}n^{2/3}}+O\left(\frac{1}{n}\right)\right\}. \qquad (A\,14)$$

Thus finally we have

$$|\rho(nl,n'l+1)|=1{\cdot}3044\sqrt{\frac{(n'+l+1)!\,(n-l-1)!}{(n'-l-2)!\,(n+l)!}}\left(\frac{n}{n'}\right)^{l+3}\frac{1}{n^{2/3}(1-n^2/n'^2)^{5/3}}$$
$$\times\left\{1+0{\cdot}1728\frac{[4+5l-(n/n')^2(5l+6)]}{(1-n^2/n'^2)^{2/3}n^{2/3}}+O\left(\frac{1}{n}\right)\right\}. \qquad (A\,15)$$

The expansion is obviously valid when $n\gg 1$, $n'\gg n$ and $l\ll n$, or when $n'\gg 1$, $n\gg n'$ and $l\ll n'$.

Since the expansion is valid for the second set of conditions, we may obtain from (A 15)

$$|\rho(nl,n'l-1)|=1{\cdot}3044\sqrt{\frac{(n+l)!\,(n'-l)!}{(n-l-1)!\,(n'+l-1)!}}\left(\frac{n'}{n}\right)^{l-2}\frac{1}{n^{2/3}(1-n^2/n'^2)^{5/3}}$$
$$\times\left\{1-0{\cdot}1728\frac{[5l+1-(n/n')^2(5l-1)]}{(1-n^2/n'^2)^{2/3}n^{2/3}}+\ldots\right\}, \qquad (A\,16)$$

with the same conditions on n, n' and l as previously. In Table A I, values of $|\rho|^2$ obtained from (A 14) and (A 15) are compared with those obtained from the exact formulae.

TABLE A I

n	l	n'	l'	$\lvert\rho\rvert^2$ Exact	$\lvert\rho\rvert^2$ Asymptotic	Error (per cent)
5	0	10	1	2·273	2·233	1·8
10	0	20	1	3·195	3·181	0·44
5	1	20	2	0·2101	0·2269	8·0
15	1	20	2	89·61	88·35	1·4
10	1	20	0	1·562	1·530	2·0
15	2	20	3	107·5	105·3	2·0

We now consider the case of bound–free transitions. By a consideration of the hydrogen bound state and continuum radial functions it is easy to show that

$$|\sigma(nl,k^2l')|=\left[\frac{\pi}{2k^3(1-e^{-2\pi/k})}\right]^{1/2}|\rho[nl,(i/k)l']|. \qquad (A\,17)$$

Hence from (A 14) and (A 15) we have that

$$|\sigma(nl,k^2l+1)|=1{\cdot}6348\left[\frac{\prod_{r=1}^{l+1}(1+r^2k^2)}{\prod_{r=0}^{l}(1-r^2/n^2)}\right]^{1/2}\frac{n^{11/6}}{(1+n^2k^2)^{5/3}}$$
$$\times\left\{1+0{\cdot}1728\frac{[4+5l+n^2k^2(5l+6)]}{(1+n^2k^2)^{2/3}n^{2/3}}+O\left(\frac{1}{n}\right)\right\} \qquad (A\,18)$$

and

$$|\sigma(nl, k^2l-1)| = 1{\cdot}6348\left[\frac{\prod_{r=1}^{l}(1-r^2/n^2)}{\prod_{r=0}^{l-1}(1+r^2k^2)}\right]^{1/2}\frac{n^{11/6}}{(1+n^2k^2)^{5/3}}$$
$$\times\left\{1-0{\cdot}1728\frac{[5l+1+n^2k^2(5l-1)]}{(1+n^2k^2)^{2/3}n^{2/3}}+O\left(\frac{1}{n}\right)\right\}, \quad (A\,19)$$

the expansions being valid for $n \gg 1$, $1/k \gg 1$ and $l \ll n$. The factor $(1-e^{-2\pi/k})^{-1/2}$ in (A 17) has been omitted since it is very nearly unity over the permitted range of k.

In Table A II values of $|\sigma|/n^2$ obtained from (A 18) and (A 19) are compared with those obtained from exact formulae.

TABLE A II

n	l	k^2	l'	$\lvert\sigma\rvert/n^2$ Exact	$\lvert\sigma\rvert/n^2$ Asymptotic	Error (per cent)
4	0	0	1	1·6504	1·653	0·2
8	0	0	1	1·3551	1·3557	0·04
12	0	0	1	1·2226	1·2229	0·02
8	1	0	2	1·5847	1·618	2·1
12	1	0	2	1·3925	1·406	1·0
8	1	0	0	0·864	0·850	1·6
12	1	0	0	0·870	0·864	0·7

Lastly we consider the case of free–free transitions. If the required matrix element is

$$\chi(k_1^2l_1, k_2^2l_2) = \int_0^\infty rF(k_1^2l_1, r)F(k_2^2l_2, r)\,dr,$$

where the continuum functions $F(k_1^2l_1, r)$ and $F(k_2^2l_2, r)$ are normalized to asymptotic amplitude $k_1^{-1/2}$ and $k_2^{-1/2}$ respectively, then it can be shown (cf. bound–free case) that

$$|\chi(k_1^2l_1, k_2^2l_2)| = \frac{\pi}{2}\left(\frac{1}{k_1k_2}\right)^{3/2}\frac{\left|\rho\left(\frac{i}{k_1}l_1, \frac{i}{k_2}l_2\right)\right|}{(1-e^{-2\pi/k_1})^{1/2}(1-e^{-2\pi/k_2})^{1/2}}. \quad (A\,10)$$

We thus obtain

$$|\chi(k_1^2l, k_2^2l+1)| = 2{\cdot}0489\left[\frac{\prod_{r=1}^{l+1}(1+r^2k_2^2)}{\prod_{r=0}^{l}(1+r^2k_1^2)}\right]^{1/2}\frac{1}{k_1^{10/3}(1-k_2^2/k_1^2)^{5/3}}$$
$$\times\left\{1-0{\cdot}1728\frac{[4+5l-(k_2/k_1)^2(5l+6)]}{(1-k_2^2/k_1^2)^{2/3}}k_1^{2/3}+O(k_1)\right\}, \quad (A\,21)$$

which is valid for $k_1 \ll 1$, $k_1/k_2 \gg 1$ and $l \ll 1/k_1$ or for $k_2 \ll 1$, $k_2/k_1 \gg 1$ and $l \ll 1/k_2$.

In the course of this work, the asymptotic expansions obtained by Menzel and Pekeris (**16**) were checked. There appears to be an error in the third term of all their expansions, e.g. in equation (A 16) of their paper the factor

$$\left(1+\frac{484}{15}\alpha^2+\alpha^4\right)$$

should be $(1-\frac{4}{3}\alpha^2+\alpha^4)$. Hence equation (1.38) for example should read

$$g_I \simeq \left[1-\frac{0{\cdot}1728(1+n'^2/n^2)}{(1-n'^2/n^2)^{2/3}(n')^{2/3}}-0{\cdot}0496\frac{(1-\frac{4}{3}n'^2/n^2+n'^4/n^4)}{(1-n'^2/n^2)^{4/3}(n')^{4/3}}+\ldots\right\}$$

similar modification being necessary in the formulae for g_{II} and g_{III}, the factor $+\frac{484}{15}$ being replaced by $-\frac{4}{3}$. As a check, in Table A III we compare exact

TABLE A III

n'	n	Δ_{exact}	$\Delta_{asymptotic}$	
			M. and P.	Corrected
5	10	$3{\cdot}4261\times10^{12}$	$3{\cdot}15\times10^{12}$	$3{\cdot}4217\times10^{12}$
10	20	$3{\cdot}6672\times10^{26}$	$3{\cdot}556\times10^{26}$	$3{\cdot}6660\times10^{26}$
20	100	$1{\cdot}3087\times10^{40}$	$1{\cdot}3069\times10^{40}$	$1{\cdot}3087\times10^{40}$

values of the quantity $\Delta\equiv[{}_2F_1(-n', -n+1; 1; x)]^2-[{}_2F_1(-n'+1, -n; 1; x)]^2$ (see equation (A 16) of Menzel and Pekeris (**16**)) with values given by using Menzel and Pekeris's expansion and with those using the correct asymptotic expansion (cf. table VI of (**16**)). We see that the corrected expansion gives much better results especially when n and n' are small.

Department of Physics,
University College London,
*W.C.*1:
1958 *May* 26.

References

(1) Baker, J. G. and Menzel, D. H., *Ap. J.*, **88**, 52, 1938.
(2) Bohm, D. and Aller, L. H., *Ap. J.*, **105**, 131, 1947.
(3) Spitzer, L. and Greenstein, J. L., *Ap. J.*, **114**, 407, 1951.
(4) Seaton, M. J., *M.N.*, **115**, 279, 1955.
(5) Green, L. C., Rush, P. P. and Chandler, C. D., *Ap. J. Suppl. Series*, **3**, 37, 1957.
(6) Gordon, W., *Ann. d. Phys.*, Series 2, **5**, 1051, 1929.
(7) Burgess, A. and Seaton, M. J., *M.N.*, in the press.
(8) Pearson, K., *Tables of the Incomplete Γ-function*, Biometrika Office, London, 1934.
(9) Menzel, D. H. and Baker, J. G., *Ap. J.*, **86**, 70, 1937.
(10) Aller, L. H., Bowen, I. S. and Minkowski, R., *Ap. J.*, **122**, 62, 1955.
(11) Berman, L., *M.N.*, **96**, 890, 1936.
(12) Aller, L. H., *Ap. J.*, **113**, 138, 1951.
(13) Minkowski, R. and Aller, L. H., *Ap. J.*, **124**, 93, 1956.
(14) Whitford, A. E., *Ap. J.*, **107**, 102, 1948.
(15) Aller, L. H. and Minkowski, R., *Ap. J.*, **124**, 110, 1956.
(16) Menzel, D. H. and Pekeris, C. L., *M.N.*, **96**, 77, 1935.
(17) Copson, E. T., *The asymptotic expansion of a function defined by a definite integral or contour integral*, Admiralty Computing Service, London, 1946.
(18) Erdélyi, A., *Asymptotic Expansions*, Dover, 1956.

INTERFEROMETRIC MEASUREMENTS OF WAVE-LENGTHS

VI. Measurements in the region 3940–4450 A

S. Nichols and S. V. M. Clube

(Communicated by the Director of the University Observatory, Oxford)

(Received 1958 June 12)

Summary

The paper describes the measurement of 17 solar and vacuum-arc wave-lengths in the region 3940–4450 A, and brings to 51 the total number of solar red-shifts obtained by the method of circular channels. This group of 17 lines is of interest in that it includes 6 iron lines from the same multiplet: a^3F–y^3F^0; a resonance line of iron: 4375·9 A; and a line of relatively great strength in the chromosphere, due to Ti^+: 4443·8 A. The red-shifts of these lines do not accord with any of the predictions which have at present been made for them. In fact, for the 51 observed lines, the general increase of solar red-shift with line strength is still the only observable regularity.

Introduction

Although the theoretical aspects are as yet uncertain, the major difficulty in interpreting the difference between solar and laboratory wave-lengths probably still arises from the scarcity of observations with small and known limits of uncertainty. In illustration we may point to the Allegheny Observatory–Bureau of Standards red-shifts quoted in Paper V of this series (**5**) for lines of the same strength (Section 2.2); these were selected as the most homogeneous available but they show a completely anomalous variation with wave-length. While this may be a genuine observational feature of red-shifts, it strongly suggests scale errors, different for the arc and solar wave-lengths in the A.O.–B.S. measures. Burns and Meggers themselves mention the possibility of scale errors in their work. We believe that such errors are substantially reduced by the technique we are now using for measuring wave-lengths (Paper IV (**4**)), and that it is therefore worthwhile to redetermine wave-lengths and red-shifts for representative solar lines over a wide range of line strengths and spectral region. The Oxford measures, so far, have included only three lines in wave-length regions shorter than 5080 A; in this paper we give results for 17 lines in the blue and violet between 3944–4450 A. The lines include some of special interest from the point of view of theoretical interpretation; these are noted in the comments following the observational results.

In Table I are recorded the lines whose solar and arc wave-lengths have been measured. The lines fall observationally into two groups, 3944–4143 A and 4376–4449 A, which are discussed separately in Sections 1 and 2. Various relevant data are included in this table. For convenience, the values of δ/λ for the lines are shown plotted against $\log(W/\lambda \times 10^6)$ in Fig. 1, where δ is the residual red-shift equal to observed red-shift minus relativity shift, W is the equivalent width of the line and λ the wave-length; both W and λ are measured in the same units. The numbering is continued from Paper V of this series. The open circles on

the figure refer to lines 1–34 (already published), and the filled circles to the new observations. Members of the same multiplet are shown joined.

TABLE I

Lines measured

No.	El.	Intensity	Wave-length	Multiplet	Transition	Ex. pot. (low)	log ($W/\lambda \times 10^6$)
(Rowland revision values)				(Reference : 10)		(volts)	(W taken from 6)
35	Al	15	3944·0 A	1	$3^2P^0–4^2S$	0·00	2·217
36	Al	20	3961·5	1	$3^2P^0–4^2S$	0·01	2·356
37	Fe	10	3969·3	43	$a^3F–y^3F^0$	1·48	2·057
38	Fe	30	4045·8	43	$a^3F–y^3F^0$	1·48	2·473
39	Fe	20	4063·6	43	$a^3F–y^3F^0$	1·55	2·324
40	Fe	15	4071·7	43	$a^3F–y^3F^0$	1·60	2·248
41	Fe	10	4132·1	43	$a^3F–y^3F^0$	1·60	1·964
42	Fe	15	4143·9	43	$a^3F–y^3F^0$	1·55	2·025
43	Fe	6	4375·95	2	$a^5D–z^7F^0$	0·00	1·520
44	Fe	15	4383·6	41	$a^3F–z^5G^0$	1·48	2·388
45	Ca	5	4434·97	4	$4^3P^0–4^3D$	1·88	1·614
46	Ca	4	4435·7	4	$4^3P^0–4^3D$	1·88	1·456
47	Fe	6	4442·3	68	$a^5P–x^5D^0$	2·19	1·554
48	Fe	3	4443·2	350	$b^3P–x^3D^0$	2·85	1·386
49	Ti^+	5	4443·8	19	$a^2D–z^2F^0$	1·075	1·464
50	Fe	6	4447·7	68	$a^5P–x^5D^0$	2·21	1·534
51	Ti	2	4449·1	160	$a^5F–y^3G^0$	1·88	1·114

1. *Strong lines of iron and aluminium in the region* 3944–4144 A

1.1. *Procedure.*—In the region 3944–4144 A, eight strong solar lines were measured: six of these are members of the iron multiplet, Fe I 43, and the other two are the interlocking lines 3962 A and 3944 A of Al I. These lines are listed in the first part of Table I. The observations were made during 1957 August and September by S.N.

The method of circular channels was used in the determination of the solar and laboratory wave-lengths and the final experimental procedure followed Paper III (**3**). The solar lines were observed at the centre of the disk over a slit height 1/10 of the diameter of the solar image. The spectrograph was employed in its three-prism, diaphragmed form giving a dispersion of about 0·63 A/mm in this region.

For the laboratory lines, a vacuum-arc with vertical pole-pieces was used and a rotary oil pump maintained the arc pressure at 4 cm of mercury; the pressure was indicated by an absolute aneroid type of gauge. With a pole-piece separation of 10 mm, currents of about 8 amps were used. Only light from the central part of the arc was used so as to avoid any possible complications due to pole-effect. Mild-steel pole-pieces were inserted for the iron lines, and carbon pole-pieces plugged with aluminium alloy for the aluminium lines. The latter were thus obtained without any indication of self-reversal.

Ilford Rapid Process Panchromatic R.40 plates were used for the solar work, and I.R.P.P. and H.P.3 plates for the arc. The plates were measured on the modified Hilger machine fitted with a rotating stage. Both the machine and the method of reduction have been fully described in the earlier papers.

1.2. *Corrections to the observed wave-lengths.*—The solar wave-lengths are corrected for the Earth's diurnal rotation and orbital motion. The arc wave-lengths have been reduced to their vacuum-arc values using Babcock's empirical relation between the depression d (cm^{-1}) of a spectral term per atmosphere, and the excitation potential V (volts) of the term. This relation is $d = 1{\cdot}15V^2 - 1{\cdot}93V$ for the triplet terms of iron (**7**), and the pressure shift is given by the difference between the depressions for the two terms involved in the transition. The same relation was also used for the aluminium lines because no other information is available. In any case, the corrections were very small and of the order of 0·0001 A.

Both solar and arc wave-lengths had to be corrected for the dispersion of air. If conditions differ greatly from N.T.P., this correction is important because of the large difference in wave-length region of the lines measured and the primary standard (Cd 6438·4696 A). Pressures and temperatures were recorded during the observations, and the measured wave-lengths were reduced to standard atmospheric conditions by using H. D. Babcock's tables (**8**). The corrections were of the order of 0·0005 A.

The phase change corrections were obtained from plates showing the line 4046 A of Hg 198, the source being a water-cooled mercury–198 isotope lamp. Because of the small wave-length range, the phase change corrections for other wave-lengths were determined with sufficient accuracy by extrapolation, the slope of the phase change–wave-length curve being known from previous work.

Although fused silica etalon plates of small wedge angle ($2\frac{1}{2}'$) were used, a correction for the differential deviation of the two cones of rays, standard and line, was made to the wave-lengths ((**1**), Section 2.2). This correction was of the order of only 0·0006 A.

1.3. *The observed wave-lengths.*—The measured wave-lengths in the region 3944–4144 A are given in Table II. In column 3 the width of the etalon spacers are given. Two spacers, $1\frac{1}{2}$ mm and $2\frac{1}{2}$ mm, were used for the Fe I line No. 38 and the results are in good agreement. For the solar lines the difference for the averages of the spacers is 0·0011 A and for the arc lines 0·0001 A. In the case of the line 3969 A, which lies in the wing of the H line of Ca^+, 1 mm and $1\frac{1}{2}$ mm spacers were used, the wave-length differences being 0·0009 A, solar, and 0·0035 A, arc. The latter difference, especially, in the arc lines is somewhat disappointing and not easy to explain, but a 1 mm spacer, which was only brought into use for the H and K lines, must strain any interferometric procedure to the limit.

TABLE II

Wave-lengths and red-shifts in region 3944–4144 A

			Sun			Arc			
No.	El.	Spacer mm	Wave-length	Std. dev.	No. of plates	Wave-length	Std. dev.	No. of plates	Red-shift
35	Al	$1\frac{1}{2}$	3944·0136 A	±0·0001	6	3944·0070 A	±0·0005	6	6·6 mA
36	Al	$1\frac{1}{2}$	3961·5320	0·0005	6	3961·5210	0·0004	6	11·0
37	Fe	1, $1\frac{1}{2}$	3969·2650	0·0015	16	3969·2581	0·0005	12	6·9
38	Fe	$1\frac{1}{2}$, $2\frac{1}{2}$	4045·8185	0·0005	12	4045·8100	0·0002	12	8·5
39	Fe	$1\frac{1}{2}$	4063·5980	0·0009	8	4063·5932	0·0003	8	4·8
40	Fe	$1\frac{1}{2}$	4071·7468	0·0011	8	4071·7383	0·0007	8	8·5
41	Fe	$1\frac{1}{2}$	4132·0688	0·0004	8	4132·0597	0·0003	8	9·1
42	Fe	$1\frac{1}{2}$	4143·8758	0·0010	8	4143·8667	0·0009	8	9·1

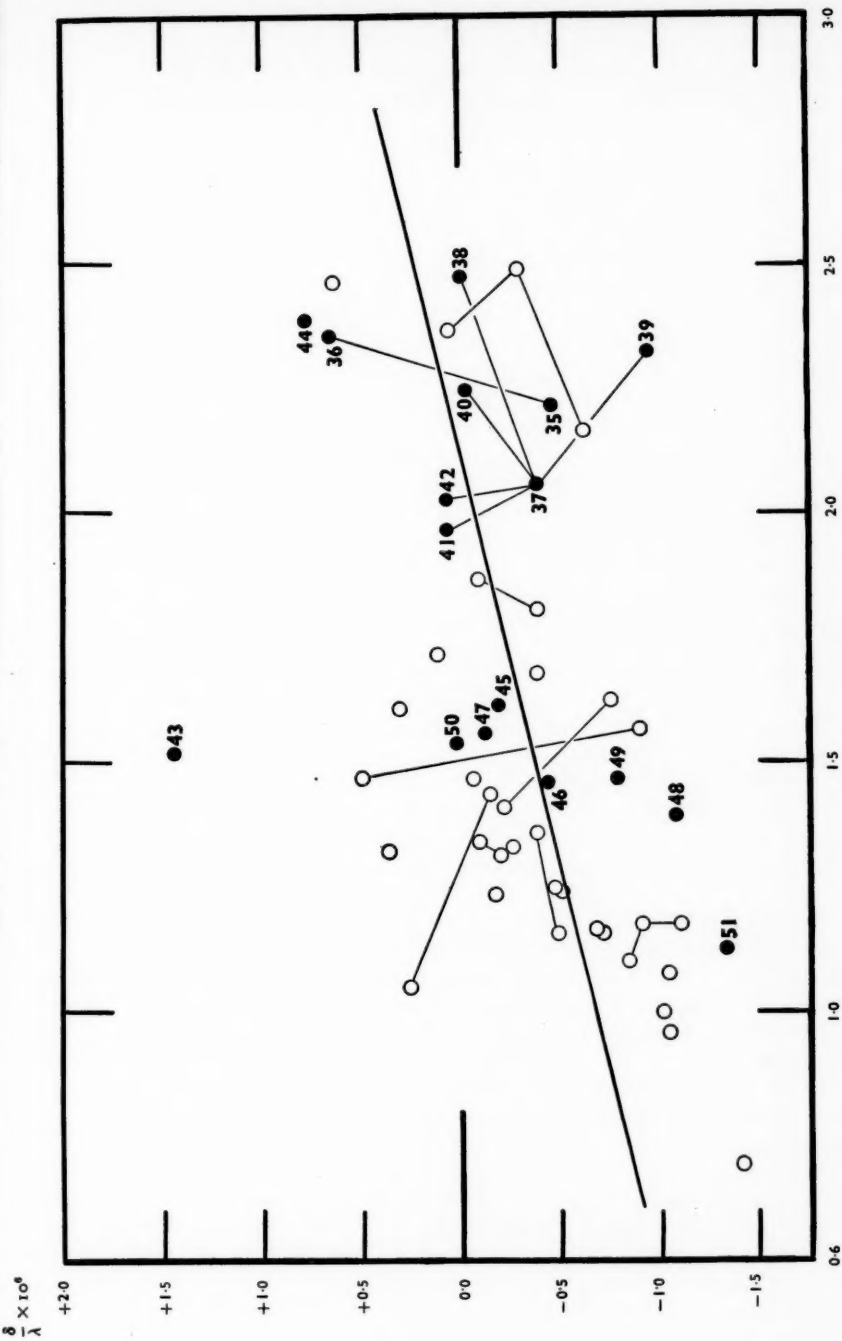

FIG. 1.—(δ/λ) *as a function of line strength.*

The relativity shift in this region is 8·6 mA, and it can be seen from Table II and Fig. 1 that all six members of the Fe multiplet, irrespective of their strengths, show approximately this value, with only the line 38 seriously different. The mean red-shift for the two aluminium lines is also closely equal to the relativity shift.

2. *Fe, Ca, Ti lines in the region* 4375–4450 A

2.1. *Observations.*—Observations for wave-lengths at the centre of the solar disk and in the vacuum-arc for the nine lines 43–51 were made by the method of circular channels, before the investigation referred to in Paper III was completed. The light patches for the standard and unknown sources were coincident on the interferometer plates but not of the same size. The spectra were obtained by Miss Adam in 1953 August, using the spectroscope in its three-prism form giving a dispersion of 0·95 A/mm. For most of the plates the spectroscope collimator was diaphragmed to its usual 3 cm strip (**11**), but in order to reduce the arc exposure time for the faint iron lines and the titanium lines the diaphragm was removed. To assess any change in the measured wave-lengths arising from this change in the optical train, the iron arc was observed through both the diaphragmed and the un-diaphragmed spectroscope. (The original vacuum-arc with horizontal pole-pieces was used for these nine lines, with the usual operating conditions; pressures were of the order of $\frac{1}{8}$ atmosphere.)

The cadmium pattern was photographed on the plate in the form of a simple cross, as in Paper I, without the "side arms", which were subsequently added following the investigations of Paper III. As is shown there, this leads to possible errors in wave-length due to irregularities in the interferometer plates, but the red-shifts obtained with the same plate-orientations for the solar and arc wave-lengths, are not systematically affected. In our results in Tables III and IV, the groups A, B, C and D, correspond to different plate-orientations and the red-shifts have always been obtained from photographic plates in the same group.

2.2. *Measurement and reduction.*—The interferometer plates were the originals, of crystalline quartz with a wedge angle of 15′. The large angle necessitated a correction (as in Paper I) for the shift of the pattern centre between the regions 6438 and 4400 A. The modification of the measuring machine, whereby the photographic plates can be measured from very near the true pattern centre, has made the application of this correction a much simpler matter than as described in Paper I. The displacement of the pattern centre due to the wedge angle can be calculated as in I, and it suffices to incorporate the component of the displacement parallel to the dispersion with the displacement $2x'$ (see (**2**)) of the Cd pattern centre from the centre of rotation of the table. The maximum error arising from this simplified procedure was estimated at 0·0002 A in our results.

The reduction of the plates otherwise followed the normal scheme. The phase-change corrections for reflection at the silvered plates of the etalon (silver coatings of similar density to those in Paper IV) were taken from Table I of Paper IV. The solar wave-lengths were corrected for Doppler effects due to the Earth's rotation and radial motion relative to the Sun, while the arc wave-lengths were corrected for the small pressure shifts according to Babcock's formulae (**7**) for iron lines—also applied to calcium and titanium lines.

Gale and Adams (**9**) have found that although pressure shifts for ionized titanium lines are generally quite large that of the line 4443·8 A is comparable to the shift for iron lines. Assuming that the variation of pressure shifts in the Ti^+ line with excitation potential followed that of the Fe lines at low pressure, a small value was deduced for the necessary correction. The pressure shift corrections made are shown in Table III.

2.3. *Wave-lengths and red-shifts.*—The observed solar and arc wave-lengths for each group are recorded in Table III. As mentioned above, the absence of "side arms" on the plates does not allow us to estimate errors in the wave-lengths due to irregularities in the etalon plates, and this has, to a certain extent, rendered our absolute values of wave-lengths uncertain. The (λ solar–λ arc) values taken from each group should however remain unaffected by these variations; these red-shifts are recorded in Table IV. In Table III, the asterisked wave-lengths were obtained from plates taken with the spectroscope undiaphragmed. It was found from the iron lines that (λ diaphragmed–λ undiaphragmed) = 0·0035 A. This correction, which is presumably due to the change in area of the etalon plates traversed by the light, was applied to the "undiaphragmed wave-lengths", prior to the calculation of red-shifts and absolute wave-lengths. The mean absolute values for the solar and arc wave-lengths are also recorded in Table III; the standard errors are rather large due to the differences in wave-length from group to group. The red-shifts between these absolute values are slightly different from those in Table IV but it is felt that the latter have more significance since errors due to alterations of the etalon plate orientation are eliminated.

TABLE III

Observed wave-lengths in the region 4400 A

Element		Fe	Fe	Ca	Ca	Fe	Fe	Ti^+	Fe	Ti
wave-length (in A)		4375·–	4383·–	4434·–	4435·–	4442·–	4443·–	4443·–	4447·–	4449·–
Pressure shift (arc)		0·0002	0·0004	0·0005	0·0005	0·0006	0·0007	0·0004	0·0006	0·0005
Group										
A	Solar (4)			·9641	·6862	·3488	·1999	·8083	·7273	
	Arc (6)			·9556	·6786	·3395	·1950		·7168	
B	Solar (3)			·9659	·6867	·3461	·1992	·8070	·7242	
	Arc (2)					·3396	·1939		·7152	
C	Solar (5)			·9656	·6871	·3505	·1997	·8087	·7261	·1472
	Arc (2–6)			·9568	·6799	·3412	·1954		·7181	
						*·3376	*·1926	*·7993	*·7143	*·1402
D	Solar (10)	·9454								
	Arc (5)	·9296								
	Solar (6)		·5581							
	Arc (8)		·5453							
	Solar	·9454	·5581	·9652	·6867	·3488	·1996	·8083	·7260	·1472
Mean		±0010	±0008	±0015	±0013	±0025	±0013	±0015	±0024	±0012
wave-lengths	Arc	·9296	·5453	·9559	·6788	·3395	·1943	·8028	·7163	·1437
		±0010	±0011	±0010	±0007	±0012	±0014	±0005	±0017	±0009

The figures in brackets indicate the number of plates measured.

TABLE IV

Red-shifts in mA (*region* 4400 A)

Wave-length (in A)	4375·95	4383·6	4434·96	4435·69	4442·35	4443·20	4443·81	4447·73	4449·15
Group									
A			8·5	7·6	9·3	4·9		10·5	
B					6·5	5·3		9·0	
C			8·8	7·2	9·4	4·0	5·9	8·2	3·5
D	15·8	12·8							
Mean*	15·8	12·8	8·6	7·5	8·9	4·6	5·9	9·3	3·5

*The mean red-shift was calculated by weighting according to the number of plates taken.

2.4. *Comments on results.*—In this group of nine lines the red-shifts of the lines Ti^+ 4443·8 A and Fe 4375·9 A are of special interest; the former both on account of the fact that it is an ionized line and also because of its relatively strong emission in the chromosphere, and the latter because it is a resonance line.

The seven lines 45–51 were taken for the most part in the same solar exposure. This is of some importance should secular effects be responsible for the large scatter amongst observed red-shifts; for these measures of seven lines on the same plate eliminate any uncertainty which may arise from the comparison of lines measured at different times. The most obvious characteristic of this group is the steady increase of red-shift with line strength. Schröter (**13**) predicts a difference between the red-shifts of neutral and ionized lines, since the lines are formed at different levels in the solar atmosphere. Also, Plaskett (**12**) has pointed out that the chromospheric emission line must be superposed on the photospheric absorption line and so any asymmetry in the former will lead to an asymmetry and apparent wave-length shift in the latter. Our present data are hardly conclusive, but this study of seven lines 45–51 does not reveal any exceptional red-shift of the Ti^+ line (see Fig. 1, showing δ/λ against $\log(W/\lambda \times 10^6)$).

The resonance line of iron, 4375·9 A, has an exceptionally large red-shift. (The Einstein shift for this region is 0·0093 A.) This is in contrast to the measured resonance lines of calcium (4226·7, 6572·8 A), aluminium (3961·5, 3944 A) and titanium (5173·8 A), whose red-shifts are more in accord with some line-strength relationship. The Utrecht Atlas shows no blending lines likely to disturb the iron resonance line, and it is therefore probable that the abnormally large red-shift is real.

Conclusion.—The results given in this paper bring to 51 the total number of red-shifts measured by the method of circular channels. The measurements now extend over the whole visible spectrum and the line strengths range from lines of Rowland No. 1 to Rowland No. 30. This statistical approach establishes only one recognizable regularity in the shifts, namely the increase in shift with line strength (Paper II). For the 51 results as shown in Fig. 1, the correlation coefficient between δ/λ and $\log(W/\lambda \times 10^6)$ is 0·458, with a significance level better than 0·001. The y on x regression line for the distribution is shown on the figure.

The present paper, VI, concludes the series of papers on interferometrically-determined red-shifts at the centre of the disk. It is proposed now to investigate special lines of theoretical interest, without restriction to method and not limiting the measurements only to the centre of the disk.

The authors express their thanks to Dr M. G. Adam for helpful discussions during the course of this work and to the D.S.I.R. for maintenance grants.

University Observatory,
Oxford:
1958 *June* 1.

References

(1) M. G. Adam, *M.N.*, **112**, 546, 1952; Comm. Univ. Obs. Oxford, No. 26. Paper I.
(2) M. G. Adam, *M.N.*, **115**, 367, 1955; Comm. Univ. Obs. Oxford, No. 49. Paper II.
(3) M. G. Adam, *M.N.*, **115**, 385, 1955; Comm. Univ. Obs. Oxford, No. 50. Paper III.
(4) M. G. Adam and S. Nichols, *M.N.*, **118**, 97, 1958; Comm. Univ. Obs. Oxford, No. 65. Paper IV.
(5) M. G. Adam, *M.N.*, **118**, 106, 1958; Comm. Univ. Obs. Oxford, No. 66. Paper V.
(6) C. W. Allen, *Mem. Comm. Solar Obs.*, **5**, 1934.
(7) H. D. Babcock, *Ap. J.*, **67**, 240, 1928.
(8) H. D. Babcock, *Ap. J.*, **111**, 60, 1950.
(9) H. G. Gale and W. S. Adams, *Ap. J.*, **35**, 10, 1912.
(10) C. E. Moore, *A Multiplet Table of Astrophysical Interest*, rev. ed., Princeton, 1945.
(11) H. H. Plaskett, *M.N.*, **112**, 99, 1952; Comm. Univ. Obs. Oxford, No. 33.
(12) H. H. Plaskett, *Obs.*, **76**, 217, 1956.
(13) E. H. Schröter, *Zs. f. Ap.*, **41**, 141, 1957.

THE QUANTUM DEFECT METHOD

M. J. Seaton

(Received 1958 May 27)

Summary

The Quantum Defect Method uses interpolated or extrapolated quantum defects to determine the asymptotic forms of atomic wave functions. The method may be used in the calculation of atomic transition probabilities and photo-ionization cross sections, in electron-ion collision calculations and also in connection with solid state problems.

The paper gives a summary of previous work on the fundamental ideas of the method and presents some new results for positive energy states and for the normalization of bound-state wave functions. Some applications of the method are discussed.

Introduction.—When calculating atomic properties one may consider semi-empirical methods which make use of known energy-level data. One approach is to construct potentials which will reproduce a number of observed levels (**1, 2, 3**) but this has the disadvantage that each individual case has to be treated separately and that the calculations may be very laborious. Hylleraas (**4**) and Bates and Damgaard (**5**) have developed more general methods for transition probability calculations. The transition integrals are tabulated directly as functions of the effective quantum numbers* ν_{nl} defined by

$$T_{nl}=\frac{Rz^2}{\nu_{nl}^2}, \tag{1}$$

where T_{nl} is the energy, measured in cm^{-1}, required to remove the nl electron, $R=109737\ cm^{-1}$ is the Rydberg wave-number and z is the residual charge ($z=1$ for neutral atoms).

The quantum defect μ_{nl}, defined by $\mu_n=n-\nu_{nl}$, usually varies slowly in a spectral series and tends to a definite limit $\mu_{\infty l}$ at the spectral head. For collisions between electrons and positive ions one requires the phase differences between the wave functions for the electron in the ion field and the corresponding wave function in a pure Coulomb field. It has been shown previously (**6**) that the zero energy phase is equal to $\pi\mu_{\infty l}$. This result has been used in various electron–ion collision problems (**7, 8, 9, 10**).

Similar methods have been developed for the study of solid-state problems (Ham (**11**)); for these problems one requires the asymptotic forms of the wave functions for negative energies other than those corresponding to eigenvalues of the free atom. The use of interpolated or extrapolated quantum defects will be referred to as the Quantum Defect Method. In the present paper the general theory of the method is developed by considering a simplified mathematical problem. Some of our analysis is a summary of the work of Ham (**11**) and of some much

* For effective quantum numbers we use ν in place of the more familiar n^*.

earlier work by Hartree (**12**). These authors were concerned with the negative energy states. In the present paper new results are given for the positive energy states and also for the normalization of bound state wave functions. We discuss the use of the method in collision problems and also its practical limitations. In a later paper (Burgess and Seaton (**13**)) the Quantum Defect Method will be used for the calculation of photo-ionization cross-sections.

1. *Valence-electron states.*—We consider an N-electron atom with nuclear charge Z and put $z=(Z-N+1)$. An approximate radial function for a valence-electron may be obtained on solving an equation of the type

$$\left[\frac{d^2}{dr^2}-\frac{l(l+1)}{r^2}-V(r)+E\right]P(E,l;r)=0 \qquad (2)$$

where r is in atomic units and E and V are in Rydberg units (13·60 eV or 109 737 cm^{-1}). The potential $V(r)$ is such that $rV(r)=-2Z$ for r small and $rV(r)=-2z$ for r large.

For $E<0$ solutions of (2) which are everywhere bounded and continuous exist only for the discrete eigenvalues E_{nl} of E. The quantum number n may be defined by stating that: n may take on the values $(l+1)$, $(l+2)$, ...; $n=(l+1)$ corresponds to the lowest eigenvalue; $E_{n'l}$ is greater than E_{nl} for $n'>n$. An equivalent definition is that the number of nodes in $P(E_{nl},l;r)$, excluding the origin and infinity, is $(n-l-1)$. We put $E_{nl}=-z^2/\nu_{nl}^2$ and $\mu_{nl}=n-\nu_{nl}$. Then $\mu_{nl}=0$ for the pure Coulomb field, $V(r)=-2z/r$.

For $E>0$ we put $E=k^2$. The solution $P(k^2,l;r)$ which is bounded at the origin will have asymptotic form

$$P(k^2,l;r)\underset{r\to\infty}{\sim}\text{const.}\times\sin\left[kr-\tfrac{1}{2}l\pi+\frac{z}{k}\ln(2kr)+\arg\Gamma\left(l+1-\frac{iz}{k}\right)+\delta_l\left(\frac{k^2}{z^2}\right)\right]. \qquad (3)$$

The phase δ_l is zero for the pure Coulomb field.

2. *Coulomb functions.*—We consider the equation

$$\left[\frac{d^2}{dr^2}-\frac{\lambda(\lambda+1)}{r^2}+\frac{2z}{r}+E\right]y=0 \qquad (4)$$

where λ is not necessarily an integer. Introducing

$$\rho=zr, \quad \epsilon=\frac{E}{z^2}=-\frac{1}{\kappa^2} \qquad (5)$$

we obtain

$$\left[\frac{d^2}{d\rho^2}-\frac{\lambda(\lambda+1)}{\rho^2}+\frac{2}{\rho}-\frac{1}{\kappa^2}\right]y=0. \qquad (6)$$

For $\epsilon<0$ we put $\kappa=\nu$ with ν real and positive and for $\epsilon>0$ we put $\kappa=i\gamma$ with γ real and positive. Then $\gamma=z/k$.

Entire analytic functions.—Let $y(\kappa,\lambda;\rho)$ be a solution of (6). Following Ham (**11**) we shall say that $y(\kappa,\lambda;\rho)$ is an entire analytic function of $\epsilon=-1/\kappa^2$ if, for ρ infinite, $y(\kappa,\lambda;\rho)$ is a single-valued analytic function of ϵ in the entire ϵ-plane save for the point at infinity. Such a function may be represented by an expansion

$$y(\kappa,\lambda;\rho)=\sum_{p=0}^{\infty}\epsilon^p f_p(\lambda;\rho) \qquad (7)$$

absolutely and uniformly convergent for $\epsilon \leqslant |\mathscr{E}| < \infty$, $\rho \leqslant |\mathscr{R}| < \infty$. Conversely, y will be an entire analytic function if such an expansion exists.

For the theory of the Quantum Defect Method we require, for the case of $\lambda = l = 0, 1, 2, \ldots$, two linearly independent solutions of (6) both of which are entire analytic functions of ϵ. We also require the asymptotic forms of these solutions for ρ large.

Solutions of the Coulomb equation.—We consider the following solutions of (6):

$$y_1(\kappa,\lambda;\rho) = \frac{\kappa^{\lambda+1}}{\Gamma(2\lambda+2)} M_{\kappa,\lambda+1/2}(2\rho/\kappa), \tag{8}$$

$$y_2(\kappa,\lambda;\rho) = y_1(\kappa,-\lambda-1;\rho)$$
$$= \frac{\kappa^{-\lambda}}{\Gamma(-2\lambda)} M_{\kappa,-\lambda-1/2}(2\rho/\kappa), \tag{9}$$

$$y_3(\kappa,\lambda;\rho) = \frac{A(\kappa,\lambda)\cos\pi(2\lambda+1)y_1(\kappa,\lambda;\rho) - y_2(\kappa,\lambda;\rho)}{\sin\pi(2\lambda+1)}, \tag{10}$$

$$y_4(\kappa,\lambda;\rho) = y_3(\kappa,\lambda;\rho) - G(\kappa,\lambda)y_1(\kappa,\lambda;\rho), \tag{11}$$

$$y_5(\kappa,\lambda;\rho) = W_{\kappa,\lambda+1/2}(2\rho/\kappa). \tag{12}$$

The functions $M_{\kappa,\lambda+\lambda/2}$ and $W_{\kappa,\lambda+1/2}$ are defined by Whittaker and Watson (**14**) and

$$A(\kappa,\lambda) = \frac{\Gamma(\kappa+\lambda+1)}{\kappa^{2\lambda+1}\Gamma(\kappa-\lambda)}, \tag{13}$$

$$G(\kappa,\lambda) = \frac{1}{2\pi}\frac{\partial}{\partial\lambda}A(\kappa,\lambda)$$
$$= \frac{A(\kappa,\lambda)}{2\pi}\{\psi(\kappa+\lambda+1) + \psi(\kappa-\lambda) - 2\ln(\kappa)\} \tag{14}$$

where $\psi(x) = d[\ln\Gamma(x)]/dx$.

The definition of y_1 may be written

$$y_1(\kappa,\lambda;\rho) = (2\rho)^{\gamma+1}\,e^{-\rho/\kappa}\Phi(\lambda+1-\kappa, 2\lambda+2; 2\rho/\kappa) \tag{15}$$

where

$$\Phi(\lambda+1-\kappa, 2\lambda+2; 2\rho/\kappa) = \sum_{\sigma=0}^{\infty} \frac{\Gamma(\lambda+1-\kappa+\sigma)\Gamma(2\lambda+2)}{\Gamma(\lambda+1-\kappa)\Gamma(2\lambda+2+\sigma)\sigma!}\left(\frac{2\rho}{\kappa}\right)^{\sigma}. \tag{16}$$

The series for Φ and for $\exp(-\rho/\kappa)$ converge absolutely and uniformly for $|\rho/\kappa| \leqslant |B| < \infty$. Since $\Gamma(\lambda+1-\kappa+\sigma)/\Gamma(\lambda+1-\kappa)$ is a polynomial in κ of order σ one may express y_1 as a series of powers of $(1/\kappa)$. By Kummer's transformation (**14**), $y_1(-\kappa,\lambda;\rho) = y_1(\kappa,\lambda;\rho)$ and therefore only even powers of $(1/\kappa)$ will occur. Therefore y_1 is an entire analytic function of ϵ. In the same way one may show that y_2 is an entire analytic function of ϵ.

For $\lambda \neq l$ ($l = 0, 1, 2, \ldots$), y_1 and y_2 provide two linearly independent solutions of (6) but on letting $\lambda \to l$ one obtains

$$y_2(\kappa,l;\rho) = -A(\kappa,l)y_1(\kappa,l;\rho). \tag{17}$$

Since

$$\lim_{|\kappa|\to\infty} y_1(\kappa,\lambda;\rho) = (2\rho)^{1/2}J_{2\lambda+1}(\sqrt{(8\rho)}), \tag{18}$$

$$\lim_{|\kappa|\to\infty} y_2(\kappa,\lambda;\rho) = (2\rho)^{1/2}J_{-2\lambda-1}(\sqrt{(8\rho)}), \tag{19}$$

$$\lim_{|\kappa|\to\infty} A(\kappa,\lambda) = 1, \tag{20}$$

in the limit of large κ (17) corresponds to the Bessel function relation

$J_{2l+1} = -J_{-2l-1}$. The Weber function is defined by

$$Y_{2\lambda+1} = \frac{\cos\pi(2\lambda+1)J_{2\lambda+1} - J_{-2\lambda-1}}{\sin\pi(2\lambda+1)} \tag{21}$$

and by the limit of (21) for $\lambda \to l$. Then $J_{2\lambda+1}$ and $Y_{2\lambda+1}$ are linearly independent for all λ. Wannier (**15**) introduced the function y_3 by analogy with (21). From equations (18) to (21) one obtains

$$\lim_{|\kappa|\to\infty} y_3(\kappa, \lambda; \rho) = (2\rho)^{1/2} Y_{2\lambda+1}(\sqrt{(8\rho)}). \tag{22}$$

Defining $y_3(\kappa, l; \rho)$ as the limit of equation (10) for $\lambda \to l$ one obtains

$$y_3(\kappa, l; \rho) = \frac{1}{2\pi}\left\{A(\kappa, l)\frac{\partial}{\partial\lambda}y_1(\kappa, \lambda; \rho) + \frac{\partial}{\partial\lambda}y_2(\kappa, \lambda; \rho) + y_1(\kappa, l; \rho)\frac{\partial}{\partial\lambda}A(\kappa, \lambda)\right\}_{\lambda=l}. \tag{23}$$

Since $y_1(\kappa, \lambda; \rho)$ and $y_2(\kappa, \lambda; \rho)$ are entire analytic functions for all λ, $\partial y_1/\partial\lambda$ and $\partial y_2/\partial\lambda$ are also entire analytic functions. Also, since

$$A(\kappa, l) = \frac{(\kappa+l)(\kappa+l-1)\ldots(\kappa-l)}{\kappa^{2l+1}} \tag{24a}$$

$$= \frac{[\kappa^2-l^2][\kappa^2-(l-1)^2]\ldots[\kappa^2-1]}{\kappa^{2l}} \tag{24b}$$

and $A(\kappa, 0) = 1$, $A(\kappa, l)$ is a polynomial in $1/\kappa^2$ of order l. But $\partial A(\kappa, \lambda)/\partial\lambda$ cannot be expressed as a convergent power series in $1/\kappa^2$ and therefore $y_3(\kappa, l; \rho)$ is not an entire analytic function of ϵ. The entire analytic function $y_4(\kappa, l; \rho)$ is obtained (**11**) on subtracting from $y_3(\kappa, l; \rho)$ the term in $\partial A/\partial\lambda$.

The required entire analytic functions are therefore $y_1(\kappa, l; \rho)$ and $y_4(\kappa, l; \rho)$. The expansions of these functions are discussed in the Appendix.

Properties of the function $G(\kappa, l)$.—It is convenient to put

$$G(\kappa, l) = \mathcal{G}(\kappa, l) + i\mathcal{H}(\kappa, l) \tag{25}$$

where $\mathcal{G}$ and $\mathcal{H}$ are real. From (14) $G(\nu, l)$ is real for ν real and positive: therefore

$$\mathcal{H}(\nu, l) = 0 \qquad (\nu \text{ real and positive}). \tag{26}$$

For γ real and positive $G(i\gamma, l)$ is complex: using

$$\psi(x) - \psi(1-x) = -\pi\cot(\pi x)$$

one obtains

$$\mathcal{H}(i\gamma, l) = \frac{A(i\gamma, l)}{[e^{2\pi\gamma}-1]} \qquad (\gamma \text{ real and positive}). \tag{27}$$

Relations involving the Whittaker function.—It is convenient to express y_3 and y_4 in terms of y_1 and the Whittaker function y_5. Using the relations

$$W_{\kappa,\lambda+1/2} = \frac{\Gamma(-2\lambda-1)}{\Gamma(-\lambda-\kappa)}M_{\kappa,\lambda+1/2} + \frac{\Gamma(2\lambda+1)}{\Gamma(\lambda+1-\kappa)}M_{\kappa,-\lambda-1/2} \tag{28}$$

(**14**) valid for $\lambda \neq l$ and

$$\Gamma(x)\Gamma(1-x) = \frac{\pi}{\sin(\pi x)} \tag{29}$$

one obtains

$$y_5 = \frac{\pi}{\sin(2\pi\lambda)}\left\{\frac{\kappa^{-\lambda-1}y_1}{\Gamma(-\lambda-\kappa)} - \frac{\kappa^{\lambda}y_2}{\Gamma(\lambda+1-\kappa)}\right\}. \tag{30}$$

We use (30) to eliminate y_2 in (10) and then let $\lambda \to l$. This gives

$$y_3(\kappa, l; \rho) = -A(\kappa, l)\cot(\pi\kappa)y_1(\kappa, l; \rho) - \frac{\Gamma(l+1-\kappa)}{\pi\kappa^l}\, y_5(\kappa, l; \rho) \tag{31}$$

and from (11)

$$y_4(\kappa, l; \rho) = -[A(\kappa, l)\cot(\pi\kappa) + G(\kappa, l)]y_1(\kappa, l; \rho) - \frac{\Gamma(l+1-\kappa)}{\pi\kappa^l}\, y_5(\kappa, l; \rho). \tag{32}$$

Asymptotic expansions.—In the limit of $\rho \to \infty$, $y_1(\kappa, l; \rho)$ ceases to be a single-valued function of κ. We therefore consider $\kappa = \nu + i\gamma$ with $\nu \geqslant 0$, $\gamma \geqslant 0$. The asymptotic expansion for y_1 is then (**16**)

$$y_1(\kappa, l; \rho) \underset{\rho\to\infty}{\sim} \kappa^{l+1} e^{-i\frac{1}{2}\pi(l-\kappa)} \left\{ \frac{(2\rho/\kappa)^{-\kappa} \exp[\rho/\kappa + i\tfrac{1}{2}\pi(l-\kappa)]}{\Gamma(l+1-\kappa)} - \frac{(2\rho/\kappa)^{\kappa} \exp[-\rho/\kappa - i\tfrac{1}{2}\pi(l-\kappa)]}{\Gamma(l+1+\kappa)} \right\}. \tag{33}$$

It is seen that $y_1(\nu, l; \rho) \to \infty$ for $\rho \to \infty$, except when $\nu = n = (l+1), (l+2), \ldots$; when $\nu = n$, $\Gamma(l+1-\nu)$ is infinite and $y_1(n, l; \rho) \to 0$ for $\rho \to \infty$.

Substitution of $\kappa = i\gamma$ in (33) gives

$$y_1(i\gamma, l; \rho) \underset{\rho\to\infty}{\sim} \frac{2\gamma^{l+1} e^{-\pi\gamma/2}}{|\Gamma(l+1-i\gamma)|} \sin(x) \tag{34}$$

with

$$x = \frac{\rho}{\gamma} - \tfrac{1}{2}l\pi + \gamma \ln(2\rho/\gamma) + \arg\Gamma(l+1-i\gamma). \tag{35}$$

Using (29) one may show that

$$|\Gamma(l+1-i\gamma)|^2 = \frac{\pi\gamma^{2l+1}A(i\gamma, l)}{\sinh(\pi\gamma)} \tag{36}$$

and therefore

$$y_1(i\gamma, l; \rho) \underset{\rho\to\infty}{\sim} \left(\frac{2\gamma}{\pi}\right)^{1/2} \left[\frac{1 - e^{-2\pi\gamma}}{A(i\gamma, l)}\right]^{1/2} \sin(x). \tag{37}$$

The asymptotic form of the Whittaker function is

$$y_5(\kappa, l; \rho) \underset{\rho\to\infty}{\sim} (2\rho/\kappa)^{\kappa} e^{-\rho/\kappa}. \tag{38}$$

Therefore, for all ν, $y_5(\nu, l; \rho) \to 0$ for $\rho \to \infty$. From (38) one obtains

$$\frac{\Gamma(l+1-i\gamma)}{\pi(i\gamma)^l} y_5(i\gamma, l; \rho) \underset{\rho\to\infty}{\sim} \left(\frac{2\gamma}{\pi}\right)^{1/2} \left[\frac{A(i\gamma, l)}{1 - e^{-2\pi\gamma}}\right]^{1/2} e^{ix} \tag{39}$$

and, using (25), (27), (32) and (36),

$$y_4(i\gamma, l; \rho) \underset{\rho\to\infty}{\sim} -\left(\frac{2\gamma}{\pi}\right)^{1/2} \left\{ \left[\frac{1 - e^{-2\pi\gamma}}{A(i\gamma, l)}\right]^{1/2} \mathcal{G}(i\gamma, l) \sin(x) + \left[\frac{A(i\gamma, l)}{1 - e^{-2\pi\gamma}}\right]^{1/2} \cos(x) \right\} \tag{40}$$

and therefore

$$[y_4(i\gamma, l; \rho) + \mathcal{G}(i\gamma, l)y_1(i\gamma, l; \rho)] \underset{\rho\to\infty}{\sim} -\left(\frac{2\gamma}{\pi}\right)^{1/2} \left[\frac{A(i\gamma, l)}{1 - e^{-2\pi\gamma}}\right]^{1/2} \cos(x). \tag{41}$$

3. *The modified Coulomb field.*—We consider

$$\left[\frac{d^2}{d\rho^2} - \frac{l(l+1)}{\rho^2} + u(\rho) + \frac{2}{\rho} - \frac{1}{\kappa^2}\right] \mathcal{F}(\kappa, l; \rho) = 0. \tag{42}$$

Let ρ_0, ρ_1 be such that $0 < \rho_0$, $\rho_0 \leqslant \rho_1 < \infty$ and let $u(\rho)$ be such that: $\rho u(\rho)$ analytic

for $\rho<\rho_0$; $u(\rho)$ piecewise continuous for $\rho_0<\rho<\rho_1$; $u(\rho)=0$ for $\rho>\rho_1$. Let $\mathscr{F}(\kappa,l;\rho)$ be a continuous solution of (42) satisfying

$$\mathscr{F}(\kappa,l;0)=0, \tag{43}$$

$$\mathscr{F}(\kappa,l;\rho)=y_1(\kappa,l;\rho)-\beta(\epsilon)y_4(\kappa,l;\rho) \qquad (\rho>\rho_1). \tag{44}$$

It is shown by Ham (**11**) that $\mathscr{F}(\kappa,l;\rho)$ will be an entire analytic function of $\epsilon=-1/\kappa^2$. Since y_1 and y_4 are entire analytic functions it follows that $\beta(\epsilon)$ will be an entire analytic function and from the fact that y_1 and y_4 are real for ϵ real it may be shown to follow that $\beta(\epsilon)$ will be real for ϵ real. Therefore $\beta(\epsilon)$ may be represented by an expansion

$$\beta(\epsilon)=\sum_{p=0}^{\infty}B_p\epsilon^p \tag{45}$$

convergent for $|\epsilon|\leqslant|\mathscr{E}|<\infty$ and the coefficients B_p will be real.

The negative energy states.—From (32) and (44)

$$\mathscr{F}(\kappa,l;\rho)=\{1+\beta(\epsilon)[A(\kappa,l)\cot(\pi\kappa)+G(\kappa,l)]\}y_1(\kappa,l;\rho)$$
$$+\beta(\epsilon)\frac{\Gamma(l+1-\kappa)}{\pi\kappa^l}y_5(\kappa,l;\rho) \qquad (\rho>\rho_1) \tag{46}$$

and since $G(\nu,l)=\mathscr{G}(\nu,l)$,

$$\mathscr{F}(\nu,l;\rho)=\{1+\beta(\epsilon)[A(\nu,l)\cot(\pi\nu)+\mathscr{G}(\nu,l)]\}y_1(\nu,l;\rho)$$
$$+\beta(\epsilon)\frac{\Gamma(l+1-\nu)}{\pi\nu^l}y_5(\nu,l;\rho) \qquad (\rho>\rho_1). \tag{47}$$

Let $\epsilon_n=-1/{\nu_n}^2$ be an eigenvalue of ϵ; then $\mathscr{F}(\nu_n,l;\rho)\to0$ for $\rho\to\infty$. If $u(\rho)$ is not identically zero we may assume $\nu_n\neq n$ and therefore $y_1(\nu_n,l;\rho)\to\infty$ for $\rho\to\infty$. The condition $\mathscr{F}(\nu_n,l;\rho)\to0$ for $\rho\to\infty$ then requires that the coefficient of y_1 should vanish in (47); this requirement is (**11**)

$$\beta(\epsilon_n)=-[A(\nu_n,l)\cot(\pi\nu_n)+\mathscr{G}(\nu_n,l)]^{-1} \tag{48}$$

or, in terms of the quantum defect defined by

$$\mu(\epsilon_n)=n-\nu_n, \tag{49}$$

it is

$$\beta(\epsilon_n)=[A(\nu_n,l)\cot(\pi\mu(\epsilon_n))-\mathscr{G}(\nu_n,l)]^{-1}. \tag{50}$$

Suppose all the eigenvalues ϵ_n to be known. Then $\beta(\epsilon_n)$ is known for an infinite sequence of values of ϵ_n and, in consequence of the possibility of the expansion (45), $\beta(\epsilon)$ is uniquely determined for all finite ϵ. A quantum defect $\mu(\epsilon)$ may therefore be defined for all finite ϵ by

$$\beta(\epsilon)=[A(\kappa,l)\cot(\pi\mu(\epsilon))-\mathscr{G}(\kappa,l)]^{-1} \tag{51}$$

together with the condition that $\mu(\epsilon)$ should be a continuous function and should satisfy (49) at the eigenvalues. Since $\mathscr{G}$ is real and $\beta(\epsilon)$ and $A(\kappa,l)$ are real for real ϵ it follows that* $\mu(\epsilon)$ will be real for real ϵ.

The η-defect.—Letting $\nu\to m$ where $m=0,1,2,\ldots l$ we find that $\mathscr{G}(\nu,l)$ remains finite but that $A(\nu,l)$ tends to zero. However $\beta(-1/\nu^2)$, as determined from the eigenvalue spectrum, does not normally tend† to $-1/\mathscr{G}(m,l)$. Therefore as $\nu\to m$, $\mu(-1/\nu^2)$ must tend to an integer in such a way that $A(\nu,l)\cot(\pi\mu)$

* The definition of $\mu(\epsilon)$ used by Ham (**11**) is obtained on replacing $\mathscr{G}$ by G in (51). For ϵ real and negative this is identical with our definition but for ϵ real and positive $\mu(\epsilon)$ as defined by Ham will be complex.

† This may be shown (**11**) by solving the radial equation for various functions $u(\rho)$.

remains finite (11). This is confirmed by examination of observed energy levels. Fig. 1 shows the values of μ for the *nd* series in K I and in Ca II; in the former case $\mu \to 0$ and in the latter $\mu \to 1$ as $\nu \to 2$.

Ham introduces the η-defect defined by

$$A(\kappa, l) \cot \pi\mu = \cot \pi\eta. \tag{52}$$

We consider that $\eta(\epsilon)$ is a continuous function and that $\eta(0) = \mu(0)$. Since η does not necessarily tend to an integer as $\nu \to m$ we may expect that η will usually vary more slowly than μ. Values of η are shown in Fig. 1.

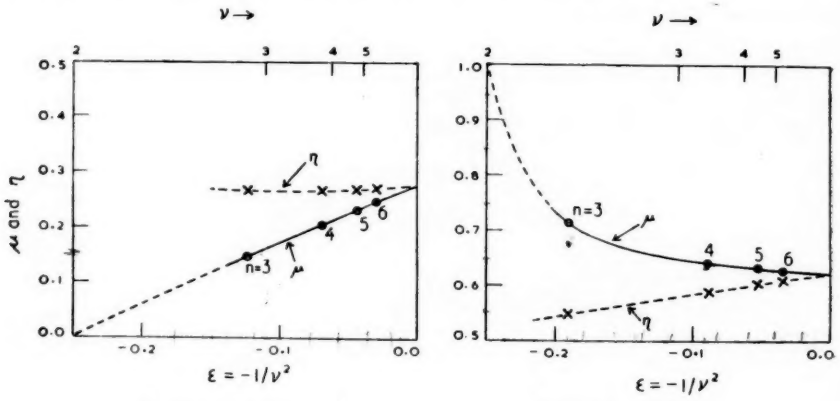

The nd series of K I. *The nd series of* Ca II

FIG. 1.—*Quantum defects and η-defects.*

The positive energy states.—Equation (44) may be written

$$\mathscr{F} = [1 + \beta\mathscr{G}]y_1 - \beta[y_4 + \mathscr{G}y_1] \qquad (\rho > \rho_1). \tag{53}$$

Using the asymptotic forms (37) and (41) we obtain

$$\mathscr{F}(i\gamma, l; \rho) \underset{\rho\to\infty}{\sim} \left(\frac{2\gamma}{\pi}\right)^{1/2} \left[\frac{1 - e^{-2\pi\gamma}}{A(i\gamma, l)}\right]^{1/2} \beta(\epsilon) \left\{\left[\frac{1}{\beta(\epsilon)} + \mathscr{G}(i\gamma, l)\right] \sin(x) + \left[\frac{A(i\gamma, l)}{1 - e^{-2\pi\gamma}}\right] \cos(x)\right\} \tag{54}$$

or

$$\mathscr{F}(i\gamma, l; \rho) \sim \left(\frac{\gamma}{\pi}\right)^{1/2} C(\epsilon) \sin[x + \delta(\epsilon)] \tag{55}$$

where

$$\tan\delta = \frac{[A/(1 - e^{-2\pi\gamma})]}{[(1/\beta) + \mathscr{G}]} \tag{56}$$

and

$$C = (2)^{1/2} \left[\frac{1 - e^{-2\pi\gamma}}{A}\right]^{1/2} \beta \left\{\left[\frac{1}{\beta} + \mathscr{G}\right]^2 + [A/(1 - e^{-2\pi\gamma})]^2\right\}^{1/2}. \tag{57}$$

Substitution of $(1/\beta) + \mathscr{G} = A \cot(\pi\mu)$ from (51) gives

$$\tan\delta(\epsilon) = \frac{\tan\pi\mu(\epsilon)}{(1 - e^{-2\pi\gamma})} \tag{58}$$

and

$$C = (2)^{1/2}[A(1 - e^{-2\pi\gamma})]^{1/2}\beta\{[\cot\pi\mu]^2 + [1 - e^{-2\pi\gamma}]^{-2}\}^{1/2}. \tag{59}$$

To the phase $\delta(\epsilon)$ defined by (55) we may add any integral multiple of π. Consistent with (58) we may define $\delta(\epsilon)$ uniquely by requiring that $\delta(\epsilon)$ be continuous and that

$$\delta(0)=\pi\mu(0). \tag{60}$$

In most applications we may assume $2\pi\gamma$ to be large. Neglecting* $\exp(-2\pi\gamma)$ in (58) and (59) we obtain

$$\delta(\epsilon)=\pi\mu(\epsilon) \qquad (2\pi\gamma\gg 1), \tag{61}$$

and

$$C=(2A)^{1/2}\beta/\sin\delta \qquad (2\pi\gamma\gg 1). \tag{62}$$

The zero-energy phase and the number of bound states.—For an attractive potential $V(r)$ which, for large r, tends to zero more rapidly than the Coulomb potential a general theorem (**17**) states that $\delta(0)=\pi N$ where N is the number of bound states obtainable with the potential V. For a potential tending asymptotically to the attractive Coulomb form the number of bound states is infinite. In such a case one may define $N(\epsilon')$ as the number of bound states with ϵ_n less than some small negative value ϵ'. Then $N(\epsilon')$ will increase by unity when $\mu(\epsilon')$ increases by unity. One may thus regard $\mu(0)$ as the increase in the number of bound states which results from the non-Coulomb part of the potential $u(r)$; this despite the fact that $\mu(0)$ is generally not an integer. The relation $\delta(0)=\pi\mu(0)$ may therefore be regarded as a generalization of the relation $\delta(0)=\pi N$.

4. *Normalization of the radial functions.*—We put

$$\left.\begin{aligned}\mathcal{F}&=\mathcal{F}(\kappa,l;\rho)\\ \mathcal{F}'&=\mathcal{F}(\kappa',l;\rho)\\ D&=\frac{d}{d\rho}\end{aligned}\right\}. \tag{63}$$

Then from (42)

$$\int_0^\rho \mathcal{F}\left[D^2-\frac{l(l+1)}{\rho^2}+u(\rho)+\frac{2}{\rho}-\frac{1}{\kappa'^2}\right]\mathcal{F}'\,d\rho=0. \tag{64}$$

Integrating by parts and using the equation satisfied by $\mathcal{F}$ one obtains

$$(\mathcal{F}D\mathcal{F}'-\mathcal{F}'D\mathcal{F})\Big|_0^\rho+\left(\frac{1}{\kappa^2}-\frac{1}{\kappa'^2}\right)\int_0^\rho \mathcal{F}\mathcal{F}'\,d\rho=0. \tag{65}$$

Assuming $D\mathcal{F}$ and $D\mathcal{F}'$ to be finite for $\rho=0$ it follows from (43) that $(\mathcal{F}D\mathcal{F}'-\mathcal{F}'D\mathcal{F})$ is zero at the lower limit and therefore

$$\int_0^\rho \mathcal{F}\mathcal{F}'\,d\rho=\frac{(\mathcal{F}'D\mathcal{F}-\mathcal{F}D\mathcal{F}')}{(1/\kappa^2-1/\kappa'^2)}. \tag{66}$$

We consider this expression in the limit of $\rho\to\infty$.

Equation (66) is the standard expression used for the normalization of positive energy radial functions. One obtains (**18, 19**)

$$\int_0^\infty \mathcal{F}(i\gamma,l;\rho)\mathcal{F}(i\gamma',l;\rho)\,d\rho=[C(\epsilon)]^2\delta(\epsilon-\epsilon') \tag{67}$$

where $\delta(\epsilon-\epsilon')$ is the Dirac δ-function.

* The condition $(2\pi\gamma)\gg 1$ is equivalent to $k\ll(2\pi z)$ where k^2 is the electron kinetic energy in units of 13·60 eV.

To obtain the normalization for bound states we put

$$\mathscr{F} = \mathscr{F}(\nu, l; \rho) \tag{68}$$

and

$$\mathscr{F}' = \mathscr{F}_n = \mathscr{F}(\nu_n, l; \rho) \tag{69}$$

where $\epsilon_n = -1/\nu_n^2$ is an eigenvalue. The integral

$$\Delta_n = \int_0^\infty \mathscr{F}_n^2 \, d\rho \tag{70}$$

is evaluated as *

$$\Delta_n = \lim_{\rho\to\infty} \lim_{\nu\to\nu_n} \left\{ \frac{\mathscr{F}_n D\mathscr{F} - \mathscr{F} D\mathscr{F}_n}{(1/\nu^2 - 1/\nu_n^2)} \right\}. \tag{71}$$

Using (33), (38) and (47) we have

$$\mathscr{F} \sim a\rho^\nu \, e^{-\rho/\nu} + b\rho^{-\nu} \, e^{\rho/\nu} \tag{72}$$

where

$$a = \frac{\beta\Gamma(l+1-\nu)}{\pi\nu^l} \left(\frac{2}{\nu}\right)^\nu, \tag{73}$$

$$b = \{1 + \beta[A \cot \pi\nu + G]\} \frac{\nu^{l+1}(2/\nu)^\nu}{\Gamma(l+1-\nu)}. \tag{74}$$

Since $\mathscr{F}_n$ is an eigenfunction,

$$\mathscr{F}_n \sim a_n \rho^{\nu_n} e^{-\rho/\nu_n} \tag{75}$$

where

$$a_n = \beta(\epsilon_n) \frac{\Gamma(l+1-\nu_n)}{\pi\nu_n^{\,l}} \left(\frac{2}{\nu_n}\right)^{\nu_n}. \tag{76}$$

Substitution of (72) and (75) in (71) gives

$$\Delta_n = -\nu_n^2 a_n \left.\frac{\partial b}{\partial \nu}\right|_{\nu=\nu_n}. \tag{77}$$

Using (74) and (51) one obtains

$$\left.\frac{\partial b}{\partial \nu}\right|_{\nu=\nu_n} = -\frac{\pi A(\nu_n, l)\beta(\epsilon_n)\nu_n^{\,l+1}(2/\nu_n)^{-\nu_n}\zeta(\nu_n)}{\sin^2(\pi\mu(\epsilon_n))\Gamma(l+1-\nu_n)} \tag{78}$$

where

$$\zeta(\nu) = 1 + \frac{\partial\mu}{\partial\nu}. \tag{79}$$

From (76), (77) and (78) the normalization integral is

$$\Delta_n = \frac{\nu_n^3\beta^2(\epsilon_n)A(\nu_n, l)\zeta(\nu_n)}{\sin^2(\pi\mu(\epsilon_n))}. \tag{80}$$

The normalized radial function $P_{nl}(r)$ is taken to satisfy

$$\int_0^\infty P_{nl}^2(r)\, dr = 1 \tag{81}$$

where the integration is over r and not $\rho = zr$. Making a convenient phase choice we put

$$P_{nl} = \frac{z^{1/2}(-1)^{n-l-1}\mathscr{F}_n}{\Delta_n^{1/2}}. \tag{82}$$

* Ham (11) quotes an expression similar to (71) and states that it can be evaluated using the Quantum Defect Method. He does not, however, give the explicit expression for the normalization factor as obtained in the present paper.

From (47) and (50),

$$\mathscr{F}_n = \frac{\beta(\epsilon_n)\Gamma(l+1-\nu_n)}{\pi\nu_n{}^l}\, y_5(\nu_n, l; \rho) \qquad (\rho > \rho_1) \tag{83}$$

and therefore

$$P_{nl} = \mathrm{K}(\nu_n, l) y_5(\nu_n, l; \rho) \qquad (\rho > \rho_1) \tag{84}$$

where

$$\mathrm{K}(\nu_n, l) = z^{1/2}[\zeta(\nu_n)\nu_n{}^2\Gamma(\nu_n + l + 1)\Gamma(\nu_n - l)]^{-1/2}. \tag{85}$$

If all the eigenvalues are known $\partial\mu/\partial\nu$ may be calculated and the exact normalized eigenfunctions determined for $\rho > \rho_1$. It may be noted that

$$\zeta(\nu) = 1 + \frac{\partial\mu}{\partial\nu} = 1 + \frac{2}{\nu^3}\frac{\partial\mu}{\partial\epsilon}. \tag{86}$$

For large ν, $\partial\mu/\partial\epsilon$ remains finite, and therefore $\zeta(\nu)$ tends to unity. The normalization factor then becomes

$$\mathrm{K}(\nu_n, l) = z^{1/2}[\nu_n{}^2\Gamma(\nu_n + l + 1)\Gamma(\nu_n - l)]^{-1/2} \qquad (\nu_n \text{ large}). \tag{87}$$

With $\nu_n = n$ this is the exact normalization factor for the pure Coulomb field (for which $\mu = 0$ and $\zeta = 1$). Hartree (**12**) has shown that the factor (87) satisfies a necessary recurrence relation for values of ν_n differing by integers. This is consistent with the exact result since the ν_n may be considered to differ by integers only when $\partial\mu/\partial\nu$ is negligible.

Numerical results for the bound-state normalization factor.—Hartree (**12**) and Bates and Damgaard (**5**) have shown that the normalization factor with $\zeta = 1$ is a good approximation when ν_n is not too small. In illustration of cases for

TABLE I

The normalization factor K *for 2p radial functions of atomic oxygen ions*

Ion	State	ν_2	K		
			Eqn. (85) with $\zeta = 1$	Eqn. (85) with $\zeta = \frac{(\nu_2-1)(\nu_2+2)}{\nu_2(\nu_2+1)}$	Exact value
O°	$2p^4\ {}^3P$	0·890	imaginary	0·61	0·78
O^{+}	$2p^3\ {}^2P$	1·296	0·38	0·67	0·67
O^{+2}	$2p^2\ {}^3P$	1·483	0·48	0·71	0·71
O^{+3}	$2p\ {}^2P$	1·672	0·51	0·69	0·65

Note that the values of ν_2 are obtained from the energy parameters in the radial equations and not from measured energies.

which this approximation is not sufficient we consider the $2p$ radial functions for atomic oxygen ions calculated by Hartree, Hartree and Swirles (**20**). Fig. 2 shows the quantum defects for the $2p$ and $3p$ states of O^{+3}. It is seen that μ goes to unity for $\nu = 1$ and that $\mu(\epsilon)$ is a nearly linear function of ϵ for ν between 1 and ν_2. Assuming an exactly linear function we obtain

$$\zeta(\nu_2) = \frac{(\nu_2 - 1)(\nu_2 + 2)}{\nu_2(\nu_2 + 1)}. \tag{88}$$

Table I gives the normalization factors as calculated with $\zeta = 1$ and as calculated using (88) and also the exact values determined from numerical evaluation of the normalization integral (81).

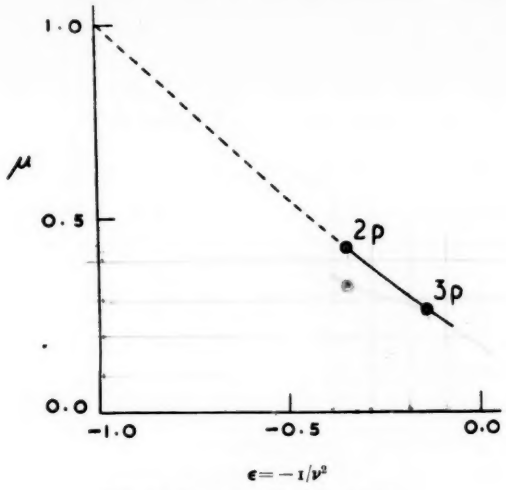

FIG. 2.—*Quantum defects for* O^{+3} *np.*

5. *Discussion of the Quantum Defect Method.*—The mathematical theory considered so far is concerned with central fields which tend to the attractive Coulomb form at large distances. A different approach would be needed in order to develop an exact theory applicable to many-electron atoms. Some of the results of the present theory may, however, be used directly.

Consider an atomic spectral series for which the ion is left in the ground state at the series limit. From the observed energy levels quantum defects may be obtained and extrapolated to positive energies. Just beyond the series limit the free electron will have a kinetic energy which will be too small for collisions to produce excitation of the ion. A single real phase parameter will then suffice to describe the asymptotic form of wave functions corresponding to definite angular momenta. In such cases there can be little doubt that accurate phases can be determined from the extrapolated quantum defects.

For higher energies the situation is more complicated. The asymptotic form of the wave function may be described in terms of a scattering matrix **S**, the off-diagonal elements of this matrix determining the probability of the free electron producing transitions between states of the ion. If all atomic energy levels were considered, including those corresponding to excitation of two or more electrons, it may be expected that information about the complete scattering matrix could in principle be deduced. The more complete theory required has not yet been developed. We consider some applications of the present form of the Quantum Defect Method.

Extrapolation procedures.—For the modified Coulomb field we have shown that the mixture parameter $\beta(\epsilon)$ can be expressed as a convergent power series in ϵ and that the quantum defect μ may be defined for all ϵ as a function of β. We have not shown that the quantum defect itself may be expressed as a convergent expansion in powers of ϵ but it may be shown (**12**) that μ may be expressed as an asymptotic expansion in powers of ϵ.

In practical applications information concerning the eigenvalues is always incomplete. Quantum defects obtained from observed energy levels may usually be represented by polynomials in ϵ containing only a few terms. These polynomials may be used for extrapolation to positive energies. The range of extrapolation is limited by incomplete knowledge of the exact eigenvalues and also by the fact that the simple theory is invalid for positive energies such that inelastic collisions may occur.

It may be convenient to extrapolate the η-defect when η varies more slowly than μ.

Comparison of calculated and empirical phases.—Such comparisons have been made in previous papers (**6, 7, 8, 9, 28**). In favourable cases, phases obtained from solutions of the continuous state Hartree–Fock equations (**21**) are in very good agreement with extrapolated quantum defects. The reason is that the Hartree–Fock equations for continuous states may be derived from a variational principle for the phase just as the equations for bound states may be derived from a variational principle for the energy. In cases for which the Hartree–Fock phases are less satisfactory it may be expected that configuration interaction is important; an example of such a case is the continuum corresponding to extrapolation of the $4snp$ series in Ca (**7**).

Calculation of elastic scattering cross-sections.—We consider ions with non-degenerate ground states. For elastic scattering of slow electrons the appropriate theory is then that for a modified Coulomb field. For scattering through an angle θ the cross-section per unit solid angle is (**22**)

$$I(\theta)=|\mathbf{a}_0 f(\theta)|^2 \tag{89}$$

where $\mathbf{a}_0$ is the Bohr radius and where

$$f(\theta)=\frac{1}{2ik}\sum_{l=0}^{\infty}(2l+1)P_l(\cos\theta)[e^{2i(\phi_l+\delta_l)}-1] \tag{90}$$

and*

$$\phi_l(\gamma)=\arg\Gamma(l+1-i\gamma). \tag{91}$$

It is convenient to put

$$I(\theta)=I_c(\theta)\mathcal{F}(\theta) \tag{92}$$

where $I_c(\theta)$ is the cross-section for the unmodified Coulomb field. The latter is given by

$$I_c(\theta)=|\mathbf{a}_0 f_c(\theta)|^2 \tag{93}$$

where $f_c(\theta)$ is obtained on putting $\delta_l=0$ in (90):

$$f_c(\theta)=\frac{1}{2ik}\sum_{l}(2l+1)P_l(\cos\theta)[e^{2i\phi_l}-1]. \tag{94}$$

This series may be summed (**22**) to give

$$f_c(\theta)=\frac{\gamma}{2k\sin^2(\theta/2)}\exp[2i(\phi_0+\gamma\ln\sin\tfrac{1}{2}\theta)] \tag{95}$$

and

$$I_c(\theta)=\left[\frac{2\mathbf{a}_0}{2k^2\sin^2(\theta/2)}\right]^2 \tag{96}$$

* We recall that $\delta_l(\gamma)$ is the phase for the l-wave due to the non-Coulomb part of the potential and that $\gamma=z/k$.

which is the Rutherford formula. From (90) and (94) we obtain

$$f(\theta)=f_c(\theta)+\frac{1}{2ik}\sum_l (2l+1)P_l e^{2i\phi_l}[e^{2i\delta_l}-1] \tag{97}$$

and, using (95),

$$\frac{f(\theta)}{f_c(\theta)}=1+\frac{2\sin^2(\theta/2)}{\gamma}\sum_l (2l+1)P_l(\cos\theta)e^{ip_l}\sin\delta_l \tag{98}$$

with

$$p_l(\theta,\gamma)=2(\phi_l-\phi_0)-2\gamma\ln\sin\theta/2+\delta_l. \tag{99}$$

It may be noted that

$$\begin{aligned} e^{2i(\phi_l-\phi_0)}&=\frac{\Gamma(l+1-i\gamma)\Gamma(1+i\gamma)}{\Gamma(l+1+i\gamma)\Gamma(1-i\gamma)}\\ &=\frac{(1-i\gamma)(2-i\gamma)\dots(l-i\gamma)}{(1+i\gamma)(2+i\gamma)\dots(l+i\gamma)} \end{aligned} \tag{100}$$

and therefore

$$(\phi_l-\phi_0)=-\sum_{m=1}^{l}\arctan(\gamma/m). \tag{101}$$

From (99) we obtain finally

$$\mathscr{I}(\theta)=X^2+Y^2 \tag{102}$$

with

$$\left.\begin{aligned} X&=1+\frac{2\sin^2(\theta/2)}{\gamma}\sum_l (2l+1)P_l(\cos\theta)\cos p_l\sin\delta_l\\ Y&=\frac{2\sin^2(\theta/2)}{\gamma}\sum_l (2l+1)P_l(\cos\theta)\sin p_l\sin\delta_l \end{aligned}\right\}. \tag{103}$$

It follows from these expressions that $\mathscr{I}(0)=1$ for all k^2 and that, for $k^2=0$, $\mathscr{I}(\theta)=1$ for all θ.

Fig. 3 shows results obtained for scattering of electrons by Na^+ ions. The phases* have been obtained using formulae given by Ham (**11**) for extrapolation of the η-defects. The cross-sections are seen to be significantly different from the corresponding Coulomb cross-sections. Complicated interference effects are particularly marked for small values of k.

Inelastic collisions.—For ions with degenerate ground states the Quantum Defect Method may be used to obtain accurate cross-sections for electron-induced transitions between ground-state fine structure components. The method has been applied (**10**) to the transitions $C^+\ 2p_{1/2}$–$2p_{3/2}$ and $Si^+\ 3p_{1/2}$–$3p_{3/2}$; these are of importance for the cooling of the interstellar gas.

For other transitions in ions produced by electron impact it has not yet proved to be possible to deduce cross-sections from quantum defect data alone. One may, however, make calculations in which the various parameters are so adjusted as to be consistent with extrapolated quantum defects (**10**).

The Quantum Defect Method may be used to obtain continuum wave functions having asymptotic forms which are virtually exact. Such functions have been used for the calculations of photo-ionization cross-sections (**13**).

* Only s- and p-phases have been taken into account. The higher order phases are small and will have little effect on the cross-section.

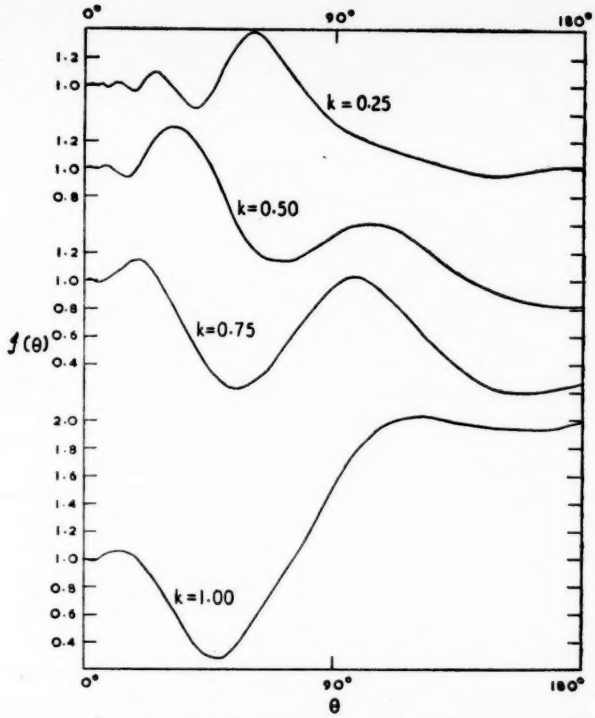

FIG. 3.—*Elastic electron scattering by Na^+ ions. $\mathcal{J}(\theta)$ is the factor by which the Coulomb cross-section must be multiplied, θ being the scattering angle. k^2 is the kinetic energy in Rydbergs (13·60 eV). Note that $\mathcal{J}(\theta)=1$ for $k=0$.*

APPENDIX

Expansions of the Coulomb functions in powers of the energy.—The expansion of the regular Coulomb function y_1 has been discussed in a number of papers (see (**23, 24, 25, 26, 27**)). One may first obtain

$$y_1(\kappa, l; \rho)=\sum_{p=0}^{\infty} a_p(\kappa, l)(2\rho)^{\frac{1}{2}(p+1)}J_{2l+1+p}(\sqrt{(8\rho)}) \qquad (A\,1)$$

where (**26**)

$$\left.\begin{aligned} &a_0=1, \qquad a_1=0, \qquad a_2=(l+1)/4\kappa^2, \\ &a_p=\frac{1}{4\kappa^2 p}\{(2l+p)a_{p-2}-a_{p-3}\} \qquad (p\geqslant 3) \end{aligned}\right\}. \qquad (A\,2)$$

Putting

$$a_p(\kappa, l)=\sum_q a_{q,p}(l)\kappa^{-2q} \qquad (A\,3)$$

one obtains

$$\left.\begin{aligned} &a_{q,p}=0 \quad \text{unless} \quad 2q\leqslant p\leqslant 3q, \\ &a_{0,0}=1, \qquad a_{1,2}=(l+1)/4, \qquad a_{1,3}=-\frac{1}{12}, \\ &a_{q,p}=\frac{1}{4p}\{(2l+p)a_{q-1,p-2}-a_{q-1,p-3}\} \qquad (q\geqslant 1, \quad p\geqslant 3) \end{aligned}\right\}. \qquad (A\,4)$$

The expansion for y_1 is

$$y_1(\kappa, l; \rho) = \sum_{q=0}^{\infty} \kappa^{-2q} \sum_{p=2q}^{3q} a_{q,p}(l)(2\rho)^{\frac{1}{2}(p+1)} J_{2l+1+p}(\sqrt{(8\rho)}). \qquad (A\,5)$$

Various expansions for irregular Coulomb functions have been proposed. It has been shown (see Section 2) that the function y_3 cannot be represented by a convergent expansion in powers of the energy. It may, however, be represented by the *asymptotic* expansion

$$y_3(\kappa, l; \rho) = A(\kappa, l) \sum_{q=0}^{Q} \kappa^{-2q} \sum_{p=2q}^{3q} a_{q,p}(l)(2\rho)^{\frac{1}{2}(p+1)} Y_{2l+1+p}(\sqrt{(8\rho)}) + O(\kappa^{-2Q-2}), \quad (A\,6)$$

(**25, 26, 27**). On expressing $A(\kappa, l)$ as a polynomial in κ^{-2}, (A 6) gives an asymptotic expansion in powers of κ^{-2}. The function $G(\kappa, l)$ (defined by equation (14)) may be represented by an asymptotic expansion in powers of κ^{-2} (**12, 27**). Substitution of the asymptotic expansions for y_3 and for Gy_1 in $y_4 = y_3 - Gy_1$ gives a convergent expansion for y_4 (Ham (**27**)). For numerical calculations the asymptotic expansion (A 6) is often convenient.

Department of Physics,
University College, London,
*W.C.*1:
1958 *May* 26.

References

(1) W. Prokofjew, *Z. Phys.*, **58,** 255, 1929.
(2) B. Trumpy, *Z. Phys.*, **61,** 54 and **66,** 720, 1929.
(3) L. Biermann, *Nachr. Akad. Wiss. Göttingen, Math-Phys., Kl.*, **2,** 116, 1946.
(4) E. A. Hylleraas, *Arch. Math. Naturv.* B, **48** No. 4, 1945.
(5) D. R. Bates and A. Damgaard, *Phil. Trans.*, A **242,** 101, 1949.
(6) M. J. Seaton, *Comptes Rendus*, **240,** 1317, 1955.
(7) M. J. Seaton, *Ann. d'Astrophys.*, **18,** 206, 1955.
(8) M. J. Seaton, *The airglow and the aurorae* (ed. E. B. Armstrong and A. Dalgarno), p. 289, Pergamon, 1955.
(9) M. J. Seaton and D. E. Osterbrock, *Ap. J.*, **125,** 66, 1957.
(10) M. J. Seaton, *Rev. Mod. Phys.*, **30,** 979, 1958.
(11) F. S. Ham, *Solid State Physics* (ed. F. Seitz and D. Turnbull), vol. **1,** p. 127, Academic Press, 1955.
(12) D. R. Hartree, *Proc. Camb. Phil. Soc.*, **24,** 89 and 426, 1927; *ibid.*, **25,** 310, 1929.
(13) A. Burgess and M. J. Seaton, *Rev. Mod. Phys.*, **30,** 992, 1958.
(14) E. T. Whittaker and G. N. Watson, *A course of modern analysis*, 4th ed., Ch. XVI, Cambridge, 1946.
(15) G. H. Wannier, *Phys. Rev.*, **64,** 358, 1943.
(16) Bateman Manuscript Project, *Higher Transcendental functions*, vol. **1,** p. 278, McGraw-Hill, 1953.
(17) P. Weiss, *Phys. Rev.*, **87,** 226, 1952.
(18) E. Fues, *Ann. d. Phys.*, **87,** 281, 1926.
(19) J. Hargreaves, *Proc. Camb. Phil. Soc.*, **25,** 75, 1929.
(20) D. R. Hartree, W. Hartree and B. Swirles, *Phil. Trans.*, A, **238,** 229, 1939.
(21) M. J. Seaton, *Phil. Trans.*, A, **245,** 469, 1953.
(22) W. Gordon, *Z. Phys.*, **48,** 180, 1928.
(23) F. L. Yost, J. A. Wheeler and G. Breit, *Phys. Rev.*, **49,** 174, 1936.
(24) J. G. Beckerley, *Phys. Rev.*, **67,** 11, 1945.
(25) T. S. Kuhn, *Quart. Appl. Math.*, **9,** 1, 1951.
(26) M. Abramowitz, *Jour. Math. and Phys.* (M.I.T.), **33,** 111, 1954.
(27) F. S. Ham, *Tables for the calculation of Coulomb Wave functions*, Tech. Rep. No. 204 Cruft Lab., Harvard, 1955.
(28) M. J. Seaton, *Proc. Phys. Soc.* A, **70,** 620, 1957.

GIANT STARS OF TYPE II

C. B. Haselgrove and F. Hoyle

(Received 1958 March 15)

Summary

Integrations along the Type II giant sequence are given that reach an evolutionary stage at which there is an appreciable energy yield from nuclear reactions in helium. The new integrations seem to be in close agreement with observation.

---

1. *Results.*—Seven evolutionary steps beyond those given in a former paper (1956 *a*) have been made for a star of mass $2{\cdot}512 \times 10^{33}$ gm., the initial composition being the same as before.

Results are set out in Table I below, the solutions being numbered so as to follow consecutively with those obtained previously. The symbols appearing in the table have the following interpretation:

R = total radius,
M = total mass,
L = luminosity,
$T_{\rm eff}$ = effective temperature,
$L_{\rm He}$ = the contribution to the luminosity from nuclear reactions that convert helium to carbon, oxygen, and neon.
P_0 = central pressure,
T_0 = central temperature,
$M_{\rm He}$ = mass of helium zone,
$M_{\rm C,O,Ne}$ = mass of carbon-oxygen-neon core.

$T_{\rm eff}$ and T_0 are in deg. K, all other quantities being measured in c.g.s. units. The method of solution was that given in an earlier paper (1956 *b*).

TABLE I

Solution	$\log_{10}R$	$\log_{10}L$	$\log_{10}L_{\rm He}$	$\log_{10}T_{\rm eff}$	$\log_{10}P_0$	$\log_{10}T_0$	$M_{\rm He}/M$	$M_{\rm C,O,Ne}/M$	$\log_{10}L/L_\odot$
17	11·756	35·208	...	3·708	21·215	7·590	0·195	...	1·630
18	11·936	35·524	...	3·698	21·425	7·615	0·218	...	1·946
19	12·126	35·851	...	3·684	21·557	7·717	0·241	...	2·273
20	12·329	36·200	...	3·675	21·770	7·767	0·264	...	2·622
21	12·652	36·757	...	3·648	22·141	7·889	0·322	...	3·179
22	11·930	35·521	34·537	3·700	20·574	8·087	0·341	...	1·943
23	12·126	35·851	35·264	3·684	20·714	8·124	0·312	0·105	2·273

The least accurate feature of the integrations lies in the treatment of the term $\partial\epsilon/\partial t$, appearing in the equations for the structure of the star (cf. 1956 *b*). The estimation of this term for any integration requires a difference to be taken between the quantity ϵ for the current integration and the value for the previous solution. Thus, for example, the value of $\partial\epsilon/\partial t$ for solution 20 depends on the difference between the value of ϵ for Solution 20 itself and the value for Solution 19. Now in operating a machine of limited capacity (the present integrations were performed

on EDSAC I) it is not possible to store the previous solution in any great detail, a circumstance that of necessity introduces some error. The extent of the error can be seen from Fig. 1, which shows that the points scatter around a mean line, the extent of the scatter being about $\pm 0{\cdot}1$ mag. Evidently an error of this order is adequately small.

The concentration of metals was taken to be so low that in all cases there was no appreciable contribution from the metals to the electron pressure at the photosphere.

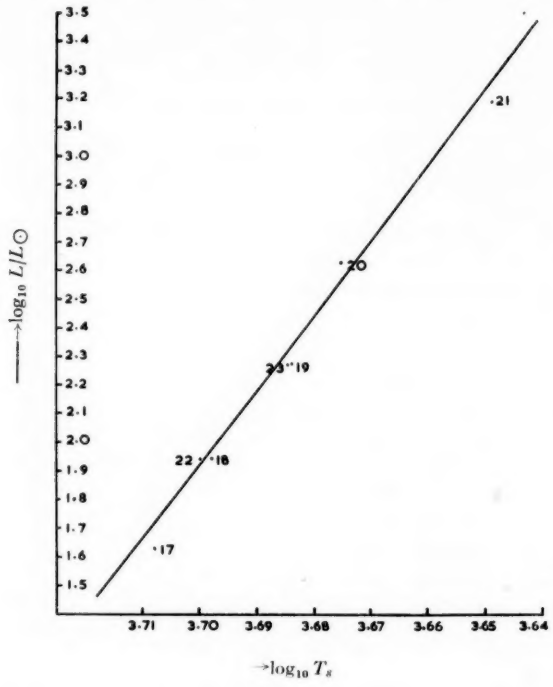

FIG. 1.

2. *Discussion of the integrations.*—The outstanding feature of the table is the marked change from Solution 21 to Solution 22. Material at the centre of the star is degenerate in Solution 21, the density being $6{\cdot}00 \times 10^5$ gm/cm^3. But no solution with a degenerate helium zone could be found that extended appreciably further than Solution 21. The reason for our failure to find such a solution can readily be understood from the following argument.

It will be observed that the central temperature T_0 rises steadily from $3{\cdot}89 \times 10^7$ deg. K at Solution 17 to $7{\cdot}75 \times 10^7$ deg. K at Solution 21. This increase is due to a temperature gradient that maintains an outward flow of energy, the energy supplied by a general gravitational compression of the helium zone. Now any appreciable extension of the evolution beyond Solution 21 demands a central temperature above 8×10^7 deg. K, when the energy yielded by nuclear reactions in helium exceeds the effect of compression. This leads to an accentuated rise of the central temperature, which in turn increases the rate of nuclear energy generation still further ... and so on. Evidently a rapid evolution of the star is to be expected

in which the helium zone becomes expanded to lower density. This expansion is necessary to reduce the opacity sufficiently to allow a more ready outflow of the energy generated in the helium.

This is just what is shown by Solution 22. The central density in this solution is reduced to $4{\cdot}05 \times 10^4$ gm/cm^3, and the helium is no longer degenerate.

Although it would have been very desirable to trace in detail all stages of the rapid evolution from Solution 21 to Solution 22, this was not possible in EDSAC I, since a prohibitively lengthy calculation would have been necessary. Our expedient was to "pick up" simply by trial and error the evolution at a stage after the expansion of the core had taken place. One important assumption was involved in this procedure: *that there was no mixing of the inner helium with the outer hydrogen during the period of rapid evolution.* Since there are no incipient signs of any such mixing at Solution 21, this seems an entirely reasonable hypothesis.

The fraction of the total luminosity arising from energy production in helium increases appreciably between Solutions 22 and 23. An attempt to follow the evolution beyond Solution 23 showed that L_{He} increased rapidly to a value close to L, and that a further instability in the structure of the star then ensued. Since in this case there were some signs that a mixing of hydrogen and helium might be important, no attempt was made to pick up the evolution beyond the second instability. More detailed computations with a substantially faster machine will be needed to follow the evolution still further.

3. *Comparison with observation.*—All the solutions given in Table I lie on what is usually called the giant branch of the representation in the Hertzsprung-Russell diagram. The relation between L and T_{eff} for Solutions 17 to 21 agrees very closely with earlier calculations by Hoyle and Schwarzschild (1955). The values of M_{He}/M for these solutions are about 20 per cent less than those obtained by Hoyle and Schwarszchild, however.

Solutions 19 and 23 fall at almost exactly the same point of the Hertzsprung-Russell diagram, showing that apparently there is no unique interior structure for stars on the giant branch with $L/L_\odot > 100$.

Provided that a unique structure is assumed at lower luminosities, in particular at Solution 17, we can compare the value of M_{He}/M obtained for this solution with that deduced by Sandage (1957) from the observed luminosity function of the stars of the globular cluster M3. Making a slight adjustment for the initial hydrogen concentration 0·9309 used in the present calculations, and interpolating for $\log_{10} L/L_\odot = 1{\cdot}630$ between Sandage's values, we obtain the following comparison:—

	M_{He}/M at $\log_{10} L/L_\odot = 1{\cdot}630$
Present paper	0·195
Sandage's semi-empirical value	0·209

A second very close agreement with Sandage's results follows from estimating the amount ΔM of the envelope that is added to the helium zone between $\log_{10} L/L_\odot = 1{\cdot}630$ and $\log_{10} L/L_\odot = 2{\cdot}273$. According to Sandage, $\Delta M/M = 0{\cdot}121$. From the way that this estimate was made, it must be interpreted as the *total* burning of the envelope material that takes place within the specified range of luminosity. Now from Table I it will be seen that burning occurs at two distinct stages. The first stage is given by the range from Solution 17 to Solution 19, and

the second stage by the range from Solution 22 to Solution 23. Writing ΔM_1, ΔM_2 for the amounts of the envelope material that is burned in these two stages, we have from the table:—

$$\frac{\Delta M_1}{M} = 0{\cdot}046, \qquad \frac{\Delta M_2}{M} = 0{\cdot}076.$$

Our calculations therefore give

$$\frac{\Delta M}{M} = \frac{\Delta M_1 + \Delta M_2}{M} = 0{\cdot}122,$$

in almost exact agreement with Sandage's estimate. It would clearly be very desirable to extend the present comparison to higher luminosities, but this unfortunately requires an extension of the calculations beyond Solution 23, and such an extension is not yet available.

Solution 21 gives the highest value of L. If we interpret this solution as giving the top of the giant branch, the magnitude of the brightest Type II stars becomes $-2{\cdot}8$. This value follows from the equation

$$M = +4{\cdot}62 - 2{\cdot}5 \log_{10} L/L_{\odot} + \text{bolometric correction},$$

where the bolometric correction at $\log T_{\text{eff}} = 3{\cdot}648$ was taken as 0·53 mag. This upper limit of $-2{\cdot}8$ is in excellent agreement with extensive data obtained by Arp (private communication) for a number of globular clusters.

It has already been stated that the present calculations were carried out on the basis that electrons derived from metal atoms do not make an appreciable contribution to the electron pressure at the photosphere. This case has a special importance in relation to the search that is being made for stars of abnormally low metal content. The effect of a small metal content to is push the top of the giant branch towards the right of the Hertzsprung-Russell diagram (Hoyle and Schwarzschild, *loc. cit.*). Hence if a giant sequence can be observed that falls near the sequence of solutions given in the above table (a sequence not pushed to the right in the H–R diagram), it is possible to infer that the stars in question have no more than a negligible trace of metals. This criterion of the presence or absence of metals may well prove to be more sensitive than a direct spectroscopic criterion.

It is a pleasure to acknowledge our gratitude to the Director of the Mathematical Laboratory, Cambridge for provision of the facilities that allowed these calculations to be made.

Department of Mathematics,
The University, Manchester 13:
1958 *March.*

St. John's College,
Cambridge.

References

Haselgrove, C. B. and Hoyle, F. (1956 *a*), *M.N.*, **116**, 527.
Haselgrove, C. B. and Hoyle, F. (1956 *b*), *M.N.*, **116**, 515.
Hoyle, F. and Schwarzschild, M. (1955), *Ap. J. Suppl.*, **2**, No. 13, 1.
Sandage, A. R. (1957), *Ap. J.*, **126**, 326.

STABILITY OF POLYTROPIC GAS SPHERES

W. B. Bonnor

(Received 1958 May 23)

Summary

It has previously been shown that an isothermal gas sphere is gravitationally unstable to small perturbations in the pressure at sufficient distance from the centre. This work is here extended to polytropic gas spheres: it is shown that this type of instability does not affect spheres with indices n given by $0<n\leqslant 3$, but that for $n>3$, a sphere larger than a certain critical size is unstable, and tends to collapse towards the centre.

---

1. *Introduction.*—It has recently been shown (**1, 3, 5**) that the isothermal gas sphere exhibits an unexpected type of instability. To understand how this arises one may think of a fixed, very large mass of gas, at uniform temperature T, subject to an experiment investigating Boyle's law. When the gas is in equilibrium with a very large volume V it satisfies the law in the form

$$pV=NkT, \tag{1.1}$$

N being the number of molecules present, k being Boltzmann's constant, and p the external pressure applied to maintain equilibrium. If p is gradually increased so that the gas passes through a series of equilibrium states, it is necessary to add to (1.1) a term representing the gravitational attraction of the molecules of gas on each other. Finally, at a certain critical pressure and volume (dependent on N and T), it is found that $\partial p/\partial V$ becomes positive, and the mass of gas unstable, with a tendency to collapse towards the centre.

A result of this phenomenon is that a sufficiently large isothermal gas sphere is unstable, and it is possible that the instability may be of importance in explaining the formation of stars of Population I (**5**). It therefore seems of interest to find out whether a similar type of instability applies to polytropic gas spheres, which are used as stellar models, and this question is investigated here.

It is known that certain complete polytropic gas spheres must exhibit an instability predicted by the virial theorem, but it has been shown (**1, 5**) that the conditions for instability according to the virial theorem are not necessarily the same as those for the instability described above, although the two phenomena are of the same general type. It does indeed turn out (Section 3) that for polytropic spheres the criteria for the two instabilities are different; in fact, the newly-discovered phenomenon gives criteria for the stability of incomplete polytropes, to which the virial theorem in its ordinary form does not apply.

2. *Perturbations in polytropic gas spheres.*—A polytropic gas sphere is called *complete* if it is surrounded by vacuum, and if the polytropic relationship applies, with the same index n, throughout its volume. It is called *incomplete* if the relation applies (with uniform n) within a sphere which is subject at its boundary to an equilibrium pressure provided by some other material. The following work will

apply to spheres which are complete or incomplete in the foregoing sense. One can also envisage annular regions of gas in polytropic equilbrium, but these are not dealt with here.

Consider a spherical mass of gas in equilibrium, and let $\rho(r)$ and $p(r)$ be the density and pressure at radius r. The hydrostatic equation is

$$\frac{dp}{dr} = -\frac{\rho G M(r)}{r^2}, \tag{2.1}$$

where $M(r)$ is the mass inside radius r, and G is the constant of gravitation. The polytropic relation is

$$p = \kappa\rho^{(1+1/n)}, \tag{2.2}$$

where κ and n are constants. Using (2.2), and also

$$M(r) = 4\pi\int_0^r \rho r^2\, dr, \tag{2.3}$$

we find that (2.1) gives

$$\frac{1}{r^2}\frac{d}{dr}\left\{\frac{r^2}{\rho}\frac{d}{dr}(\rho^{1+1/n})\right\} = -\frac{4\pi G}{\kappa}\rho. \tag{2.4}$$

Eqn. (2.4) determines $\rho(r)$ up to two arbitrary constants.

Let us introduce new variables θ and ξ by the formulae

$$\rho = \lambda\theta^n, \qquad \xi = r/\alpha \tag{2.5}$$

where

$$\alpha = \left[\frac{\kappa(1+n)}{4\pi G\lambda^{(1-1/n)}}\right]^{1/2}, \tag{2.6}$$

λ being a constant; then (2.4) gives

$$\frac{1}{\xi^2}\frac{d}{d\xi}\left\{\xi^2\frac{d\theta}{d\xi}\right\} = -\theta^n. \tag{2.7}$$

This is Emden's equation of index n. The constant λ does not appear in it, and so may be taken as arbitrary. The solutions of (2.7) with

$$\theta = 1, \quad \frac{d\theta}{d\xi} = 0 \quad \text{at} \quad \xi = 0$$

correspond to polytropic spheres, of central density λ.

Now consider a sphere S_0 of radius r_0 inside and concentric with the polytropic sphere, and containing mass M. Let us contemplate a small variation in r_0 such that

(i) M remains constant;
(ii) eqn. (2.1) is satisfied throughout S_0 after the variation, and at the new boundary of S_0 the pressure is that appropriate to equilibrium;
(iii) eqn. (2.2) is satisfied during the variation.

We may imagine that the variation takes place in the course of fluctuations of the molecules of the polytrope or, if the latter is incomplete and of radius r_0, from fluctuations in the material outside.

From (2.3), (2.5) and (2.6), we find

$$M = 4\pi\alpha^3\lambda\int_0^{\xi_0}\xi^2\theta^n\, d\xi,$$

which gives, with the use of (2.7),

$$M = -4\pi\alpha^3\lambda\,\xi_0^2\left(\frac{d\theta}{d\xi}\right)_0. \tag{2.8}$$

Here, and elsewhere, a suffix o means that the value of the quantity concerned is to be taken on the boundary of S_0. Now put

$$\alpha = \beta\lambda^{-(1-1/n)/2} \tag{2.9}$$

so that

$$\beta = \left[\frac{\kappa(1+n)}{4\pi G}\right]^{1/2}; \tag{2.10}$$

then (2.8) becomes

$$M = -4\pi\beta^3\lambda^{-(1-3/n)/2}\,\xi_0^{\,2}\left(\frac{d\theta}{d\xi}\right)_0. \tag{2.11}$$

As M is to remain constant as r_0 (or ξ_0) varies we have

$$0 = \delta M = -4\pi\beta^3\lambda^{-(1-3/n)/2}\left\{\frac{d}{d\xi}\left[\xi^2\frac{d\theta}{d\xi}\right]\right\}_0\delta\xi_0 + 2\pi\beta^3\lambda^{-3(1-1/n)/2}\left(1-\frac{3}{n}\right)\xi_0^{\,2}\left(\frac{d\theta}{d\xi}\right)_0\delta\lambda. \tag{2.12}$$

The change in λ allows for the slight alteration in central density which occurs during the variation. From (2.5) and (2.9) we have

$$\delta\xi_0 = \delta\left(\frac{r}{\alpha}\right)_0 = \frac{1}{\alpha}\delta r_0 + \frac{r_0}{2\beta}\left(1-\frac{1}{n}\right)\lambda^{-(1+1/n)/2}\delta\lambda. \tag{2.13}$$

Substituting (2.13) into (2.12) and using (2.7) and (2.11), we find after a calculation

$$\delta r_0 = \left\{\frac{(1-3/n)M}{8\pi\lambda r_0^{\,2}\rho_0} + \frac{(1/n-1)r_0}{2\lambda}\right\}\delta\lambda. \tag{2.14}$$

From (2.2) we have

$$\frac{\delta p}{p} = \left(1+\frac{1}{n}\right)\frac{\delta\rho}{\rho} = \left(1+\frac{1}{n}\right)\left\{\frac{\delta\lambda}{\lambda}+\frac{n}{\theta}\delta\theta\right\}. \tag{2.15}$$

Further

$$\delta\theta_0 = \left(\frac{d\theta}{d\xi}\right)_0\delta\xi_0,$$

so that after a calculation, in which (2.8) and (2.13) are used

$$\delta\theta_0 = -\frac{M}{4\pi\lambda^{1/n}\beta^2 r_0^{\,2}}\delta r_0 - \frac{(1-1/n)M}{8\pi\beta^2 r_0\lambda^{(1+1/n)}}\delta\lambda.$$

Substituting this into (2.15) we find with the help of (2.5) and (2.14)

$$\frac{1}{p_0}\frac{\delta p_0}{\delta r_0}\left[\left(1-\frac{3}{n}\right)M + \left(\frac{1}{n}-1\right)4\pi\rho_0 r_0^{\,3}\right]4\pi\rho_0^{\,1/n}\beta^2 r_0^{\,2} = 32\pi^2\left(1+\frac{1}{n}\right)\beta^2\rho_0^{\,1+1/n}r_0^{\,4} - (1+n)\left(1-\frac{3}{n}\right)M^2. \tag{2.16}$$

Simplifying this further, and using (2.2) and (2.10) we eventually find

$$\left(\frac{\partial p}{\partial V}\right)_0 = -\frac{2(n+1)p_0}{3(n-1)V_0}\frac{1-\dfrac{(n-3)GM^2}{(n+1)8\pi p_0 r_0^{\,4}}}{1-\dfrac{n-3}{n-1}\dfrac{M}{3\rho_0 V_0}}. \tag{2.17}$$

If we put $G=0$ and take the density as uniform, we find

$$\left(\frac{\partial p}{\partial V}\right)_0 = -\frac{n+1}{n}\frac{p_0}{V_0},$$

which is the formula obtained at once by differentiating (2.2) and using $\rho V = \text{const}$.

Formulae (2.16) and (2.17) are those required for the discussion of stability in the next Section. If in (2.17) we let $n \to \infty$, we get a formula for the isothermal gas sphere which agrees with that in (1).

3. *Stability.*—It is easily shown that the polytropic gas sphere will be unstable to small variations in p_0 and V_0 if $(\partial p/\partial V)_0$ is positive. It follows at once from (2.17) that $(\partial p/\partial V)_0$ is negative for all r_0 if

$$1 < n \leqslant 3.$$

This means that a polytropic sphere with an index in this range is stable to the type of perturbation described in Section 2. This result is true whether or not the sphere is a complete polytrope.

The case in which

$$0 < n \leqslant 1 \tag{3.1}$$

is best dealt with by considering (2.16). With this range of n the right-hand side of (2.16) is positive, and $(\partial p/\partial V)_0$ will be positive if the term in square brackets on the left is positive, that is, if

$$\left(1 - \frac{3}{n}\right) M + \left(\frac{1}{n} - 1\right) 4\pi\rho_0 r_0^3 > 0,$$

that is, if $$4\pi\rho_0 r_0^3 (1-n) > (3-n) M. \tag{3.2}$$

If we write (3.2) in the form

$$\frac{1-n}{1-n/3} > \frac{\bar{\rho}}{\rho_0}, \tag{3.3}$$

$\bar{\rho}$ being the mean density within radius r_0, we see that $(\partial p/\partial V)_0$ cannot be positive, with n satisfying (3.1), if the density diminishes as the radius increases. Because if the latter condition is fulfilled the right-hand side of (3.3) is greater than unity whereas the left-hand side is less than unity. We conclude that no physically interesting case of instability arises if n satisfies (3.1).

If we ignore, as being of no physical interest, spheres for which $n \leqslant 0$, there remain those with

$$n > 3.$$

If these are *complete* it follows from an application of the virial thoerem (2) that they are unstable. It was emphasized in the case of the isothermal gas sphere that this theorem applies only if the gas is surrounded by vacuum, and if this is not so the situation may be quite different. The work in Section 2 holds for a polytrope which is incomplete provided that it is surrounded by gas at the appropriate equilibrium pressure. We can use this work to find how the stability of incomplete polytropes depends on the radius for $n > 3$.

To do this we need to study how the sign of $(\partial p/\partial V)_0$ in (2.17) depends on r_0. We can do this most easily by transforming to the variables ξ and θ, and using Emden's calculations (4). For $n > 3$ it is clear from (2.17) that $(\partial p/\partial V)_0$ has the sign of

$$-\frac{1 - \dfrac{n-3}{n+1}\dfrac{GM^2}{8\pi p_0 r_0^4}}{1 - \dfrac{n-3}{n-1}\dfrac{M}{3\rho_0 V_0}},$$

and by using (2.2), (2.5), (2.6) and (2.8), we can transform this expression into

$$-\frac{1-\frac{n-3}{2}\left(\frac{d\theta}{d\xi}\right)_0^2\theta_0^{-(n+1)}}{1+\frac{n-3}{n-1}\xi_0^{-1}\theta_0^{-n}\left(\frac{d\theta}{d\xi}\right)_0}. \tag{3.4}$$

For given n, this expression can be worked out as a function of ξ_0 by the use of Emden's tables. One finds that for small ξ_0 (i.e. small r_0) (3.4) is negative, but when ξ_0 is increased to a certain value, ξ_0 (crit.), the numerator changes sign. For this value of ξ_0, $(\partial p/\partial V)_0$ becomes positive and the sphere becomes unstable. By arguments such as those used for the isothermal gas sphere, one can easily show that for all larger radii the polytropic sphere must be unstable, and that the instability must result in a tendency to collapse towards the centre.

Table I shows (in the second column) the values of ξ_0 (crit.) for polytropes with various values of n (>3). These have been calculated from Emden's tables by interpolation, and are given to the nearest 1/10 of a unit of ξ. The appropriate values of r_0 can be obtained from (2.5) and (2.6). In the third column of Table I, ξ_1 indicates the greatest possible value of ξ, that is, the value of ξ for which the pressure vanishes.

TABLE I

n	ξ_0 (crit.)	ξ_1
4	3·5	14·999
4·5	3·2	32·143
4·9	3·0	169·4678
5	3·0	∞
6	2·7	∞

It follows that incomplete polytropes with radii less than those referred to in Table I are stable to the type of perturbation considered in this paper. (One cannot of course assert from this that they would be stable to other perturbations.) It is clear from the work of McCrea (**5**, p. 563 *et seq.*) that the instability envisaged is of the same general type as that predicted by the virial theorem, but the method used here enables one to take account of the presence of a surrounding medium. One may therefore take this work as supplementing the well-known criterion obtained from the virial theorem that complete polytropes are unstable if $n>3$, and as showing that the criterion cannot be extended to incomplete polytropes of sizes less than that given by ξ_0 (crit.).

Queen Elizabeth College
(University of London),
Campden Hill Road,
London, W.8:
1958 *May* 22.

References

(1) Bonnor, W. B., *M.N.*, **116**, 351, 1956.
(2) Chandrasekhar, S., *An Introduction to the Study of Stellar Structure*, Chicago, 1939, p. 52.
(3) Ebert, R., *Z. Astrophys.*, **37**, 217, 1955.
(4) Emden, R., *Gaskugeln*, Leipzig and Berlin, 1907.
(5) McCrea, W. H., *M.N.*, **117**, 562, 1957.

ERRATA

M.N., **113**, No. 4, pp. 455–467, 1953:

J. G. Porter and D. H. Sadler, *The Accurate Calculation of Apparent Places of Stars.*

The statement " sec δ may be replaced approximately by tan δ " in para 9 (*c*) on p. 460 applies only to magnitude and not to sign. The substance and conclusions of the paper are unaffected by this error; but the formulae for the tabulation method of correction (*c*) apply only for northern (positive) declinations.

For southern (negative) declinations: $(1-\sin\delta)$ in the coefficients of the residual second-order terms No. 12 should be replaced by $(1+\sin\delta)$; and the signs of the terms $2gh$ in the definitions of J, J' in equations (14), (15) on p. 460 should be negative. Separate tabulations of the values of J, J' are therefore required for northern and for southern declinations.

We are grateful to Dr T. Lederle of the Astronomisches Rechen-Institut, Heidelberg, for pointing out this error to us.

J. G. P.
1958 *June* 25. D. H. S.

M.N., **117**, No. 6, p. 581, 1957:

List of Fellows elected:

for Matthew Leslie Billis *read* Matthew Leslie Bellis.

РЕЗЮМЕ ДОКЛАДОВ, В ПЕРЕВОДЕ НА РУССКИЙ ЯЗЫК

ПРЕИМУЩЕСТВО НЕЗАВИСИМОЙ АСТРОЛЯБИИ ДЛЯ ОСНОВНОЙ АСТРОНОМИИ

Лекция имени Джорджа Дарвина, прочитанная профессором Андрэ Данжоном 9 го мая 1958 г.

ИЗУЧЕНИЕ ОПРЕДЕЛЕНИЯ АТМОСФЕРНОГО СОДЕРЖАНИЯ СОЛНЦА

Д. Магглстоун

Изучается определение солнечных атмосферных содержаний с помощью наблюдаемых интенсивностей слабых линий Фраунгофера. Метод весовых функций, пользующийся результатами наблюдаемого потемнения края диска, разбирается в деталях. Предлагается дополнительный метод—метод градиента Планкка, который не нуждается в наблюдениях потемнений к краям диска, но всецело зависит от физических характеристик рассматриваемой модели солнечной атмосферы.

В статье делается ссылка на случай азота (потенциал ионизации = 14,54 вольта), главным образом для сравнения результатов, полученных обоими вышеуказанными методами. В статье рассматриваются девять линий поглощения и даются определения содержания азота по каждой из них. Обнаружено значительное расхождение между результатами полученными обоими методами. Из теоретического разбора следует вывод, что в случае азота, да и вообще для всех элементов высокого потенциала ионизации, метод весовых функций совершенно ненадёжен и надо пользоваться методом градиента Планкка.

Рассматриваются три атмосферных модели и, для азота, выводятся средние результаты, полученные последним методом (принимая $\log A_H = 12{,}00$): модель Клааса — $\log A_N = 7{,}71$, модель Витензи — $\log A_N = 7{,}81$, модель Суихарта — $\log A_N = 7{,}93$ (для сравнения: по Хюнаертсу 9,02, а по Унсёльду 8,61).

ТЕМПЕРАТУРЫ ВОЗБУЖДЕНИЯ ДЛЯ CN-ИЗЛУЧЕНИЯ НИЖНЕЙ ХРОМОСФЕРЫ

Д. В. Томас

Микрофотометрирована область системы полос CN при 3883 A, являющейся заметной особенностью спектрограммы вспышки, полученной Редманом при затмении в 1952 г. Полосы CN сильно искажены совпадениями, но оказалось достаточно неискаженных линий, чтобы можно было измерить распределение ротационной интенсивности в полосе o–o на трех высотах ниже ~ 400 км. Самопоглощение значительно, в особенности у границ полос и произведена оценка его влияния. Измерения указывают на отрицательный градиент температуры возбуждения; температура на высоте в ~ 400 км оказывается $\simeq 4500°$, а величина ее градиента неопределенна. Между тем CN-излучение может оказаться в соответствии с положительным градиентом кинетической температуры в последней моделе хромосферы по де Ягеру, при условии учета отклонения от локального термодинамического равновесия и несовершенности результатов наблюдений.

СПЕКТР РЕКОМБИНАЦИИ ВОДОРОДА

А. Бёрджесс

Дано решение каскадных уровнений радиативного захвата для водорода, принимая при этом во внимание вырождённость орбитального углового момента атомных уровней. Рассмотрены все уровни (n, l) с $n < 13$, также как и континуум.

Применяется метод перевала для получения асимптотических разложений дипольных матричных элементов водорода, явно включающих квантовое число l, а при помощи других методов выведены полезные приблизительные выражения. Приведены таблицы сечений фотоионизации водорода для всех уровней (n, l) с $n < 13$, а также коэффициентов рекомбинации для температур электронов $T_e = 10^4$ и $2 \cdot 10^4$ °K.

Даны решения каскадных уравнений для обоих случаев A и B при $T_e = 10^4$ и $2 \cdot 10^4$ °K. Население отдельных уровней l для данного n отнюдь не пропорционально их статистическому весу. По данным расчетам получаются для обоих случаев A и B бальмеровские декременты, подобные декрементам, выведенным Бэкером и Менцелем для случая B.

Наблюдаемые бальмеровские декременты шести планетарных туманностей, с поправкой на покраснение, хорошо совпадают с вычисленными декрементами.

ИНТЕРФЕРОМЕТРИЧЕСКИЕ ИЗМЕРЕНИЯ ДЛИН ВОЛН VI. ИЗМЕРЕНИЯ В ОБЛАСТИ 3940–4450 А

С. Никольс и С. В. М. Клюб

Описано измерение 17 солнечных и вакуум-дуговых длин волн в области 3940–4450 А. Общее число солнечных красных смещений, измеренных методом круговых каналов, сведено к 51. Эта группа линий интересна потому, что она содержит 6 линий железа из одного мультиплета: a^3F–y^3F^0, резонансную линию железа: 4375,9 А и относительно сильную линию в хромосфере, по причине Ti^+: 4443,8 А. Красные смещения этих линий не согласуются ни с одним из существующих предположений. Для 51 наблюдаемой линии общее возрастание солнечного красного смещения с интенсивностью линии является единственной наблюдаемой закономерностью.

МЕТОД КВАНТОВОГО ДЕФЕКТА

М. Дж. Ситон

В методе квантового дефекта применяются интерполированные или экстраполированные квантовые дефекты для определения асимптотических видов атомных волновых функций. Этот метод можно применять при вычислениях вероятностей атомных переходов и сечений фотоионизации, при расчетах столкновений между электронами и ионами, а также при решении проблем твердого состояния.

Данная статья содержит обзор прежних работ, касающихся основных целей метода и дает несколько новых результатов, относящихся к состояниям положительной энергии и к нормировке волновых функций связанных состояний. Обсуждены некоторые приложения метода.

ЗВЕЗДЫ-ГИГАНТЫ ТИПА II

К. Б. Хэзелгроув и Ф. Хойль

Даны интеграции по последовательности звезд-гигантов типа II, приводящие к стадии эволюции, в которой выход энергии из ядерных реакций по гелию значителен. Результаты этих интеграций видимо хорошо согласуются с наблюдениями.

УСТОЙЧИВОСТЬ ПОЛИТРОПИЧЕСКИХ ШАРОВ ГАЗА

В. Б. Боннор

Ранее было доказано, что изотермический шар газа является гравитационно неустойчивым при малых возмущениях давления на достаточно большом расстоянии от центра. Эти выводы прилагаются здесь к политропическим шарам газа: доказывается, что эта неустойчивость не влияет на шары, показатель n которых удовлетворяет условию $0<n\leqslant 3$, но для $n>3$ и радиуса шара, превосходящего определенную критическую величину, шар неустойчив и склонен к сплющиванию по направлению к центру.